ADVANCED SLIDING MODE CONTROLLERS AND THEIR INNOVATIVE APPLICATIONS USING SMART MATERIALS

A Dissertation

Presented to

the Faculty of the Department of Electrical and Computer Engineering

University of Houston

In Partial Fulfillment

of the Requirements for the Degree

Doctor of Philosophy

in Electrical Engineering

by

Mithun Singla

August 2012

ADVANCED SLIDING MODE CONTROLLERS AND THEIR INNOVATIVE APPLICATIONS USING SMART MATERIALS

Mithun Singla

Approved:

Chair of the Committee
Dr. Gangbing Song, Professor
Electrical and Computer Engineering
Mechanical Engineering

Co-Chair of the Committee
Dr. Leang-San Shieh, Professor Emeritus
Electrical and Computer Engineering

Committee Members:

Dr. Heidar Malki, Professor and Chair
Engineering Technology
Electrical and Computer Engineering

Dr. Ji Chen, Associate Professor
Electrical and Computer Engineering

Dr. Matthew Franchek, Professor
Mechanical Engineering

Dr. Karolos Grigoriadis, Professor
Mechanical Engineering

Dr. Suresh K. Khator, Associate Dean
Cullen College of Engineering

Dr. Badrinath Roysam, Professor and Chair
Electrical and Computer Engineering

To my Maa and Paa

Acknowledgments

This dissertation would not have been possible without the immense help and support from my advisors, students, friends and parents. First of all, I would like to acknowledge my advisor and mentor Dr. Gangbing Song for his continued support both financially and technically for all these years. He helped me throughout all my studies and most importantly during my difficult times. I would like to thank him for giving me a chance to work with him on many interesting and challenging tasks. Without his support and trust in my abilities, I would not be able to make it here.

I would like to thank Dr. Leang-San Shieh for sharing his vast knowledge of controls with me. He mentored and taught me many aspects of controls and guided me on my research objectives. I am very grateful to him for all the help and suggestions he has given me, thus bettering my understanding of this field.

I would like to thank all of the committee members for accepting my request of serving on my PhD dissertation defense committee. I thank my colleagues all for their continuous friendship and moral support. In particular, Dr. Claudio Olmi and Christiana Chang, thank you for proofreading my papers without complaining; Dr. Haichang Gu for his help on introducing me to smart materials; Mr. Devendra Patil, for his mechanical engineering support, and Dr. Luyu Li for his deep knowledge of math and controls. I would like to give a special thanks to Mr. Peng Zhang and Mr. Pranab Narayan Jha for their help and time in mathematical modeling. Lastly, I acknowledge my family for their love and support, without this I would not be able to meet my goals.

ADVANCED SLIDING MODE CONTROLLERS AND THIER INNOVATIVE APPLICATIONS USING SMART MATERIALS

An Abstract

of a

Dissertation

Presented to

the Faculty of the Department of Electrical and Computer Engineering

University of Houston

In Partial Fulfillment

of the Requirements for the Degree

Doctor of Philosophy

in Electrical Engineering

by

Mithun Singla

August 2012

Abstract

This dissertation focuses on the following two research topics involving smart materials: 1) the advanced sliding mode controllers and their applications and 2) the development of an automatic de-icing system for roads by the electrical heating of embedded carbon fiber.

Sliding mode control has widely been used in many different applications. In this dissertation, the active sliding mode control behavior was realized through analyzing the vibration suppression of vortex induced vibrations (VIV) of a jumper pipe structure via pounding tuned mass damper (PTMD) integrated with viscoelastic material. The force generated by the PTMD is analogous to the active sliding mode control. Comparison between simulation and experimental results demonstrated the similarity between the PTMD and the active sliding mode control.

Sliding mode controllers are robust to uncertainties and immune to disturbances, but suffer chattering problems due to discontinuities in the control law. In this dissertation, an advanced sliding mode control using the continuous sign function and LQR approach to alleviate chattering is proposed. The desired sliding surface was designed using the stable eigenvectors of the controlled system. Simulation results show that the proposed approach is effective in disturbance rejection and chattering reduction. The robustness of the proposed optimal controller was demonstrated through the implementation of active vibration control on a flexible beam with mass uncertainty. The experimental results show that the vibrations of the beam with mass uncertainty can be well controlled by the proposed approach.

Due to the inability to guarantee stability of a system with unmatched uncertainties, the proposed approach is improved by replacing the LQR approach with the H_∞ approach. The stability of the proposed approach was verified with the H_∞ approach. The simulation results show that the control input generated by the proposed robust approach was very smooth compared to conventional sliding mode controllers. The experimental implementation for vibration control of a base-isolated structure equipped with an MR damper, where the nonlinear force generated by the MR damper acted as an uncertainty to the system, showing the effectiveness of the approach.

Lastly, an innovative de-icing system using carbon fiber as the heating element was developed. A test sidewalk was prepared by embedding electrically powered carbon fiber frames into the concrete pavement. A LabVIEW interface controlled the de-icing process through two sidewalk surface temperature controllers (ON-OFF and Fuzzy Logic) and enabled the user to keep track of the environmental conditions. The experimental results showed that the proposed technique effectively prevented the formation of ice on the pavement surface and that the advanced temperature controller was 80% more power efficient compared to a manual on-off switch.

Keywords: Smart Material, Sliding Mode Control, Scalar Sign Function, Pounding Tuned Mass Damper, Vibration Control, Carbon fiber, Electrical heating, de-icing

Table of Contents

List of Figures

List of Tables

Chapter 1. Introduction

Intelligent materials, more popularly known as smart materials, have emerged as a key component of recent technological advancements. Their unique ability to respond to change in a physical parameter or quantity has introduced new horizons in engineering applications. Smart materials have their applications in almost every field and with each passing day new and innovative applications are designed, further advancing technology. To properly use these smart materials, different control algorithms are used to incorporate smart materials into these applications. Among them, sliding mode controllers are known for their robustness and stability. This dissertation aims at the development of optimal sliding mode control and applications of smart materials in advanced and novel industrial applications. In the following section, the motivation and objective of this dissertation are discussed.

1.1 Motivation and Objective

Vibrations of the flexible structures have always been a major concern for structural engineers. Undesired vibrations of the structure can lead to structural failure. Although many researchers are introducing different control algorithms to develop vibration controllers using active or semi-active control approaches, the industry still prefers passive control systems. The main advantages of passive control systems are 1) no external power needed, 2) simple and easy implementation and maintenance and, most importantly, 3) low cost. However, passive control systems require understanding of the passive device and tuning of system parameters to perform effectively. This makes the design of passive control systems very cumbersome. Many researchers have offered different design techniques and mathematical models to understand and design passive

damping devices. However, an active vibration control approach has never been realized through analyzing a passive system.

In this study, the sliding mode control approach is used to simulate the process of a passive damping device to suppress the vibrations of a pipe structure used in the oil and gas industry. The passive device using viscoelastic material, called a Pounding Tuned Mass Damper (PTMD), has been developed at the University of Houston (UH). The PTMD controls the vibrations of the system by dissipating the energy through pounding the PTMD device on a viscoelastic material. The passive vibration suppression process is analyzed as the sliding mode control effect, where the system is first pushed towards the stable region and then is kept under constraints so that the system states remains in the stable region.

The concept of Sliding Mode Control (SMC) has received much attention in the past few decades. In sliding mode control, an appropriate control input is provided to the system's states so that the system states are confined to a desired manifold of the state space. For the last few decades, the sliding mode controller has evolved. Many researchers are using this approach to develop new applications. The main advantages of sliding mode control are its ability to reject disturbances and its robustness to systems with uncertainties.

Much research has been done to improve the sliding mode approach and work continues to develop its function. One particular area researchers are concentrating on is the chattering phenomenon commonly seen in sliding mode control. This phenomenon occurs when the system states are pushed very near to the sliding surface and these states start oscillating near the sliding surface due to high frequency oscillations from the

discontinuous switching function. A high gain is generally associated with this switching function to reduce the chattering. It has been seen that though many researchers are working on the optimal design of the sliding mode controller, few are attempting the optimal design of the controller gain associated with the switching function.

In this dissertation, an optimal sliding mode control algorithm is proposed using the continuous sign function. The proposed sliding mode control law is divided into two parts. The first part of the controller attracts the plant states into a stable plane using the LQR approach. The second part of the controller is designed as a solution to a constrained tracking problem, where the control law makes the system states track the desired stable sliding surface/manifold and then the states are made to converge into a desired manifold. The matrix sign function approach is used to calculate the stable eigenvector. The desired stable sliding manifold is designed by using the stable eigenvector of the controlled plant to ensure optimal convergence of the system states to the desired surface. Also, the continuous scalar sign function is used to replace the discontinuous switching function. The continuous scalar sign function will help in the alleviation of chattering introduced by the discontinuous sign function. The stability of the proposed approach can be explained by Lyapunov's second theorem.

Sliding mode control approaches are famous for their disturbance rejection and robustness to matched or structured uncertainties. However, in the case of unstructured or unmatched uncertainties, the sliding mode approaches cannot guarantee the stability of the controlled system. Also, the LQR approach does not provide a prescribed degree of stability for unstructured uncertainties. It is very necessary for a controller to prove its stability for unmatched or unstructured uncertainties. In order to deal with unmatched

uncertainties, many researchers use the H_∞ control approach, where uncertainties of the system are assumed to be bounded.

In this dissertation, the proposed optimal sliding mode approach using the LQR approach is improved by replacing the LQR approach with H_∞ control approach to deal with both matched and unmatched uncertainties. The objective of combining the H_∞ approach and continuous sign function is to deal with matched and unmatched uncertainties of the system and to reduce the chattering effect. Both proposed sliding mode approaches are implemented on a simulated system and compared with a conventional sliding mode controller individually to test their effectiveness. Also, both approaches are implemented as active vibration control examples for uncertain systems.

Control of undesired vibrations of the flexible structures has always been a major challenging task for structural engineers. System uncertainties due to model inaccuracies and structure nonlinearities and external disturbances make this challenging task more difficult. Many advanced control approaches have been discussed and implemented to suppress structural vibrations. Due to their immunity to system uncertainties and external disturbances, the sliding mode control approach has been popularly employed in active vibration control of flexible structures.

The proposed robust optimal sliding mode approaches are implemented as active vibration control approaches on smart flexible systems to show their effectiveness against uncertainties and disturbances. The optimal sliding mode controller with LQR approach is implemented to control the multimodal vibrations of a smart flexible beam with mass uncertainty. This mass uncertainty can be treated as matched uncertainty of the system.

The piezoceramic sensor and actuator are used to sense and control the vibrations, respectively.

The H_∞ based robust optimal sliding mode controller is implemented on a two story base-isolated system to suppress the vibrations of the structure during earthquake. The proposed robust approach provides the excitation voltage to an MR damper controlling the vibrations of the system. The force generated by the MR damper shows highly nonlinear behavior. Also, the force generated by the MR damper depends upon many factors, such as concentration and sedimentation of iron particles, the type of oil in the MR fluid, viscosity of the MR fluid when no voltage is provided, etc. All these factors make MR dampers highly uncertain. This uncertainty due to the MR damper can be structured in to a system model and thus can be considered as matched uncertainty. Since the earthquakes are considered as undesired random disturbance, the effect of earthquake disturbance on the system states is considered an unmatched uncertainty to the system.

Apart from advanced sliding mode controllers' development, an automatic de-icing system is also reported in the dissertation. The motivation and objective behind the development of automatic de-icing system is explained. The presence of snow and ice causes damages to roads, as well as many road accidents. Different techniques have been used to deal with the de-icing issue. All these techniques have disadvantages, such as how salting of the roads can accelerate cavity formation in concrete, in addition to being laborious. Heat exchangers are expensive and use large amounts of power. Snow movers are both expensive and laborious. There is a need of a power efficient system. In this dissertation, an advanced de-icing system using carbon fiber embedded into the concrete

as the heating element is reported. An advanced fuzzy logic based temperature controller is implemented to control the surface temperature of the pavements. This advanced controller takes consideration of weather parameters and their effect on de-icing. Upon electrically heating the carbon fiber with the advanced controller, the surface temperature of the roads can be controlled and the de-icing system can be made more power efficient and economical.

1.2 Organization

The dissertation includes eight chapters. Chapter One gives the motivation, problem statement, contribution of research done for the dissertation and dissertation organization. Chapter two introduces different smart materials such as piezoceramics, MR fluids, viscoelastic material and carbon fiber as resistive heating element and their basics with application examples. Chapter three presents the introduction and literature review of sliding mode control and the evolution of sliding mode controls over the years and their applications.

Chapter four presents the realization of active sliding mode control law through vibration suppression of large flexible pipe structures by a passive device called a Pounding Tuned Mass Damper (PTMD). The force generated by the passive device is compared with the active sliding mode control law. The simulation results of the active approach are effectively compared with the experimental results of the passive device.

Chapter five talks about the development of the optimal sliding mode controller with the Linear Quadratic Regulator (LQR) approach. The chapter includes the development of the optimal control approach and its subsequent simulation examples. To test the robustness of the approach, the implementation of the proposed controller as an

active vibration control of a flexible beam using a piezoceramic actuator and sensor is presented.

Chapter six describes the use of H∞ based sliding mode control to deal with systems with matched and unmatched uncertainties and noise rejection. A simulation example is provided to show the effectiveness of the approach. In chapter seven, the proposed optimal sliding mode controller for uncertain systems was later implemented on a two story building structure for vibration control under various earthquake excitation signals by a shaker table for example the Kobe, Northridge and El Centro earthquakes.

Chapter eight explains the development of an automatic de-icing/anti-icing system for roads in very cold regions using carbon fiber as heating elements. This chapter talks about the development of the de-icing system, and field testing results. Two temperature controllers, the ON/OFF controller and Fuzzy logic based controller, are discussed and implemented to keep the surface temperature of roads above freezing point. A power cost analysis is presented to show the cost effectiveness of the proposed approach. Chapter nine includes the conclusions and future work related to research finding provided in this dissertation.

1.3 Contribution

The significant outcomes described in this dissertation are as follows:

An analogy is successfully established between an active sliding mode control law and force generated by PTMD with viscoelastic material to suppress the vibrations of structure. This analogy is used to realize the active sliding mode control law through force generated by the PTMD. The simulation and experimental results supports the proposed relation between the sliding mode approach and passive device.

An LQR based optimal sliding mode controller using sign function is developed. The stability of the proposed controller is explained. The simulation results explain that the proposed controller uses less energy to converge the system states than the conventional sliding mode controller. The optimal controller is successfully implemented to control the vibrations of a smart beam with mass uncertainty using a piezoceramics sensor and actuator. The simulation and experimental results show that the proposed approach is very effective in rejecting disturbance and dealing with system uncertainties.

Later, the optimal control gains are calculated using H∞ approach to deal with external disturbances and unmatched system uncertainties. The performance of the robust optimal controller is evaluated by implementing the controller to suppress the vibrations of a two story structure with nonlinear MR damper. The effect of the nonlinear MR damper is considered a highly matched uncertainty and the external earthquake excitation as an unmatched uncertainty. The experimental results show the effectiveness of the robust optimal sliding mode controller in dealing with matched and unmatched uncertainties.

A cost effective de-icing system is developed using carbon fiber as the heating element and embedded into concrete pavements. Two control algorithms, the ON/OFF controller and the fuzzy logic based controller, are designed to control the surface temperature of the road. The fuzzy logic controller is based on surface temperature and weather parameters such as environmental temperature, dew point and chances of rain/snow. The power consumption cost is analyzed and from the analytical results, the fuzzy logic based controlled de-icing system is proven to be more economical than other de-icing technologies.

Chapter 2. Introduction to Smart Materials

Smart materials are defined as materials that exhibit coupling between multiple physical domains. The coupling between physical domains is manifested as a transformation of energy in one form to another in useful quantity. For example, piezoelectric materials will generate a charge signal when subjected to mechanical strain and vice versa. Commonly used smart materials include piezoceramics, shape memory alloy, magneto-rheological fluids (MR fluids), and fiber optical sensors, etc.

Smart materials are called 'smart' due to their responsive nature to physical changes. Sometimes smart materials are also described as active materials or intelligent materials due to their unique nature [1]. There are some materials which do not exhibit change in shape, but rather have some other properties which make them special, such as, magneto-rheological fluids and electro-rheological fluids which change their viscosity when under the influence of a magnetic field and an electric field, respectively.

Smart materials, or active materials, can be used as a sensor or an actuator based on the response they generate. Upon application of a stimulus, the material can respond by change in shape or length and this change in shape or length can be used as an actuation principle for the system. Similarly, an input to the system can be sensed by the sensor. While working as a sensor, smart materials provide some signal or change that can be analyzed which corresponds to the physical behavior that is being sensed by the sensor.

2.1 Classification of Smart Materials

Smart materials are used to describe the system and its behavior. There are various approaches to categorize smart materials into groups. In a more standard way,

smart materials can be classified into various categories depending on the physical property they are responsive to and the output response from them; such as electrical field, magnetic field, light, or chemical composition.

The first category of smart materials depends on the electrical field, where the electrical field is used as the medium to provide some change in the property of the materials, for example piezo-ceramics and ER fluids. The second category depends upon the magnetic field and examples are MR fluids and Magnetic Shape Memory Alloy (MSMA) material.

Some smart materials are also responsive to thermal energy or changes in temperature, such as Shape Memory Alloys (SMA). Smart materials are also classified by dependence upon light. Fiber Bragg Grating sensors (FBGs) and photovoltaic cells comes under this category. There are some materials that are responsive to changes in chemical properties of the medium. For example, ionic polymer gels are used to measure the concentration of the chemical by measuring its pH value. In this dissertation, different smart materials have been used for different applications. A brief description of these smart materials is given in the following sections.

2.2 Piezoceramics

The piezoelectric effect in materials, by which a material changes shape when an electric field is applied to it and vice versa, was discovered in the nineteenth century. There are various applications of piezoceramics in research as well as in commercial applications. As a sensor, piezo materials are used in microphones, accelerometers and ultrasonic transducers. As actuators, piezo materials are used in ultrasonic motors, ultrasonic welders, and drilling and vibration control of flexible structures.

Piezoelectric materials refer to substances with unique properties of generating electric charge when it changes in shape and vice versa. Natural piezoelectric materials are quartz, tourmaline and Rochelle salt. Later, other piezoelectric ceramics were developed by using ferroelectric materials with the perovskite crystal structure, such as barium titanate and Lead Zirconium Titanate, commonly known as PZT.

2.2.1 Piezoceramics as a Sensor

As discussed earlier, piezoceramic devices are extensively used as a sensor to detect the vibration and strain in structures. One of the most used piezoceramics is PZT. The piezoceramic sensor effect can be described in the following Figure 2-1, where a beam is attached with a piezoceramics sensor. The beam is bent in the upward and downward direction. The voltage induced by bending the beam is opposite to the direction of poling. When no load is applied, no voltage is induced.

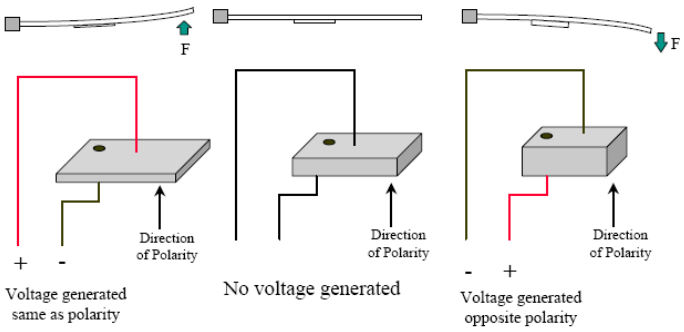

Figure 2-1 Piezoceramics as sensor

Piezoceramics are used as sensors in various applications such as gas and cigarette lighters, gramophone pick-ups and electric guitars.

2.2.2 Piezoceramics as an Actuator

Piezoceramic materials can also be used as actuators for vibration control, shape control and micro level positioning applications. The PZT is the most commonly used

piezoceramic actuator. The actuator effect can be explained by the following in Figure 2-2, where a PZT patch as actuator is attached to the beam. When voltage is applied to the beam the patch expands and provides a lateral movement in the beam as compared to no movement when no voltage is applied.

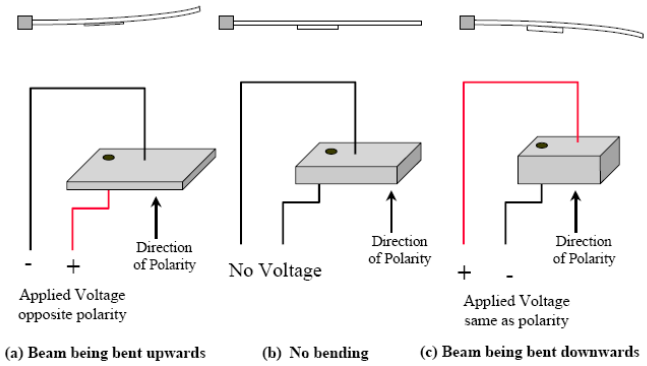

Figure 2-2 Piezoceramics as actuator

If a sinusoidal voltage signal is provided to the patch, the beam will have a sinusoidal motion and this makes the beam vibrate. There are various types of piezo actuators, such as PZT patches, stack actuators, tube actuators, and bimorph and bender actuators.

2.3 MR Fluids

Magneto-Rheological (MR) fluid is one of the smart materials used in research. MR fluid shows dramatic changes in rheological behavior upon application of the magnetic field, depending upon the strength of the applied magnetic field. When subjected to large enough magnetic fields, MR fluid can instantly change its viscosity and change form from a free-flowing fluid to a semi-solid.

MR fluids are typically composed of a carrier fluid with suspended magnetic metal particles. Synthetic oils, mineral oils, glycol or water is used as carrier fluid and pure soft iron particles consisting of a diameter around 3 to 5 microns are used as

suspended metal particles (composing 10-50% by volume). The magnetization induced by the magnetic field makes the suspended particle line up as columnar structures parallel to the applied field. To discourage gravitational settling and to promote particle suspension, enhance lubricity, modify viscosity and inhibit wear, a variety of proprietary additives can be added in most MR fluids

In recent years, MR fluid has shown great promise in the field of smart materials. MR fluid has been used in many commercial applications such as vehicle seat vibration control, automotive suspension systems, flow control valves and exercise modules.

2.4 Viscoelastic Materials

Viscoelastic material can be defined as a material that exhibits a time or frequency dependent relationship between stress and strain. An elastic material, much like a spring, retracts to its original position when stretched and released, whereas a viscous fluid, such as putty, retains its extended shape when pulled. A viscoelastic material (VEM) combines these two properties—it returns to its original shape after being stressed, but slowly enough to oppose the next cycle of vibration. The other affecting parameters other than time and frequency are temperature, dynamic strain rate, static pre-load, ageing etc.

Viscoelastic materials often used to increase the damping of structures and vehicles. Since structural metal have low damping, viscoelastic layers are of use as attached layers in providing additional damping by introducing relative energy dissipation between layers [2]. Viscoelastic materials are used in many applications for example in passive noise reduction earplugs, the vibration control of structures, seals and gasket, sports equipment etc.

2.5 Carbon Fiber

Carbon fiber is a light material with high tensile strength. The crystal alignment of carbon atoms gives the fiber a high strength to volume ratio. The carbon fiber is a material with high stiffness, high tensile strength, low weight, high chemical resistance, high temperature tolerance and low thermal expansion. The carbon fiber materials are very popular in aerospace and civil engineering, the military, and motor sports in reinforced composite material.

According to the manufacturer [3], carbon fiber has a tensile strength of 170 ksi with a density of 0.057 pci. Its electrical resistivity is in the range of 8-40m Ωm [4]. Taking advantage of the high tensile strength and electrical resistivity, carbon fiber material can be used in the de-icing of roads in the sub-tundra region during winter time by heating the carbon fiber embedded roads.

Chapter 3. Sliding Mode Controller

The sliding mode control is famous for its ability of disturbance rejection and robustness. For the past few decades, this advantage has attracted many researchers all over the world. This chapter explains the literature review of sliding mode control and its development and improvements during these years.

3.1 Introduction to Sliding Mode Controller

Control system engineers always have to deal with the presence of uncertainties and disturbances in real systems, which affect the performance of a controller in a negative way. These uncertainties not only can worsen the performance of the system, but can lead to system instability. During the control system design, the issues of uncertainties are given higher priorities and the stability of the controller is guaranteed. Many control algorithms have been proposed to mitigates the effects of uncertainties in a control system such as fuzzy logic based controllers, model predictive controllers, adaptive and robust control techniques, etc.

Sliding Mode Controller (SMC) is one such technology which is famous for its simple approach and ability to reject the effects of uncertainties and modeling errors. The concept of SMC has received much attention in the past few decades. Utkin [5] first proposed the concept of sliding mode control as an extension of the Variable Structure System (VSS) controller and showed that a sliding mode could be achieved by changing the controller structure. In a sliding mode controller, the system state trajectory is forced to move along a chosen stable manifold, called the sliding manifold, in the state space. The sliding manifold is always chosen in such a way that it itself guarantees system

stability once the control restrictions are achieved. Young *et al.* [6] presented a guide for control engineers to design different sliding mode controllers.

A sliding mode controller is composed of two parts; the first includes the estimation term to approximate the system dynamics (linear or nonlinear) and the second part consists of a robust compensator which deals with model uncertainties and disturbances to ensure stability. The stability of the sliding mode controller is defined by Lyapunov's second theorem. The robust compensator usually consists of an upper bounding of the system uncertainty with a discontinuous mathematic function, such as a sign function or a saturation function. The control input for the sliding mode controller can be mathematically described as

$$\overline{u} = -\lambda \dot{x} - \hat{f}\left(x, \dot{x}\right) - \left(F + \eta\right) \mathrm{sgn}\left(s\right), \tag{3-1}$$

$$s\left(t\right) = \lambda x\left(t\right) + \dot{x}\left(t\right), \quad \lambda > 0, \tag{3-2}$$

where λ is a positive constant, η is the adjustable parameter of arrival condition, $\hat{f}\left(x, \dot{x}\right)$ represents the dynamics of any nonlinear system, F is the upper limit of external excitation, and s is the sliding surface variable.

Sliding mode controllers can be designed in a systematic approach to the problem of maintaining stability and dealing with model inaccuracies and uncertainties to provide a consistent performance. This is the reason that sliding mode controllers are employed in many industrial applications [7]. A basic theory is given for the derivation of sliding mode control law to explain the basic aspects of the nonlinear controller design from Slotine *et al.* [7].

3.1.1 Basic Theory

Consider a second-order system,

$$\ddot{x}(t) = f\left(x(t), \dot{x}(t)\right) + u(t), \tag{3-3}$$

where $u(t)$ is the control input, $x(t)$ is the output of interest and $f\left(x(t), \dot{x}(t)\right)$ are the unknown dynamics of the system. The unknown dynamics of the system can be estimated by $\hat{f}\left(x(t), \dot{x}(t)\right)$ which can be bounded by some known function $F\left(x(t), \dot{x}(t)\right)$:

$$\left|\hat{f}\left(x(t), \dot{x}(t)\right) - f\left(x(t), \dot{x}(t)\right)\right| \le F\left(x(t), \dot{x}(t)\right), \tag{3-4}$$

In order to have the system track $x(t) \equiv x_d(t)$, the sliding surface can be defined as $s(t) = 0$, namely

$$s(t) = \left(\frac{d}{dt} + \lambda\right)\tilde{x}(t) \quad \lambda > 0, \tag{3-5}$$

where $\tilde{x}(t) = x_d(t) - x(t)$ is defined as the error of tracking. λ is chosen to be positive because the solution of Equation (3-5) at $s(t) = 0;$ gives

$$\tilde{x}(t) = \tilde{x}(t_0)e^{\left[-\lambda(t-t_0)\right]}, \tag{3-6}$$

which implies that, for $\lambda > 0$, the system output error $\tilde{x}(t)$ tends exponentially to zero. Now, the system stability can be defined with Lyapunov's second theorem [8], which is

$$s(t)\dot{s}(t) \le 0, \tag{3-7}$$

The control input $u_1(t)$ is then defined as

$$u_1(t) = -k\,\mathrm{sgn}\left(s(t)\right), \tag{3-8}$$

where $\mathrm{sgn}\left(s(t)\right) = \begin{cases} -1 & s(t) > 0 \\ 1 & s(t) < 0 \end{cases}$. This implies that $k > 0$. With large gain k, the switching can ensure the existence of the sliding mode even in the presence of matched

uncertainties and model error [9]. Once the system achieves the sliding manifold, it becomes independent from uncertainties and modeling errors. Then,

$$\dot{s}(t) = \ddot{x}(t) - \ddot{x}_d(t) + \lambda\dot{\tilde{x}}(t). \tag{3-9}$$

From Equation (3-3), the Equation (3-9) can be written as

$$\dot{s}(t) = f\left(x(t), \dot{x}(t)\right) + u(t) - \ddot{x}_d(t) + \lambda\dot{\tilde{x}}(t). \tag{3-10}$$

The best approximation for the control law $\hat{u}(t)$, when $\dot{s}(t) = 0$, is

$$\hat{u}(t) = -\hat{f}\left(x(t), \dot{x}(t)\right) + \ddot{x}_d(t) - \lambda\dot{\tilde{x}}(t). \tag{3-11}$$

Now after adding the Equation (3-8) and Equation (3-11), the control law can be derived as

$$u(t) = \hat{u}(t) - u_1(t) = -\hat{f}\left(x(t), \dot{x}(t)\right) + \ddot{x}_d(t) - \lambda\dot{\tilde{x}}(t) - k\,\mathrm{sgn}\left(s(t)\right). \tag{3-12}$$

The Equation (3-12) can be written as

$$\dot{s}(t) = f\left(x(t), \dot{x}(t)\right) - \hat{f}\left(x(t), \dot{x}(t)\right) - k\,\mathrm{sgn}\left(s(t)\right). \tag{3-13}$$

Now, stability of the sliding mode control law can be defined by Lyapunov's function

$$\frac{1}{2}\frac{d}{dt}s^2(t) = \dot{s}(t).s(t) = \left[f\left(x(t), \dot{x}(t)\right) - \hat{f}\left(x(t), \dot{x}(t)\right) - k\,\mathrm{sgn}\left(s(t)\right)\right]s(t), \tag{3-14}$$

$$\frac{1}{2}\frac{d}{dt}s^2(t) = \left[\left(f\left(x(t), \dot{x}(t)\right) - \hat{f}\left(x(t), \dot{x}(t)\right)\right)s(t) - k\left|s(t)\right|\right]. \tag{3-15}$$

Now, letting

$$k = F + \eta, \tag{3-16}$$

from Equation (3-4), the stability condition can further be derived as

$$\frac{1}{2}\frac{d}{dt}s^2(t) \le -\eta\left|s(t)\right|. \tag{3-17}$$

Now, from the control law in Equation (3-12), it can be seen that the sliding mode control law does not depend upon the system model parameters such as $f\left(x(t),\dot{x}(t)\right)$ or system states $\left(x(t),\dot{x}(t)\right)$. Thus, it can be stated that the sliding mode controller is able to deal with system uncertainties due to modeling errors or external disturbances.

The above derivation of the sliding mode control law shows that sliding mode control is very robust to system modeling error and other uncertainties. This advantage has made the sliding mode control algorithm very popular in many applications. Many researchers are using this approach in different research and commercial applications. A literature review of the development of sliding mode controller is given in the following section.

3.2 Literature Review

For the past few decades, the sliding mode controller has attracted the interests of control system engineers all over the world due to their advantages of simplicity, robustness [10], independence from system modeled uncertainties and ability for disturbance rejection. Sliding mode control was introduced in the early 1940's and after the 1970's it became one of the most promising robust control strategies [11]. The sliding mode technique is currently being used in tracking, observer design, identification, stabilization and other control problems. Many modifications to the original sliding mode concept have been proposed and practically implemented [12]. The sliding mode controller has even been implemented for stochastic processes [13, 14]. Young *et al.* provided a guide to control engineers to understand the many different aspects of sliding mode control [15]. In their paper, different types of sliding mode controllers and their possible implementation techniques were discussed in detail.

Since its introduction, the sliding mode control approach has been used in many different applications involving different strategies. Wang *et al.* proposed a smooth sliding mode controller and filter based on state feedback. The proposed controller used model reference states for the control law [16]. Hsu *et al.* proposed a model referenced output feedback based sliding mode controller for multivariable nonlinear systems. A model reference adaptive control is employed for control parameterization with unmatched disturbances [17]. Chang developed an output feedback based sliding mode controller by using H_∞ theory with mismatched disturbances [18]. Sivaramakrishnan *et al.* developed a sliding mode controller for unstable first order systems with time delay. They compared the robustness of the controller with a PID controller by checking the delay-time constant. Shieh *et al.* [19] proposed a robust sliding mode control approach for magnetic levitation systems. In their approach, integral sliding mode control with a robust optimal approach was developed to achieve high performance in position tracking. Li *et al.* [20] implemented a PD-sliding mode hybrid controller to control the speed of a permanent magnet synchronous motor robustly.

You *et al.* implemented a sliding mode controller based on genetic algorithms. The genetic algorithm uses partial state feedback to model uncertainties and external disturbances and to give optimal gains for the control law. A robust observer was designed for the state and perturbation of the Stewart platform [21]. Mohammadi developed a flexible neuro-fuzzy based sliding mode controller for magnetic levitation systems [22]. The neuro-fuzzy approach is used to eliminate the Jacobean of the plant.

Many complex hybrid sliding mode controller structures also have been proposed in association with other techniques, such as adaptive control techniques and

fuzzy control techniques [23-28]. These techniques ensure asymptotical stability and the reduction of chattering. However, most of these hybrid controllers require complex implementation algorithms.

The sliding mode controller is considered to be an effective technique for the control of systems with uncertainties. It is always required that these system uncertainties should be matched with sliding mode control. Researchers are developing sliding mode control approaches to deal with unmatched system uncertainties. Chan *et al.* proposed a sliding mode controller for linear systems with unmatched uncertainties [29]. Choi developed a sliding mode controller based on LMI approach. Based on LMIs, an explicit formula is given which guarantees the stability of the system with unmatched uncertainties [30]. Levant and his group studied and proposed higher order sliding mode controllers with finite time convergence [31-33]. They proved that higher order sliding mode controllers provide higher accuracy when properly used and reduced the chattering effect. In their approach, they tried to reduce the parameter estimation error by a proposed algorithm to produce an infinite number of valid parameters sets from a given one [31].

Due to advances in embedded systems, digital implementation of sliding mode control has garnered great attention. Controller implementation is generally done with the control gain designed to be constant over a single sampling instant. Young *et al.* discussed a sampled data based sliding mode controller for linear time invariant systems with uncertainties and external disturbances [15]. Bartoloni *et al.* proposed a digital second order sliding mode controller scheme. In their approach, it was shown that the direct discretization of continuous time control law guarantees the finite time attainment

of a motion in the sliding manifold; then an iterative learning procedure kept the states in the sliding manifold asymptotically [34]. Digital implementation of a sliding mode controller for a nonlinear system with time delay has been reported [35]. Yu *et al.* provide a design methodology based on the model reference approach for the discrete sliding mode controller [36].

The sliding mode control approach has also been employed in optimal control design by many researchers. A literature review about optimal sliding mode control and chattering phenomenon is given in the following sections.

3.2.1 Optimal Sliding Mode Controller

It has been shown in analysis of an optimal control problem with restricted control that the optimal trajectory enters sliding mode for a finite time provided that the control horizon is sufficiently large [37]. Recent developments in mathematical tools have enabled engineers to envision practical implementation of many applications in the field of robotics and mechatronics, high precision aerospace engineering, network-based control and signal processing, fault detection, bioengineering, optimally scheduled logistics and many industrial applications [37].

Young *et al.* introduced a robust sliding mode control design method to solve linear optimal control problems with fixed terminal time and fixed terminal constraints [38]. Lu *et al.* has introduced a simplex sliding mode control for nonlinear uncertain systems [39]. In their approach, they used chaos optimization to calculate the sliding manifold to speed-up the convergence and to reduce chattering. Dinuzzo *et al.* developed a higher order sliding mode controller by robust generalization of Fuller's problem [40]. The high order sliding control approach was designed to provide optimal finite time

reaching of the sliding manifold. Sakamoto developed an optimal sliding mode control approach by adding a neural network based optimal control problem [41]. Pukdeboon and Zinober applied the Lyapunov function based optimal sliding mode controllers to attitude tracking of a spacecraft [42]. The integral sliding mode control is applied to combine the sliding mode with optimal control.

Xu *et al.* [9] proposed an optimal sliding mode controller to solve the infinite time optimal control problem. Xu used an LQR approach to calculate the optimal gain for the sliding mode controller and to deal with uncertainties stochastically. Laghrouche *et al.* [43] proposed another higher order sliding mode control based on an optimal LQR approach. Edwards proposed a sliding mode controller using linear matrix inequalities using convex optimization problems [44].

Nikkah *et al.* [45] proposed a novel method based on nonlinear predictive control to design optimal linear sliding surfaces for control of under-actuated systems. In this method, the proposed sliding surface is a combination of the classic linear surface and an adaptive time varying linear component. In their approach, even if optimization of the system is not feasible, the controller has to be implemented, making this approach a bit cumbersome. On the other hand, Niu *et al.* [46] proposed an improved sliding mode control algorithm for discrete time systems. They proposed a new reaching law for the sliding surface. There are some conditions given in the paper, which must be satisfied for the reaching law.

Azhmyakov proposed a theoretic framework for general optimal problem associated with sliding mode controllers [47]. The sliding manifold is assumed as a special constraint to the main optimization problem. Based on these constraints, some

approximation schemes are discussed which are numerically stable and can be applied to many different applications.

From the above literature review of the optimal sliding mode controller, it was found that many researchers have proposed optimal sliding mode approaches, however, most of these approaches can be treated either suboptimal or partial optimal. A complete optimal sliding mode approach is still sought after. Some strategies use the optimal control law to track the desired sliding surface which is not optimally designed, as the gain associated with the switching function is not optimally calculated. Generally a high scalar gain is associated with the compensator, so that the states of the system quickly converge to the vicinity of the sliding surface. This high gain, if not properly selected, can also cause chattering in the closed loop system.

3.2.2 Chattering Phenomenon

Chattering was discussed as the main obstacle for sliding mode to be one of the most significant modern control theories. Chattering is generally referred to as the high frequency motion of system states around the sliding manifold due to the discontinuous function in sliding mode control law. This discontinuous function may excite the above mentioned high frequency motion due to un-modeled system modes and time delays, etc. The behavior is harmful because it leads to low control accuracy, high heat losses in power circuits, high wear in mechanical moving parts [48]. Many analytical design methods have been proposed to reduce chattering [49, 50].

Researchers have analyzed the chattering phenomenon in detail [11] and proposed a system approach algorithm to analyze this phenomenon quantitatively and qualitatively. There are three main approaches to deal with chattering. The most common approach to

reduce the effects of chattering is to introduce a piecewise linear or smooth approximation of the discontinuous switching function. Song and Mukherjee proposed a continuous smooth tangent hyperbolic function to replace the discontinuous switching functions to alleviate chattering [51]. A comparative study was provided to show the effectiveness of the hyperbolic function compared with bang-bang and saturation based compensators. To show the effectiveness of the smooth robust compensator, sliding mode control was implemented on a smart flexible beam [52]. The experimental results showed that the tangent hyperbolic function can be used effectively to replace the high frequency oscillation exciting switching sign function.

The second approach is to use the observer based sliding mode control. With this method, the system states are estimated by an observer since the model imperfections of the observer are smaller than those present in the system. Also, the discontinuous function take only estimated states into account not the actual physical states [15]. It is assumed that the observer error will be reduced to zero asymptotically. However, this approach may lead to the deterioration of robustness of the controller due to a mismatch between the observer and plant dynamics [11]. The third approach is to use higher order sliding manifolds. This approach enables finite time convergence to zero of not only the so-called sliding variable but its derivative also. This approach has been very attractive to researchers for the past few years [11, 30-34, 40]. Mathematically, chattering can be eliminated from the system using this approach. However, no model can estimate the dynamics of a system exactly; chattering cannot be eliminated practically but can be greatly reduced [11] and the use of smooth robust compensators is the most preferred way to deal with the chattering phenomenon due to its very simple implementation. In

this dissertation, a matrix/scalar sign function is used to calculate the control gains of the proposed optimal sliding mode control. A brief introduction of this function is given in following section.

3.2.3 Introduction to Matrix Sign Function

The matrix sign function can be described as an extension of the scalar sign function considering the scalar sign function as a special case of a 1×1 matrix. The conventional scalar signum function can be defined over the complex plane minus the imaginary axis [53] as

$$\operatorname{sgn}(z)=\begin{cases}1 & \text{if } \operatorname{Re}(z)>0\\ \textit{undefined} & \operatorname{Re}(z)=0\\ -1 & \text{if } \operatorname{Re}(z)<0\end{cases}, \tag{3-18}$$

where $z\in C^{0}$ (i.e., $C^{+}\cup C^{-}$), and C^{-},C^{+} and C^{0}, respectively, denote the open right-half complex pane, the open left-half complex plane and the imaginary axis.

Shieh *et al.* [54] developed an alternative form to represent the scalar sign function, which is as follows:

$$sign(z)=\begin{cases}\dfrac{g(z)}{z} & \text{if } \operatorname{Re}(z)>0\\ \textit{undefined} & \operatorname{Re}(z)=0\\ -\dfrac{g(z)}{z} & \text{if } \operatorname{Re}(z)<0\end{cases}, \tag{3-19}$$

where $g(z)=\sqrt{z^{2}}$ is the principal square-root of the complex value z^{2} and can be expressed as

$$g(z)=\begin{cases}z & \text{if } \operatorname{Re}(z)>0\\ -z & \text{if } \operatorname{Re}(z)<0\end{cases}. \tag{3-20}$$

Again, Re*(z)* = 0 is not included in the definition. Shieh *et al.* [54] had shown that *g(z)* can be expressed by the continued fraction expansion form below:

$$g(z) = \sqrt{z^2} = 1 + \frac{z^2 - 1}{2 + \frac{z^2 - 1}{2 + \cdots}}, \tag{3-21}$$

where $z \in C^+ \cup C^-$. Also, it has been shown that the jth truncation of the continued fraction expansion of *g(z)* can be written as

$$g_j(z) = z\frac{(1+z)^j - (1-z)^j}{(1+z)^j + (1-z)^j}, \text{ for j = 1, 2…} \tag{3-22}$$

Substituting Equation (3-22) into Equation (3-19) gives an exact expression of scalar sign function as

$$sign(z) = \frac{g(z)}{z} = \lim_{j\to\infty} \frac{g_j(z)}{z} = \lim_{j\to\infty} sign_j(z), \tag{3-23}$$

$$sign_j(z) \approx \frac{(1+z)^j - (1-z)^j}{(1+z)^j + (1-z)^j}, \tag{3-24}$$

and $sign_j(z)$ is the jth-order approximation of the scalar sign function in Equation (3-18). $sign_j(z)$ can be then expressed as

$$sign_j(z) = \begin{cases} +1, \text{ for } z > 0 \text{ and } j \to \infty \\ 0, \quad \text{for } z = 0 \\ -1, \text{ for } z < 0 \text{ and } j \to \infty \end{cases}. \tag{3-25}$$

As shown above, $sign_j(z)$ is a continuous and differentiable function that includes $z = 0$ in the definition. Since the matrix sign function can be written as

$$sign_j(\mathbf{Z}) = \left((\mathbf{I}+\mathbf{Z})^j + (\mathbf{I}-\mathbf{Z})^j\right)^{-1}\left((\mathbf{I}+\mathbf{Z})^j - (\mathbf{I}-\mathbf{Z})^j\right), \tag{3-26}$$

where $\mathbf{Z} \in \mathbf{R}^{n\times n}$ and $\mathbf{I} \in \mathbf{R}^{n\times n}$ is the identity matrix.

As shown in Equation (3-24) and Equation (3-25), when $j=\infty$, $sign_j(z)$ is exactly the sign function $sign(z)$. Hence, for securing satisfactory accuracy, j in Equation (3-24) is naturally preferred to be a large number with which a precise approximation can be efficiently accomplished. This fact can be found from Figure 3-1-Figure 3-5. When j becomes bigger, the accuracy improves in the scalar sign function. In the following figures, the proposed scalar sign function approach is explained by plotting the scalar sign function using even and odd values of truncation parameter j.

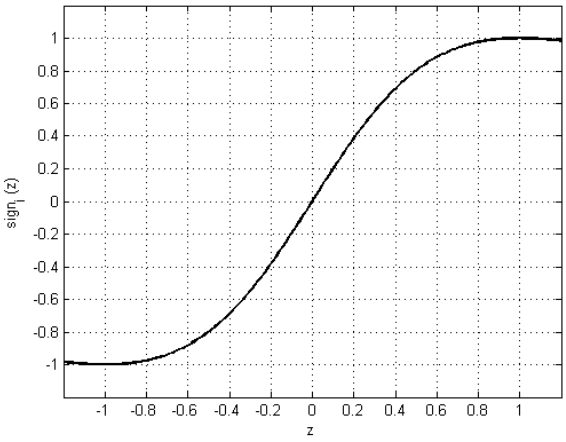

Figure 3-1 Signum function with $j = 2$

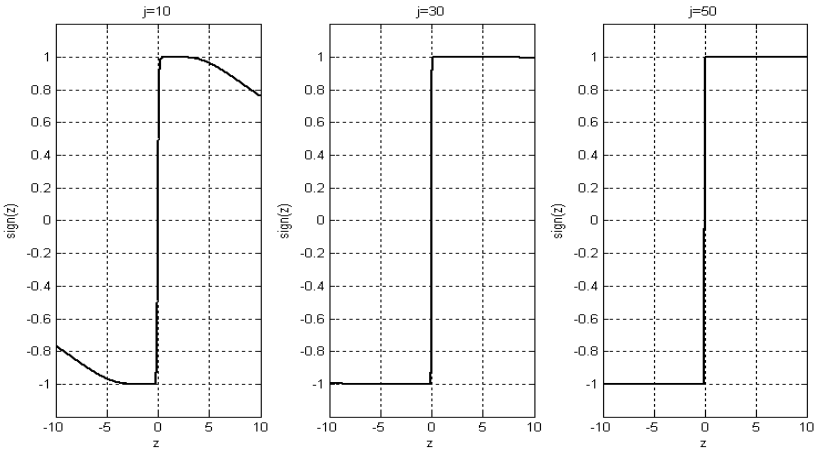

Figure 3-2 Scalar Sign Function Response with high z and even j

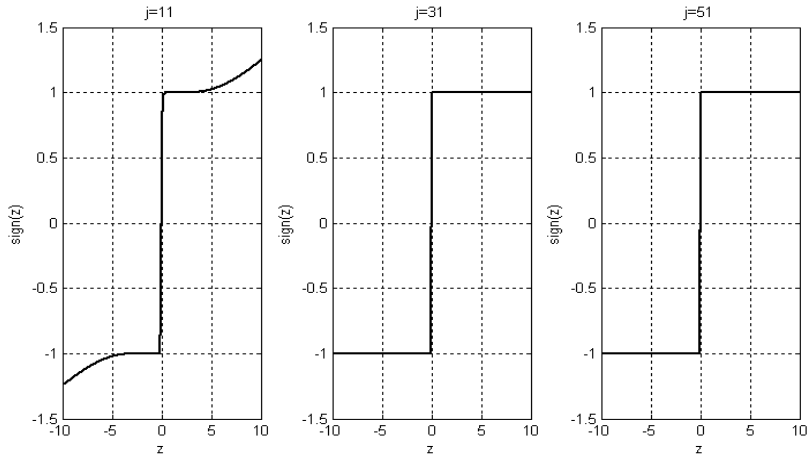

Figure 3-3 Scalar Sign Function Response with high z and odd j

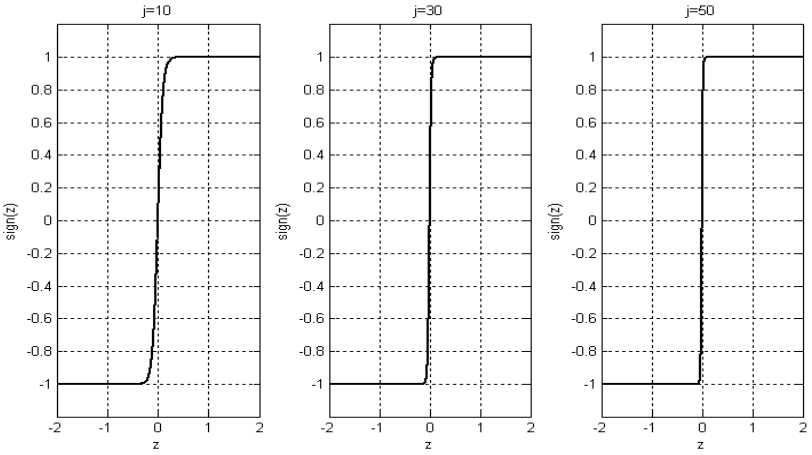

Figure 3-4 Scalar Sign Function Response for Low z and even j

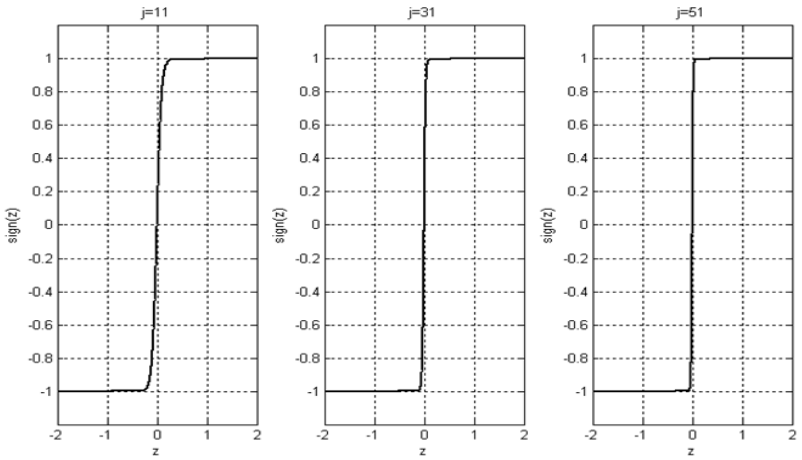

Figure 3-5 Scalar Sign Function Response for Low z and odd j

It can be seen in these figures that for an even number of j, the value of the scalar sign function always remains within the limits of $[-1,1]$. However, with an odd number of j, if the input z is large, the scalar sign function can be $-1 \le sign_j(z) \ge 1$. Therefore, it is always recommended to use even value of j. In the case of both the value of z and index j becoming significantly large, the proposed sign function can create numerical difficulty. To overcome this difficulty, a recursive algorithm was proposed by Shieh *et al.* [54] which is simply represented using

$$sign_j(z) = sign_{j_n}[sign_{j_{n-1}}[...[sign_{j_1}(z)]]], \tag{3-27}$$

where $j = \prod_{m=1}^{n} j_m$, and j_m is a positive integer. The simple form discussed in Equation (3-25) is used instead of the recursive form in Equation (3-27) to approximate the scalar sign function.

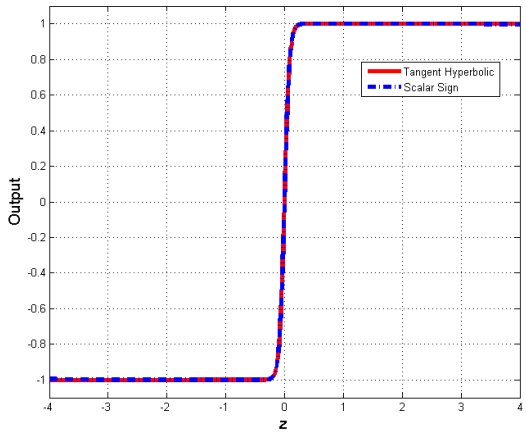

Figure 3-6 Comparison of tangent hyperbolic and scalar sign function

In the literature review of solution to the chattering problem of sliding mode controller, a tangent hyperbolic function is proposed by Song *et al.* [51]. A comparative study of tangent hyperbolic function with discontinuous sign function and saturated type compensator has been effectively done. It was concluded that the tangent hyperbolic

function can replace the discontinuous sign function as a smooth continuous switching function. In Figure 3-6, the comparison between outputs of tangent hyperbolic and scalar sign function (j=12) has been shown. It can be seen from Figure 3-6 that scalar sign function and tangent hyperbolic function both tend to mimic the signum function and can replace the discontinuous function with a smoother continuous function. It was found that the sign function can also be termed as a linear approximation of tangent hyperbolic function, where tangent hyperbolic function is

$$\tanh(jz) = \frac{e^{jz} - e^{-jz}}{e^{jz} + e^{-jz}}. \tag{3-28}$$

After truncation of higher order terms, e^z can be written as $e^z \approx \frac{1}{1-z}$. This implies that

$$\tanh(jz) \approx \frac{\left(\frac{1}{1-z}\right)^j - \left(\frac{1}{1+z}\right)^j}{\left(\frac{1}{1-z}\right)^j + \left(\frac{1}{1+z}\right)^j} = \frac{(1+z)^j - (1-z)^j}{(1+z)^j + (1-z)^j} = sign_j(z). \tag{3-29}$$

As shown in Figure 3-2 and Figure 3-3, it is shown that for the larger values of z the scalar sign function approach does not saturate at +1 or -1. This can be dealt with by using a recursive sign function approach. Compared to the traditional expression of the signum function, the proposed continuous sign function approach can replace the discontinuous switching function to alleviate chattering. The above mentioned sign function can also be used to calculate the stable eigenvectors of the system to design the sliding surface.

The stability of sign function has been analyzed by various researchers. Attarzadeh [55] and Mattheys [56] explains the stability of matrix sign function for linear time-invariant systems. Tsai *et al.* [57] provided a fast and stable algorithm for

computing the principal nth root of a complex matrix using matrix sign function. In their paper, the authors proved that the matrix sign function is numerically stable for small perturbations or errors. Tsai *et al.* successfully applied the numerically stable matrix sign function to continuous to discrete model conversion for the system with a singular system matrix [58].

From the above literature review, it can be seen that the sliding mode control is a very well researched and very famous approach. It is attracting many researchers and engineers due to its advantages of rejecting noise and uncertainties, simplicity and good performance. Researchers are still employing and developing new ways to implement or modify the sliding mode controller for various industrial applications as described in the following subsection.

3.2.4 Application of Sliding Mode Controller

The sliding mode controller has been used in many industrial applications of electromechanical systems such as controls of electric drives, AC/DC motors, power converters and advanced robotics [59]. Sliding mode control has been used in the automotive industry for vehicle suspension control, steering control, and tracking control. Fei *et al.* [60] proposed an adaptive sliding mode controller for semi-active vehicle suspension systems.

Lee *et al.* [61] proposed a controller for torque and pitch control of permanent magnet synchronous generator (PMSG) wind power systems based on the sliding mode approach. Their simulation results suggest that the sliding mode control approach is effective in controlling the wind turbine parameters for better performance. Afkham and

Ehteram [62] recently used the sliding mode control approach to control the displacement of buildings under earthquake excitation.

The sliding mode control approach has its application in the aerospace industry also. Pukdeboon [63] proposed an optimal sliding mode controller to control the attitude of a flexible spacecraft. An integral sliding mode controller was applied to combine the first-order sliding mode with optimal control. This controller was used to control attitude maneuvers with external disturbances.

SMC approaches have found their application in chemical processing plants also. Camacho and Rojas [64] proposed that the sliding mode control approach can be used for a nonlinear chemical process. The proposed sliding mode controller was successfully tested for different systems such as MIMO systems and minimum and non-minimum systems with different experimental conditions (i.e. disturbances, noise and modeling errors). The simulation results for the proposed approach were very encouraging. Camacho *et al.* developed an integral model sliding mode controller to approximate the parameters of a nonlinear chemical process. The blend of internal model control and sliding mode control concepts have been used to design the controller [65]. Chen *et al.* proposed a sliding mode controller for the non-linear regulation control of chemical processes, which integrates an identified second-order plus dead-time (SOPDT) model, an optimal sliding surface and a delay-ahead predictor [66]. Demirci *et al.* proposed a sliding mode controller for underwater vehicles. In their approach, the sliding mode controller is re-configured based on disturbances information from the shallow water conditions [67].

Takahashi *et al.* [68] have proposed the application of sliding mode controller to high speed optical disc drives. In their approach they dealt with the system having high numerical aperture and a narrow track, thus requiring high performance from the servo system. Their experimental results confirmed the effectiveness of the sliding mode controller to provide high accuracy, accessibility and defect resistance.

Because of their immunity towards system uncertainties due to modeling inaccuracies, sliding mode control algorithms have been used extensively by researchers in vibration control of flexible structures. Song *et al.* [52] implemented a sliding mode based controller to suppress the vibrations of a flexible beam. In their approach, a robust smoother tangent hyperbolic function is used to replace the discontinuous switching function to alleviate the chattering effect. Later, Gu *et al.* [69] implemented a fuzzy logic based adaptive sliding mode controller for controlling the vibration of flexible aerospace structures. In their approach, the fuzzy logic based smooth compensator is used to alleviate chattering. Li *et al.* [70] proposed and successfully implemented a dynamic neural network based adaptive fuzzy sliding mode approach for nonlinear structural vibration suppression.

In this chapter, a literature review of sliding mode control development over the years and their applications has been discussed in detail. It can be concluded that even though many researchers have proposed robustly stable optimal sliding mode approaches, a sliding mode approach which can deal with optimality issues and the chattering problem is still desired. Also, few system have been addressed which are optimal which explains the stability of the highly uncertain systems.

This dissertation reports a robust optimal sliding mode controller using the continuous sign function approach which will fulfill the requirement of being a completely optimal sliding mode approach thus guaranteeing the stability of the system for bounded matched and unmatched uncertainties. The simulation and experimental results are shown to prove the effectiveness of the proposed optimal approach.

The literature review also found that the sliding mode controller has been used in active vibration control techniques for some time. However, for passive system design this approach has never been heard of. In this dissertation, the classic sliding mode control law is used to guide the design of a passive damping device, called the Pounding Tuned Mass Damper with a viscoelastic layer, to suppress the vibrations of a pipe structure used in the oil and gas industry.

Chapter 4. Pounding Tuned Mass Damper- An Innovative Realization of Sliding Mode Control using a Passive Approach

Passive devices are the oldest and the most preferred approaches to control the vibrations of structures. A passive control system consists of a device or set of devices, which affects the system damping or stiffness to control the undesired vibrations. Different types of passive control systems have been devised and their mathematical models have been developed and discussed. The mathematical model of any system is very important to understand the concept behind the working of the system. It also helps researchers to optimally design the control system. In this chapter, mathematical modeling of a novel passive vibration control device, called Pounding Tuned Mass Damper (PTMD) is studied. The passive force generated by PTMD is analyzed through classical active sliding mode control law. An analogy is provided between the force generated by the PTMD to control the vibrations and sliding mode control law.

4.1 Introduction

Commercial pipes structures, such as jumpers, and risers used in the on-shore and off-shore oil and gas industry, are often subjected to different environmental conditions, such as internal and external temperature variations, earthquakes, and pulsating internal fluid flow. These structures have low natural frequencies and low structural damping due to their flexible geometry. Such geometry causes these to be susceptible to Vortex Induced Vibrations (VIV) in areas with a significant excitation source such as a wind or water current. The combined effect of the above factors can create excessive and/or harmful vibrations in which VIV plays a major role. These VIVs can trigger fatigue in the structure due to vibrations and potentially lead to failure of the pipe structure.

There are a number of ways to control vibrations of these large size structures through active, semi active and passive control devices. Each individual approach has its own advantages and limitations. Historically, passive control devices are the first ones to be implemented. The biggest advantage of passive control systems is that they do not require an external power source.

A passive control system can be defined as a mechanical system embedded or attached to a structure which is designed to modify the structural damping or stiffness so that this mechanical device can generate a control force to suppress the vibrations without requiring external power. This mechanical device can consist of a single device or set of devices [71-73]. Many different examples of passive control systems have been developed and implemented for control of structural vibrations e.g. Tuned Mass Dampers (TMD), tuned liquid dampers, tuned sloshing dampers, pendulum dampers and base isolation systems [73, 74].

Many new concepts of active control are being developed these days for many types of applications. These new concepts include a number of control strategies/algorithms such as modern controls, sliding mode control, fuzzy logic based control and adaptive control. These control techniques are very flexible and tunable, and, can be designed to be robust and adaptable to uncertainties. These control strategies have been implemented also for structural vibration control, but these active control systems require large external power which makes them almost impractical for structural vibration control [72, 73, 75-78]. In order to have advantages for both types of systems, passive and active, a promising technique is used these days by researchers and engineers. This is called the semi-active technique [75-79]. Researchers have

implemented semi-active controllers for structural vibration in many applications using smart materials [80-82].

Smart materials always play an important part in structural vibration control irrespective of the type of control systems. Many smart materials in the form of sensor or actuators are being used for vibration suppression e.g. piezoceramics materials are used to control the vibrations of flexible aeronautical structures [83], magneto-rheological dampers are used for semi-active vibration control of automotive and civil structures [80]. Many researchers are working on controlling the vibration of structures by various means. Some are using passive techniques to control the vibration in the system by using damping materials. The properties of some commercially available damping materials and associated damping techniques have been studied by Nashif [84]. Various materials are used commercially to increase the damping of the structures, such as MR fluids and visco-elastic tapes, etc. Viscoelastic materials are one of the oldest in the field of structural vibration and noise control and have been used in many civil structures around the world for vibration controls for a very long time [85-87]. Soong and Dargush have provided a detailed study of passive energy dissipation and active control [88].

Researchers, scientists and engineers have studied and implemented various passive vibration control devices and active algorithms for structural vibrations. They even combined both approaches for performance, flexibility and robustness enhancement. Mathematical models have been discussed and analyzed for passive devices for their better design. Franchek *et al.* [89] have discussed the design of an adaptive passive vibration control system. However, using a passive device and strategies to design an active control system is almost left untouched. In this chapter, the control force generated

by the PTMD, a passive device, is compared with active sliding mode control law. Once the relation between the passive force and active control law is established, it will be very easy for engineers to tune the passive system according to structure.

The sliding mode control, which was introduced by Utkin [5], is very robust to model uncertainty and have good disturbance rejection properties. Sliding mode controller strategy has since evolved with time. Researchers and engineers all over the world have proposed and introduced this strategy combined with other modern control techniques for different applications. This chapter explains the analogy between the force generated by PTMD to an active sliding mode control approach. The physical design of PTMD is described in section 2. This chapter presents the simulation and experimental results of a jumper structure setup at the Structures Lab in the Civil Engineering Department at the University of Houston. The simulation results of vibration suppression with analogical sliding mode control law for the structure verify the proposed approach.

4.2 Description of System

In simple terms, a pounding tuned mass damper is a constrained TMD integrated with viscoelastic damping material. The damper's movement is limited by a limiter or other devices attached to the structure. The vibration amplitude of the structure is reduced by first transferring momentum between the structure and the added mass of the PTMD; then the consumed mechanical energy is dissipated as heat energy when impact occurs between the constrained mass and the viscoelastic damping material. A ring with viscoelastic (VE) materials is used as a delimiter to limit the vibration of the mass damper and to provide damping to the structure. The effectiveness of the PTMD depends on the dynamic characteristics of the mass damper component, such as the stroke, the

amount of added mass, and the damping properties of the damping VE material. Figure 4-1 illustrates the structure of a pounding tuned mass damper.

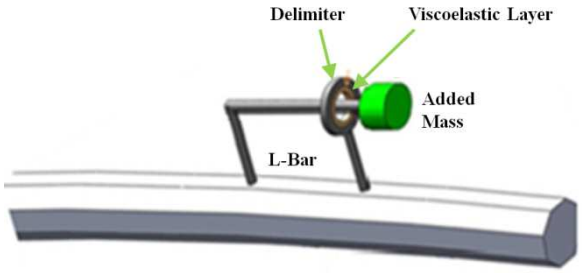

Figure 4-1 Pounding Tuned Mass Damper

4.3 Experimental Setup

An experimental model of a jumper was set up in the Structural Research Laboratory in Civil Engineering at UH, as shown in Figure 4-2-Figure 4-4. The proposed damping system consisted of an L-shaped circular rod and a specially designed damping element. The L-shaped rod was built using two sections of 5/8 inch steel rods: 12 inch vertical and 24 inch horizontal. The diameter of the rod was 0.625 inch.

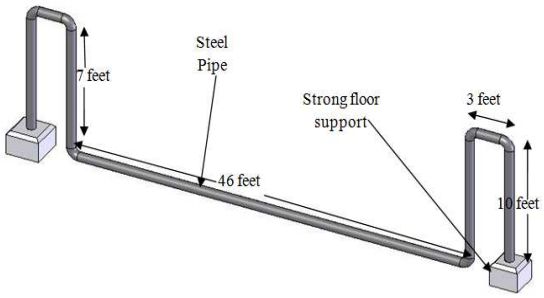

Figure 4-2 Experimental Jumper Setup

Figure 4-3 Jumper Model in Structure Lab at University of Houston, TX

Figure 4-4 PTMD Device on Jumper Model

As shown in Figure 4-4 the damping element consisted of a delimiter covered by a viscoelastic material. The constraints provided by the delimiter served the following two purposes: the first is to limit the motion of the TMD and the second is to dissipate the energy transmitted from the original structure to the TMD during impact. To simulate the effect of VIV, vibrations of the structure were induced manually by providing the harmonic force. The vibration response was measured by an accelerometer from an Analog Device (203EB) attached in the center section of the jumper model.

4.4 Modeling of PTMD as Passive Sliding Mode Controller

For a typical pipe structure with PTMD, the equation of motion can be described as

$$m\ddot{x}(t)+c\dot{x}(t)+kx(t)=c_a\dot{z}(t)+k_a z(t)+f(t), \tag{4-1}$$

$$m_a\ddot{z}(t)+c_a\dot{z}(t)+k_a z(t)+f_v(t)=-m_a\ddot{x}(t), \tag{4-2}$$

where m,c,k are mass, coefficient of damping and stiffness of the structure, m_a,c_a,k_a are mass, coefficient of damping and stiffness of the damper, and $x(t),z(t)$ are the displacement of the structure and relative displacement of the damper with respect to the structure. $f(t)$ is the disturbance and $f_v(t)$ is force exhibited by the pounding of damper on the circular ring covered by viscoelastic layer. After taking Laplace transformation of (4-1) and (4-2) assuming zero initial conditions

$$(ms^2+cs+k)X(s)=(c_a s+k_a)Z(s)+F(s), \tag{4-3}$$

and $$\left(m_a s^2 + c_a s + k_a\right) Z(s) + F_v(s) = -m_a s^2 X(s), \tag{4-4}$$

$$\Rightarrow Z(s) = \frac{-m_a s^2}{\left(m_a s^2 + c_a s + k_a\right)} X(s) - \frac{1}{\left(m_a s^2 + c_a s + k_a\right)} F_v(s). \tag{4-5}$$

Now, after putting (4-4) in (4-3)

$$(ms^2 + cs + k) X(s) = \left(c_a s + k_a\right) \begin{pmatrix} \dfrac{-m_a s^2}{\left(m_a s^2 + c_a s + k_a\right)} X(s) \ldots \\ -\dfrac{1}{\left(m_a s^2 + c_a s + k_a\right)} F_v(s) \end{pmatrix} + F(s). \tag{4-6}$$

Equation (4-6) can be rewritten as

$$\begin{aligned} (ms^2 + cs + k) X(s) &= -\left(c_a s + k_a\right) \left(\frac{m_a s^2}{m_a s^2 + c_a s + k_a} \right) X(s) \ldots \\ \ldots &- \left(\frac{c_a s + k_a}{m_a s^2 + c_a s + k_a} \right) F_v(s) + F(s). \end{aligned} \tag{4-7}$$

After taking the inverse Laplace, the Equation (4-7) can be written in time domain as

$$m\ddot{x}(t) + c\dot{x}(t) + kx = -K_p (c_a \dot{x}(t) + k_a x(t)) - \beta_p f_v(t) + f(t), \tag{4-8}$$

where $K_p = \left| \dfrac{m_a s^2}{m_a s^2 + c_a s + k_a} \right|_{s=j\omega}$, $\beta_p = \left| \dfrac{c_a s + k_a}{m_a s^2 + c_a s + k_a} \right|_{s=j\omega}$, and ω is the excitation frequency of the structure and damper. All these variables will be of maximum value when the damper is excited at the natural frequency. The viscoelastic pounding force on the system is introduced by putting the motion constraints on the mass damper by adding a circular ring with the viscoelastic layer. Linear and nonlinear force generated by the viscoelastic pounding have been studied and proposed by many researchers [90-93]. In this paper, the nonlinear model given by R. Jankowski [94] is used to explain the force generated by the pounding of PTMD on the viscoelastic layer. The force exhibited by pounding phenomenon can be explained as

$$f_v(t)=\begin{cases} f(\delta,t) & y(t)>r \\ 0 & y(t)<r \end{cases}, \tag{4-9}$$

where $y(t)$ is the absolute displacement of the damper, r is the radius of the circular ring for pounding including the viscoelastic tape thickness, and $f(\delta,t)$ is the viscoelastic pounding force on the structure during the pounding phenomenon and δ is the deformation of the viscoelastic surface during pounding. The pounding force $f(\delta,t)$ during impact between structures [94] is expressed as:

$$f(\delta,t)=\begin{cases} \phi\delta(t)^{3/2}+\xi\dot{\delta}(t) & for \quad \dot{\delta}(t)>0 \\ \phi\delta(t)^{3/2} & for \quad \dot{\delta}(t)<0 \end{cases}, \tag{4-10}$$

where $\dot{\delta}$ denotes the relative velocity between damper and pipe structure, ϕ is the impact stiffness parameter depending on material properties and the geometry of colliding bodies and ξ is the impact damping. The deformation $\delta(t)$ of viscoelastic layer depends upon the displacement $y(t)$ of PTMD; when it hits the viscoelastic layer and the direction of displacement. This means that viscoelastic force $f_v(t)$ can be further redefined as

$$f_v(t)=f(\delta,t)H, \tag{4-11}$$

where H is a function, defined for direction of motion of PTMD. That is

$$H=\begin{cases} 1 & \delta>r \\ -1 & \delta<-r \\ 0 & otherwise \end{cases}, \tag{4-12}$$

where r is the radius of the viscoelastic ring. The positive and negative sign defines the direction of motion of PTMD. The control force by PTMD to control the vibrations of structure can be extracted from Equations (4-8) and (4-11), resulting in

$$f_c(t) = -K_p\left(c_a\dot{x}(t) + k_a x(t)\right) - \beta_p f_v(t). \tag{4-13}$$

From (4-11) and (4-12), the force generated by PTMD to counter the vibrations of structure can be rewritten as

$$f_c(t) = -K_p\left(c_a\dot{x}(t) + k_a x(t)\right) - \beta_p f(\delta, t)H. \tag{4-14}$$

4.4.1 Comparison of PTMD and Sliding Mode Control Law

The sliding mode controller is a robust controller. The sliding mode controller is composed of two parts; the first includes the estimation term to approximate the system dynamics (linear or nonlinear) and the second part consists of a robust compensator which deals with model uncertainties and disturbances to ensure stability. The stability of the sliding mode controller is defined by Lyapunov's second theorem. The robust compensator usually consists of an upper bounding of the system uncertainty with a discontinuous mathematic function, such as a sign function. The control input for the sliding mode controller for vibration suppression can be mathematically described as [52]

$$u(t) = -K_d s(t) - \gamma\,\mathrm{sgn}\left(s(t)\right), \tag{4-15}$$

$$s(t) = c_1 x(t) + \dot{x}(t), \qquad c_1 > 0, \tag{4-16}$$

where $c_1 = \dfrac{k_a}{c_a}$ is a positive constant, γ is the adjustable parameter of arrival condition, and $s(t)$ is the sliding surface variable. The signum function $\mathrm{sgn}()$ in Equation (4-15) is a discontinuous function. Since the modeling of PTMD is supposed to be continuous, the signum function can be replaced with the continuous sign function [95] defined in (3-24) and (3-25).

Also, the output of the signum function is +1 or -1 depending upon the positive or negative sign of the input. However, for practical considerations, the force generated

by this part of control law has to be continuous and converging. In Figure 4-5, the output of scalar sign function is converging with time and the output of the signum function keeps fluctuating between +1 and -1, the continuous scalar sign function is a more logical choice than the discontinuous signum function.

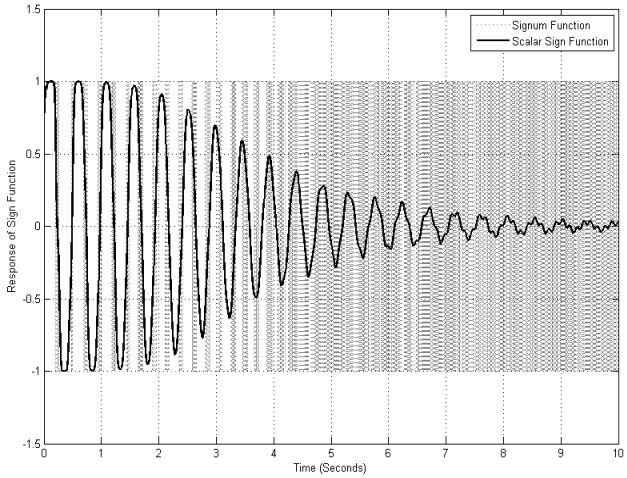

Figure 4-5 Comparison of scalar sign function with signum function

The Equation (4-15) can further be rewritten as

$$u(t) = -K_d\left(c_1 x(t) + \dot{x}(t)\right) - \gamma sign\left(s(t)\right), \tag{4-17}$$

$$\Rightarrow \quad u(t) = -K_d \frac{k_a}{c_a} x(t) - K_d\, \dot{x}(t) - \gamma sign\left(s(t)\right). \tag{4-18}$$

Now, on comparing the forms of Equations (4-14) and (4-18), it is found that the right hand terms of both control forces are analogous to each other.

Also, from both Equations (4-14) and (4-18), it is very clear that the PTMD is controlling the vibrations of the structure by first constraining the motion in to a smaller range under the constraints of the circular viscoelastic layered ring. These dynamics in this constrained area can be defined as the sliding surface of the structure. Once the motion is constrained in to this area, the vibration energy is dissipated by the pounding of the mass damper on the viscoelastic layer, which can be linked to the switching

phenomenon of a sliding mode control to keep the states in the sliding surface. The analogy between both controls forces are shown in Table 4-1.

Table 4-1 Analogy between passive sliding mode controller and PTMD

Passive Sliding Mode Control law	Pounding Tuned Mass Damper control force
$K_d \frac{k_a}{c_a}$	$K_p k_a$
K_d	$K_p c_a$
γ	β_p
$sign(s(t))$	$f(\delta,t)H$

4.5 Comparison of Simulation and Experimental Results

A finite element analysis based mathematical model of the jumper structures explained in an earlier section of the experimental setup was prepared using SAP2000. The jumper model was divided into 11 lump elements. The stiffness matrix was modified to match the real experimental data from the jumper system. The damping matrix of the structure was calculated using the Rayleigh's method. The overall damping ratio of the real system was calculated to be about 0.25%. The natural frequencies of the jumper model were 1.85 Hz for out-plane vibrations and 1.97 Hz for in-plane vibrations. A Simulink model was built to simulate the control of the jumper with sliding mode control law. The parameters for PTMD are given in the following Table 4-2.

Table 4-2 Parameters for PTMD

S. no	Parameters	
1	Mass (m_a)	18.18 Kg
2	Stiffness (k_a)	2325.6 Nm
3	Damping Coefficient (c_a)	83.24 Ns/m

4.5.1 Simulation Results

The following simulations procedures were carried out on a Matlab/Simulink environment to analyze PTMD as a passive sliding mode control algorithm for in-plane (vertical) and out-plane (horizontal) vibrations. The jumper models were simulated for

free in-plane and out-plane vibrations with and without PTMD, where PTMD is modeled as a sliding mode control law. Figure 4-6 shows the comparison of in-plane vibrations of the structure and Figure 4-7 shows the force generated by sliding mode control law to control the in-plane vibrations of structure. It can be seen that that the force limits to control the vibrations are within the practical limits.

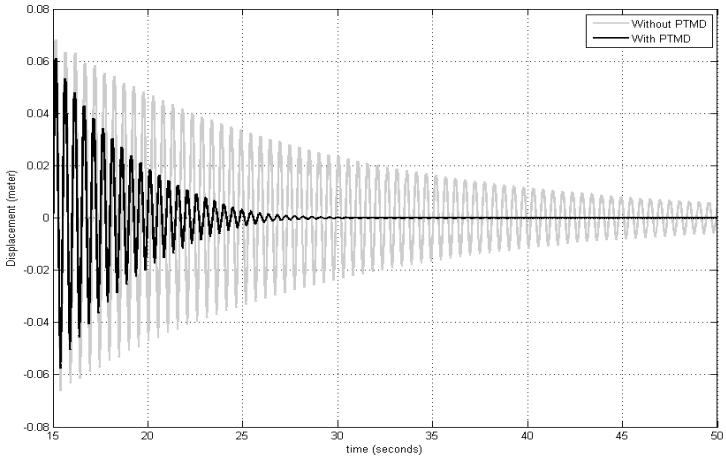

Figure 4-6 Simulated in-plane vibrations of jumper with and without PTMD

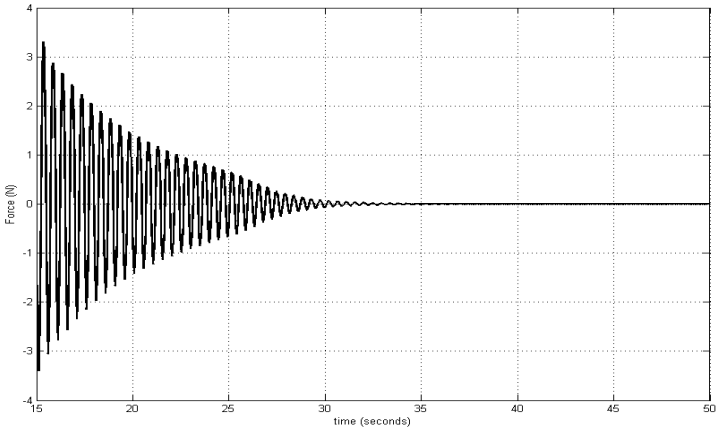

Figure 4-7 Force generated by PTMD for in-plane vibration suppression

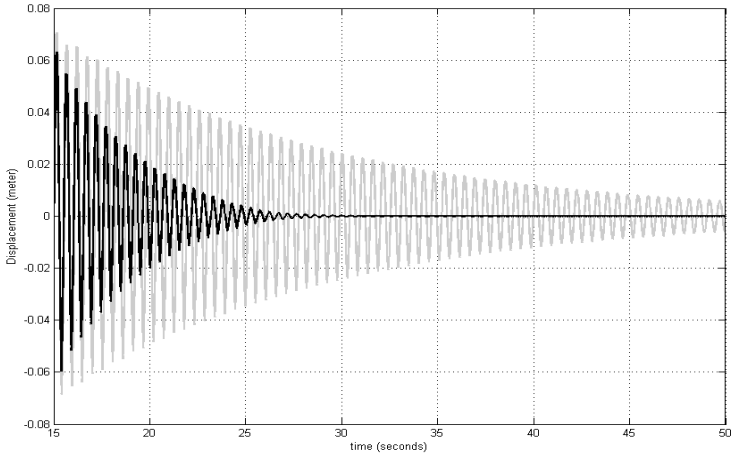

Figure 4-8 Simulated out-plane vibrations of jumper with and without PTMD

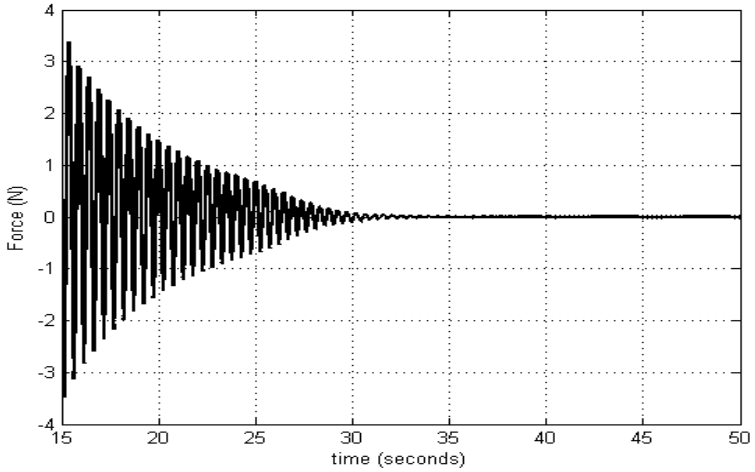

Figure 4-9 Force generated by PTMD for out-plane vibration suppression

Figure 4-8 and Figure 4-9 show the comparison of out-plane vibrations of structure with and without PTMD as passive sliding mode controller, and, the force generated by PTMD to control the out-plane vibrations of the structure.

4.5.2 Experimental Results

The experimental study was conducted in two stages. In the first stage, free vibrations of the structure were excited in the vertical direction and the response of the system with and without PTMD were recorded. In the second stage, the jumper model was excited in the horizontal direction and then the response of the jumper with and without PTMD was recorded. Since the first few modes are the dominant modes, only the

first two modal vibrations of the structure were targeted for control; thus a noise filter of 20 Hz cut off frequency was used.

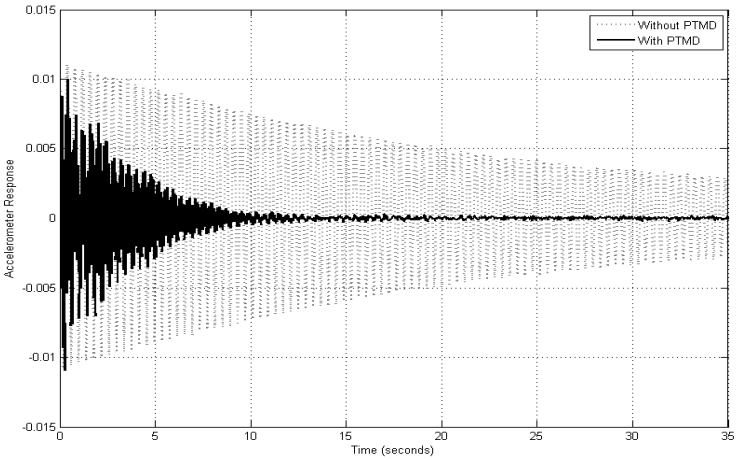

Figure 4-10 In-plane vibrations of with and without control

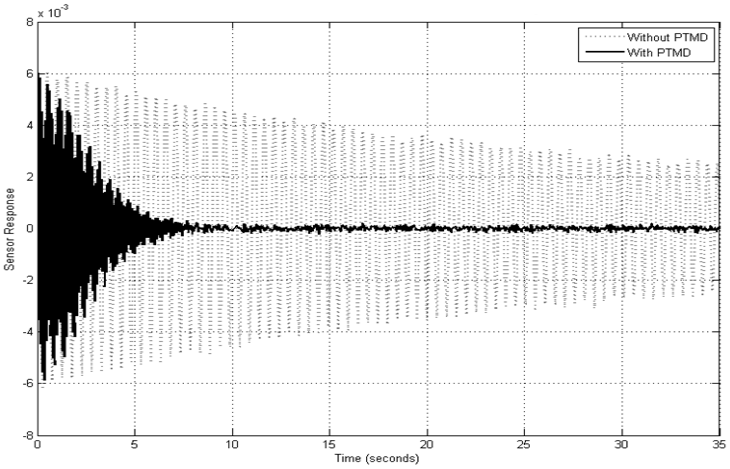

Figure 4-11 Horizontal vibrations of with and without

The damping ratio (ς) of the structure during horizontal and vertical vibrations were calculated using the log decrement formula as shown in Equation (4-19),

$$\varsigma = \frac{\frac{1}{n-1}\left(\ln\frac{x_1}{x_2}\right)}{\sqrt{4\pi^2 + \left[\frac{1}{n-1}\left(\ln\frac{x_1}{x_2}\right)\right]^2}}, \tag{4-19}$$

where n is number of oscillations, x_1 is amplitude of first oscillation and x_n is amplitude of nth oscillation. The damping ratios of structural vibrations in both directions were calculated with PTMD enabled and PTMD disabled. Table 4-3 compares the damping ratios of in-plane and out-plane vibrations of the jumper for three cases; with the simulated PTMD as passive sliding mode controller, with physical PTMD and with PTMD disabled.

Table 4-3 Comparison of damping ratio with and without PTMD

Structural Vibrations	Damping Ratio (without PTMD)	Damping Ratio (PTMD Simulated)	Damping Ratio (PTMD Experiment)
Horizontal vibrations	0.26%	3.08 %	3.33%
Vertical vibrations	0.24%	2.18 %	2.02%

4.6 Conclusion

This chapter presents the realization of pounding tuned mass damper with the classical sliding mode control algorithm. The control force generated by PTMD was derived and the analogy between components of control force of PTMD and sliding mode control law was prepared. The simulation results of the proposed technique are compared with the experimental results. The simulation results support the proposed hypothesis. In conclusion, the vibration suppression of the jumper via PTMD can be comprehended as the sliding mode control law which will help to optimally design the PTMD on a different structure in an analytical way.

Chapter 5. Development of Optimal Sliding Mode Control using Sign Function with LQR approach

A novel optimal sliding mode control approach is proposed in this chapter. The optimal sliding mode control law is designed using the LQR approach and matrix sign function. The stable sliding manifold is designed using the stable eigenvectors of the robustly stable system to ensure the convergence of the states. This chapter includes the development of the new approach and the stability proof. The performance of the proposed approach is evaluated by comparing the simulation results of the optimal approach with that of the conventional system. Later, the proposed controller is implemented to control the multimodal vibrations of a flexible beam. The robustness of the controller is tested by adding a mass uncertainty to the beam.

5.1 Introduction

In this chapter, a new optimal sliding mode control strategy is proposed based on an optimal LQR approach. First, a robustly stable system is designed using the LQR approach by optimally placing the poles of the system in a vertical strip of the left half of the s-plane. The sliding surface will be chosen with stable eigenvectors and the controller designed using scalar and matrix sign functions [96], ensuring the satisfaction of the conditions in [46] and convergence of states to the desired sliding surface. As constrained optimization, the states of the robustly stable system track the desired sliding surface. The desired eigenvectors are calculated using the matrix sign function to avoid the complex eigenvectors of system. The chapter includes the development of an optimal control algorithm incorporating the scalar and matrix sign function method. A stability analysis of the proposed controller is also provided. The developed control algorithm is simulated as

an example and compared with the classical sliding mode control technique [8]. The sign function is used to calculate the eigenvectors which are used to design the stable sliding surface and to replace the signum function in the sliding mode control algorithm.

5.2 Design of the Optimal Sliding Mode Controller using the LQR Approach

The optimal controller is defined as the controller which operates the dynamic system at a minimum cost. The minimum cost is the energy usage to regulate the system for desired results. This energy cost function is defined with a linear quadratic equation involving the system states and the control input known as the Linear Quadratic Regulator (LQR). In this section, an optimal sliding mode controller law is derived using the LQR approach with scalar sign function.

Consider the optimal sliding mode controller design for the state-space model which is both controllable and observable as

$$\begin{aligned} \dot{x}(t) &= \mathbf{A}x(t) + \mathbf{B}u(t) \\ y(t) &= \mathbf{C}x(t) \end{aligned}, \tag{5-1}$$

where $\mathbf{A} \in \mathbf{R}^{n\times n}, \mathbf{B} \in \mathbf{R}^{n\times m}, \mathbf{C} \in \mathbf{R}^{m\times n}, x(t) \in \mathbf{R}^{n}, u(t) \in \mathbf{R}^{m}$ and $y(t) \in \mathbf{R}^{m}$. The initial condition is $x(0) = \alpha$. The proposed sliding mode controller can be expressed as

$$u(t) = -\mathbf{K}_c x(t) + \mathbf{E}_c sign(S(t)), \tag{5-2}$$

where $\mathbf{K}_c \in \mathbf{R}^{m\times n}$ and $\mathbf{E}_c \in \mathbf{R}^{m\times m}$ are control gains calculated by the optimal control law. $S(t) \in \mathbf{R}^{m}$ is defined as the sliding surface variable to be determined. The sliding mode controlled system becomes

$$\dot{x}(t) = \mathbf{A}_c x(t) + \mathbf{B}\mathbf{E}_c sign(S(t)), \tag{5-3}$$

where $\mathbf{A}_c = \mathbf{A} - \mathbf{B}\mathbf{K}_c$. The objectives of the sliding mode controller design in Equation (5-2) are as follows:

1. The optimally designed system in Equation (5-2) is robustly stable.
2. The stable sliding surface can be chosen so that the designed state trajectory can converge to the equilibrium point.
3. The designed system will optimally converge to the sliding manifold $S(t) = 0$.
4. The designed system has reduced the chattering response.

To achieve the aforementioned design objectives, we first review the following optimal regional pole assignment method. The regional pole assignment method will ensure that the controlled system's poles will stay either inside the designated vertical strip in the left half of the s-plane. If any pole of the system is already located to the left of the vertical system, the controller will keep that pole location unchanged.

Lemma 1 LQR with optimal eigen-value placement [97]

Let the quadratic cost function for the system in Equation (3-27) be

$$J = \int_0^\infty \left[x^T(t)\mathbf{Q}x(t) + u^T(t)\mathbf{R}u(t) \right] dt, \tag{5-4}$$

where $\mathbf{Q} \geq 0$ and $\mathbf{R} > 0$. The optimal state-feedback control law is given by

$$u(t) = -\mathbf{K}_c x(t), \tag{5-5}$$

and $\mathbf{K}_c = \mathbf{R}^{-1}\mathbf{B}^T\mathbf{P}$, where $\mathbf{P} > 0$ is the solution of the following Riccati equation,

$$\mathbf{A}^T\mathbf{P} + \mathbf{P}\mathbf{A} + \mathbf{Q} - \mathbf{P}\mathbf{B}\mathbf{R}^{-1}\mathbf{B}^T\mathbf{P} = \mathbf{0}. \tag{5-6}$$

Then, to optimally place the closed-loop eigenvalues in a vertical strip $\{-h_2, -h_1\}$ with $h_2 > h_1 \geq 0$, as shown in Figure 5-1, the optimal control gain in Equation (5-4) can be modified as

$$\mathbf{K}_c = \gamma\mathbf{R}^{-1}\mathbf{B}^T\mathbf{P}, \tag{5-7}$$

where $\mathbf{P} > 0$ is the solution of the following modified Riccati equation

$$\hat{\mathbf{A}}^T\mathbf{P}+\mathbf{P}\hat{\mathbf{A}}-\mathbf{P}\mathbf{B}\mathbf{R}^{-1}\mathbf{B}^T\mathbf{P}=\mathbf{0}, \tag{5-8}$$

in which $\hat{\mathbf{A}}=\mathbf{A}+h_1\mathbf{I}_n, \gamma=0.5+\dfrac{h_2-h_1}{tr(\mathbf{B}\mathbf{R}^{-1}\mathbf{B}^T\mathbf{P})}$, and $tr(\square)$ denotes the trace of $(\square)$.

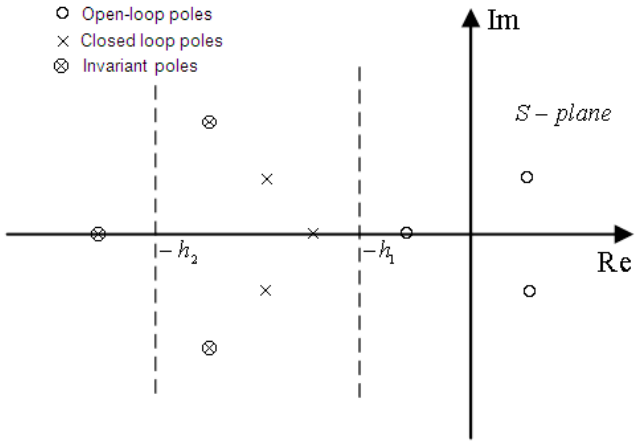

Figure 5-1 Region of interest in the continuous-time s-plane

Remark 1. If the open-loop system matrix $\mathbf{A}$ has stable eigenvalues and $h_2>\max\left|\mathrm{Re}\left[\lambda^-(\mathbf{A})\right]\right|$, then all of the closed-loop eigenvalues lie in the vertical strip, where $\lambda^-(\square)$ designates the stable eigenvalues of $(\square)$ and $\mathrm{Re}(\square)$ denotes the real part of $(\square)$. It should be noted that for any $h_2>h_1\geq 0$, the open-loop stable eigenvalues, which lie within and to the left of the vertical strip, remain invariant as the closed-loop eigenvalues, and all the other closed-loop eigenvalues lie in the vertical strip.

It is well-known that a stable eigenvalue with a small absolute magnitude gives a slow response, whereas a stable eigenvalue with a large absolute magnitude yields a fast response, which becomes negligible after the settling time. Hence, the whole system response can be approximated by the slow response after the settling time. As a result, the small (slow) eigenvalue can be known the dominant eigenvalue and its eigenvector as the dominant eigenvector. In this approach, the dominant eigenvector is utilized to construct a

specific sliding surface called as the eigen-surface. Based on the optimal regional pole assignment method and the aforementioned design objectives, we have the following design steps for the optimal sliding mode control law.

Design step 1: To achieve design objective 1, we assign the value of h_1 in Lemma 1, which indicates the degree of relative stability or robust stability. Also, to achieve design objective 2, we assign the value of h_2, which indicates the speed of the system response. The larger value of h_2 results in large feedback gains and larger designed eigenvalues. Hence, the values of h_1 and h_2 become design parameters. Therefore, the first optimal controller for the system in Equation (5-1) can be designed as

$$u^{(1)}(t) = -\mathbf{K}_c^{(1)} x(t), \tag{5-9}$$

where $\mathbf{K}_c^{(1)}$ is determined from Lemma 1. The optimally designed system becomes

$$\dot{x}(t) = \mathbf{A}_c^{(1)} x(t), \tag{5-10}$$

where $\mathbf{A}_c^{(1)} = \mathbf{A} - \mathbf{B}\mathbf{K}_c^{(1)}$. The superscript in Equation (5-9) in $u^{(1)}(t)$, $\mathbf{K}_c^{(1)}$ and $\mathbf{A}_c^{(1)}$ designates that the associated input function, feedback gain and system matrix are obtained in design step 1. From the designed system in Equation (5-10), we can determine the dominant eigen-values (designated as $\left\{\lambda_k^{(1)}, k = 1, \cdots, m\right\}$) and their associated dominant eigenvector matrix (designated as $\mathbf{M}_1^{(1)} \in \mathbf{R}^{n \times m}$). This dominant eigenvector matrix $\mathbf{M}_1^{(1)}$ can be utilized to construct the sliding surface $S(t)$ as

$$S(t) = \mathbf{C}^{(1)} x_c(t), \tag{5-11}$$

where $\mathbf{C}^{(1)} \in \mathbf{R}^{m\times n}$, and $\mathbf{C}^{(1)}\mathbf{M}_1^{(1)} = \mathbf{0}$ with $\mathbf{M}_1^{(1)} =$ any m independent column vectors in the matrix $\mathbf{M} \in \mathbf{R}^{n\times n}$, where the matrix $\mathbf{M}$ with $\hat{h}_2 > \hat{h}_1 \geq 0$ can be computed from the matrix sign function in Equation (3-25) as

$$\mathbf{M} = \frac{1}{2}\left(sign(\mathbf{A}_c^{(1)} + \hat{h}_2\mathbf{I}_n) - sign(\mathbf{A}_c^{(1)} + \hat{h}_1\mathbf{I}_n)\right), \tag{5-12}$$

The dominant eigenvalues $\left\{\lambda_k^{(1)}, k = 1,\cdots,m\right\}$ associated with the dominant eigenvectors in $\mathbf{M}_1^{(1)}$ are lying in the vertical strip $\left\{-\hat{h}_2, -\hat{h}_1\right\}$ [54]. The reason to choose the dominant eigenvector matrix $\mathbf{M}_1^{(1)}$ to construct the sliding surface $\mathbf{S}(t) = \mathbf{C}^{(1)}x_c(t) = 0$ with $\mathbf{C}^{(1)}\mathbf{M}_1^{(1)} = \mathbf{0}$ is due to the fact that any state trajectory lies on the specific sliding surface (the stable eigen-surface) will surely converge to the equilibrium point. Also, the eigenvector matrix $\mathbf{M}_1^{(1)}$ enables

$$\dot{\mathbf{S}}(t) = \mathbf{C^{(1)}}\dot{\mathbf{x}}_\mathbf{c}(t) = \mathbf{C^{(1)}}\mathbf{A_c^{(1)}}\mathbf{x}_\mathbf{c}(t) = \mathbf{C}^{(1)}\mathbf{A}_c^{(1)}\mathbf{M}_{1k}^{(1)} = \lambda_k^{(1)}\mathbf{C}^{(1)}\mathbf{M}_{1k}^{(1)} = 0, \tag{5-13}$$

where $\mathbf{M}_{1k}^{(1)} \in R^{n\times 1}$ is an eigenvector in $\mathbf{M}_1^{(1)} \in R^{n\times m}$ associated with the eigen-value $\lambda_k^{(1)}$ for $k = 1,\cdots,m$. Hence, we have the two sliding conditions as $S(t) = \mathbf{C}^{(1)}x_c(t) = 0$ and $\dot{S}(t) = \mathbf{C}^{(1)}\dot{x}_c(t) = 0$ for $\mathbf{C}^{(1)}\mathbf{M}_1^{(1)} = 0$. The orthogonal matrix $\mathbf{C}^{(1)}$ of the dominant eigenvector matrix $\mathbf{M}_1^{(1)}$ for $\mathbf{C}^{(1)}\mathbf{M}_1^{(1)} = \mathbf{0}$ can be determined from a Hermitian matrix [23]. To construct the Hermitian matrix $\mathbf{H} \in \mathbf{R}^{n\times n}$ [24], we compute the following matrix $\mathbf{N} \in \mathbf{R}^{n\times n}$ via the matrix sign function in Equation (3-25) as:

$$\mathbf{N} = \frac{1}{2}\left[sign(\mathbf{A}_c^{(1)} + \hat{h}_2\mathbf{I}_n) + sign(\mathbf{A}_c^{(1)} + \hat{h}_1\mathbf{I}_n)\right]. \tag{5-14}$$

The non-dominant eigenvalues $\left\{\lambda_k^{(1)}, k = m+1, \cdots, n\right\}$ in $\mathbf{A}_c^{(1)}$ are lying outside the vertical strip $\left\{-\hat{h}_2, -\hat{h}_1\right\}$. The associated non-dominant eigenvector matrix (denoted as $\mathbf{M}_2^{(1)} \in \mathbf{R}^{n\times(n-m)}$) can be determined from the matrix $\mathbf{N}$ in Equation (5-14) [24] as $\mathbf{M}_2^{(1)} =$ any $n-m$ independent column vectors in $\mathbf{N}$.

The Hermitian matrix $\mathbf{H} \in \mathbf{R}^{n\times n}$ and its inverse matrix $\mathbf{V} \in \mathbf{R}^{n\times n}$ can be expressed as

$$\mathbf{H}^{-1} = \begin{bmatrix} \mathbf{M}_1^{(1)} & \mathbf{M}_2^{(1)} \end{bmatrix}^{-1} = \mathbf{V} = \begin{bmatrix} \mathbf{V}_1 \\ \mathbf{V}_2 \end{bmatrix}, \tag{5-15}$$

where $\mathbf{M}_1^{(1)} \in \mathbf{R}^{n\times m}, \mathbf{M}_2^{(1)} \in \mathbf{R}^{n\times(n-m)}, \mathbf{V}_1 \in \mathbf{R}^{m\times n}$ and $\mathbf{V}_2 \in \mathbf{R}^{(n-m)\times n}$ for $n \geq 2m$. Since $\mathbf{VH} = \mathbf{I}_n$, hence, $\mathbf{V}_2\mathbf{M}_1^{(1)} = \mathbf{0}_{(n-m)\times m}$ and $\mathbf{V}_2 = C^{(1)} \in \mathbf{R}^{(n-m)\times n}$. For $n < 2m$, the corresponding block eigenvectors are chosen as $\mathbf{M}_1^{(1)} \in \mathbf{R}^{n\times(n-m)}$, $\mathbf{M}_2^{(1)} \in \mathbf{R}^{n\times m}$, $\mathbf{V}_1 \in \mathbf{R}^{(n-m)\times n}$ and $\mathbf{V}_2 \in \mathbf{R}^{m\times n}$. Hence, $\mathbf{V}_2\mathbf{M}_1^{(1)} = \mathbf{0}_{m\times(n-m)}$ and $\mathbf{V}_2 = \mathbf{C}^{(1)} \in \mathbf{R}^{m\times n}$. It is noted that when $n < 2m$, the number of the dominant eigenvectors in $\mathbf{M}_1^{(1)}$ is chosen as $n-m$ but not m. In addition, the $\lambda_k^{(1)}$ can also be complex eigen-values, and their eigenvectors become complex eigenvectors. To avoid the use of the complex eigenvector as the sliding surface, an alternative real eigenvector can be obtained from the block eigenvector $\mathbf{M}_1^{(1)}$ obtained in Equation (5-15).

Design step 2: To achieve the design objective 3, we design the second optimal tracker for the system in Equation (5-10), so that the output of the designed system is able to optimally track and stay in the desirable sliding surface. For simplicity in notation, we consider a 2-input and 2-output system model as

$$\begin{aligned} \dot{x}_c(t) &= \mathbf{A}_c^{(1)}x(t) + \mathbf{B}u(t) \\ S(t) &= \mathbf{C}^{(1)}x(t) \end{aligned}, \tag{5-16}$$

where $\mathbf{A}_c^{(1)} \in \mathbf{R}^{4\times4}, u(t) \in \mathbf{R}^{2\times1}, \mathbf{C}^{(1)} \in \mathbf{R}^{2\times4}$, and $\mathbf{C}^{(1)}\mathbf{M}_1^{(1)} = \mathbf{0}$. $S(t) \in \mathbf{R}^{2\times1}$ is the sliding surface and $\mathbf{M}_1^{(1)} \in \mathbf{R}^{4\times2}$ are the dominant eigenvector matrices obtained by using the Equation (5-15). The sliding surface equation in (5-16) can be expressed as

$$S(t) = \mathbf{C}^{(1)}x(t) = \begin{bmatrix} C_{11}^{(1)} & C_{12}^{(1)} \\ C_{21}^{(1)} & C_{22}^{(1)} \end{bmatrix}\begin{bmatrix} x_1(t) \\ x_2(t) \end{bmatrix} + \begin{bmatrix} C_{13}^{(1)} & C_{14}^{(1)} \\ C_{23}^{(1)} & C_{24}^{(1)} \end{bmatrix}\begin{bmatrix} x_3(t) \\ x_4(t) \end{bmatrix} = \begin{bmatrix} 0 \\ 0 \end{bmatrix}. \qquad (5\text{-}17)$$

The constrained equation can be written as

$$\begin{bmatrix} x_{c1}(t) \\ x_{c2}(t) \end{bmatrix} = -\begin{bmatrix} C_{11}^{(1)} & C_{12}^{(1)} \\ C_{21}^{(1)} & C_{22}^{(1)} \end{bmatrix}^{-1}\begin{bmatrix} C_{13}^{(1)} & C_{14}^{(1)} \\ C_{23}^{(1)} & C_{24}^{(1)} \end{bmatrix}\begin{bmatrix} x_3(t) \\ x_4(t) \end{bmatrix} \square \begin{bmatrix} q_{13} & q_{14} \\ q_{23} & q_{24} \end{bmatrix}\begin{bmatrix} x_3(t) \\ x_4(t) \end{bmatrix}. \qquad (5\text{-}18)$$

Suppose the output of the system in Equation (5-16) is chosen as

$$y(t) = \begin{bmatrix} x_1(t) \\ x_2(t) \end{bmatrix} = \begin{bmatrix} 1 & 0 & 0 & 0 \\ 0 & 1 & 0 & 0 \end{bmatrix}\begin{bmatrix} x_1(t) \\ x_2(t) \\ x_3(t) \\ x_4(t) \end{bmatrix} = \mathbf{C}x(t). \qquad (5\text{-}19)$$

The performance index for the tracking problem can be defined as

$$J = \int_0^\infty \left[\left[y(t) - S(t) \right]^T \mathbf{Q}_1 \left[y(t) - S(t) \right] + u^T(t)\mathbf{R}u(t) \right] dt. \qquad (5\text{-}20)$$

Letting $\mathbf{Q}_1 = \mathbf{I}_2$ and substituting the output function in Equation (5-19) and the constrained Equation (5-18) into Equation (5-20), we obtain $S(t) = 0$ and

$$\begin{aligned} J &= \int_0^\infty \left[x_1^2(t) + x_2^2(t) + u^T(t)\mathbf{R}u(t) \right] dt \\ &= \int_0^\infty \left[\hat{q}_{33}x_3^2(t) + 2\hat{q}_{34}x_3(t)x_4(t) + \hat{q}_{44}x_4^2(t) + u^T(t)\mathbf{R}u(t) \right] dt, \\ &= \int_0^\infty \left[x^T(t)\hat{\mathbf{Q}}x(t) + u^T(t)\mathbf{R}u(t) \right] dt \end{aligned} \qquad (5\text{-}21)$$

where $\hat{\mathbf{Q}} = \begin{bmatrix} 0 & 0 & 0 & 0 \\ 0 & 0 & 0 & 0 \\ 0 & 0 & \hat{q}_{33} & \hat{q}_{34} \\ 0 & 0 & \hat{q}_{34} & \hat{q}_{44} \end{bmatrix}$, $\hat{q}_{33} = q_{13}^2 + q_{23}^2, \hat{q}_{34} = q_{13}q_{14} + q_{23}q_{24}$ and $\hat{q}_{44} = q_{14}^2 + q_{24}^2$. Thus, the constrained optimization problem for the sliding surface tracking in Equations (5-16), (5-17) and (5-20) can be converted into an equivalent LQR problem in the following. Rewriting Equation (5-16) and Equation (5-21) yields

$$\dot{x}(t) = \mathbf{A}_c^{(1)} x(t) + \mathbf{B}u(t), \tag{5-22}$$

$$J = \int_0^\infty \left[x^T(t)\hat{\mathbf{Q}}x(t) + u^T(t)\mathbf{R}u(t) \right] dt, \tag{5-23}$$

The optimal control law becomes $u^{(2)}(t) = -\mathbf{K}_c^{(2)} x(t) = -\mathbf{R}^{-1}\mathbf{B}^T\mathbf{P}x(t)$, where $\mathbf{P} > 0$, the solution of the following Riccati equation is

$$\mathbf{A}_c^{(1)T}\mathbf{P} + \mathbf{P}\mathbf{A}_c^{(1)} + \hat{\mathbf{Q}} - \mathbf{P}\mathbf{B}\mathbf{R}^{-1}\mathbf{B}^T\mathbf{P} = \mathbf{0}. \tag{5-24}$$

Then, the second optimal controller for the system (5-22) is

$$u^{(2)}(t) = -\mathbf{K}_c^{(2)} x(t), \tag{5-25}$$

where $\mathbf{K}_c^{(2)}$ is determined from the solution of the equivalent LQR problem described in Equations (5-22), (5-23) and (5-24). The designed system becomes

$$\dot{x}_c(t) = \mathbf{A}_c^{(2)} x(t), \tag{5-26}$$

where $\mathbf{A}_c^{(2)} = \mathbf{A}_c^{(1)} - \mathbf{B}\mathbf{K}_c^{(2)}$. Subsequently, the total sliding mode controller in (5-2) for the system in (5-1) can be determined from (5-9) and (5-25) as

$$\begin{aligned} u(t) &= u^{(1)}(t) + u^{(2)}(t) + \mathbf{E}_c sign(S(t)) \\ &= -(\mathbf{K}_c^{(1)} + \mathbf{K}_c^{(2)})x(t) + \mathbf{E}_c sign(S(t)) \\ &= -\mathbf{K}_c x(t) + \mathbf{E}_c sign(S(t)) \end{aligned}, \tag{5-27}$$

where $\mathbf{K}_c = \mathbf{K}_c^{(1)} + \mathbf{K}_c^{(2)}$. The optimally designed sliding mode controlled system becomes

$$\begin{aligned} \dot{x}_c(t) &= (\mathbf{A} - \mathbf{B}\mathbf{K}_c)x(t) + \mathbf{B}\mathbf{E}_c sign(S(t)) \\ y(t) &= \mathbf{C}x(t) \end{aligned} . \tag{5-28}$$

Since $sign(S(t))$ is a constant vector with each component $+1$ or -1, the final value theorem can be applied to (5-28) to determine the forward gain $\mathbf{E}_c$ in (5-28) as

$$\mathbf{E}_c = -\left[\mathbf{C}(\mathbf{A} - \mathbf{B}\mathbf{K}_c)^{-1}\mathbf{B}\right]^{-1}. \tag{5-29}$$

The optimally designed controller in (5-27) is able to minimize the tracking error between the output trajectory $y(t)$ and the sliding surface $S(t)$ in (5-20) and enables the controlled state trajectory to satisfy the constrained equation in (5-18) or stay in the sliding surface $S(t) = 0$ in (5-11) and (5-17).

Design step 3: To achieve the design objective 4, the chattering effects caused by a non-smooth signal, such as the signum (sgn) function in (3-18), can be reduced by introducing the smooth sign function discussed in (3-24). Because the i^{th} entry $x_i(t)$ in $x(t)$ can be represented as $x_i(t) = |x_i(t)| sign(x_i(t)) \cong |x_i(t)| sign_j(x_i(t))$, the sliding surface is rewritten as

$$S(t) = \mathbf{C}^{(1)}x(t) \cong \mathbf{C}^{(1)}\left[|x_1(t)| sign_j(x_1(t)), |x_2(t)| sign_j(x_2(t)), ..., |x_n(t)| sign_j(x_n(t))\right]^T, \tag{5-30}$$

Since $|a| = a \cdot sign_j(a)$, (5-30) can be written as

$$S(t) \cong \mathbf{C}^{(1)}\left[x_1(t)sign_j^2(x_1(t)), x_2(t)sign_j^2(x_2(t)), ..., x_n(t)sign_j^2(x_n(t))\right]^T. \tag{5-31}$$

The term $x_i(t)sign_j^2(x_i(t))$ in (5-31) is a nonlinear smooth function. According to Wu *et al.* [98] and [8], we can use a single variable function approach such that

$$\dot{x} = f(x), \tag{5-32}$$

where $f(x)$ is a nonlinear single variable function. The optimized linear model can be written as

$$\dot{x} = a_k x, \tag{5-33}$$

where $a_k = \dfrac{f(x_k)}{x_k}$ is an exact linear model of the nonlinear function $f(x)$ at any operating point $x_k \neq 0$ [95, 98]. When $x_k = 0$, the a_k in (5-33) reduces to the gradient value of $f(x)$ in (5-32) evaluated at the operating point $x = x_k$. Thus, the exact linear model of the nonlinear function $x_i(t)sign^2(x_i(t))$ can be expressed as

$$x_i(t)sign_j^2(x_i(t)) \approx d_i x_i(t), \tag{5-34}$$

where $0 \le d_i \approx sign_j^2(x_i(t)) \le 1$ for $i = 1, 2, 3, ..., n$ and even values of j. It follows that

$$\Rightarrow \mathbf{S}_i(t) = \mathbf{C^{(1)}}\left[d_1 x_1(t), d_2 x_2(t), ..., d_n x_n(t)\right]^T = \mathbf{C_d} x(t), \tag{5-35}$$

where $S_i(t)$ is the optimally linearized sliding surface of $S(t)$ in (5-31) with $\mathbf{C}^{(1)} = \left[C_1^{(1)}, C_2^{(1)}, ..., C_n^{(1)}\right]$ and $\mathbf{C_d} = \left[C_1^{(1)} d_1, C_2^{(1)} d_2, ..., C_n^{(1)} d_n\right]$.

Subtracting (5-35) from (5-11), we obtain the following modified sliding mode surface

$$\mathbf{S_e}(t) = \mathbf{S}(t) - \mathbf{S}_i(t) = (\mathbf{C^{(1)}} - \mathbf{C_d})x(t) = \hat{\mathbf{C}}x(t), \tag{5-36}$$

where $\hat{\mathbf{C}} = \mathbf{C^{(1)}} - \mathbf{C_d} = \left[(1-d_1)C_1^{(1)}, (1-d_2)C_2^{(1)}, ..., (1-d_n)C_n^{(1)}\right]$, $d_i \approx sign_j^2((x_i))$ and $0 \le d_i \le 1$ for even values of j. It is observed that $\mathbf{S_e}(t) = 0$ when $d_i = 1$. It can be seen from the developments in (5-30) to (5-35) that with the tuning parameters d_i, we can map the value of the modified sliding surface function $\mathbf{S_e}(t) = \hat{\mathbf{C}}\mathbf{x}(t)$ in (5-36) into the interval $[-1, \ 1]$ smoothly and without changing its sign thus it can be used to reduce chattering in

sliding mode control. The comparison of the magnitudes of $sgn(C^{(1)}x(t))$ and $sign_j(\hat{C}x(t))$ is shown in Figure 5-2.

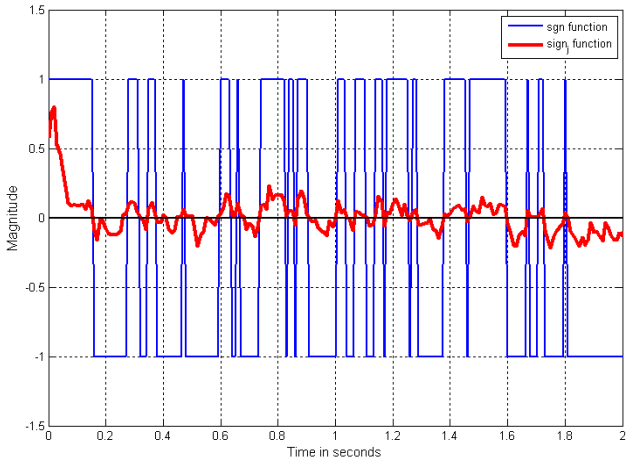

Figure 5-2 Magnitude of $sgn(\mathbf{C}^{(1)}\mathbf{x}(t))$ and $sign_j(\hat{\mathbf{C}}\mathbf{x}(t))$ with $d_1 = d_2 = 0.6, j = 2$ and white noise

It is observed that both functions have the same sign, but different magnitude. Hence, the sliding mode controller in (5-27) can be implemented as

$$\mathbf{u}(t) = -\mathbf{K}_c\mathbf{x}(t) + \mathbf{E}_c sign_j(\mathbf{S}_e(t)), \tag{5-37}$$

where $\mathbf{S}_e(t) = \hat{\mathbf{C}}\mathbf{x}(t)$ for a small even value of j in $sign_j(\mathbf{S}_e(t))$, and small components in $\hat{\mathbf{C}}$ with large values of d_i for $i = 1, 2, ...n$ in (5-36). The optimally designed sliding mode controlled system with the controller in (5-37) becomes

$$\dot{\mathbf{x}}(t) = \mathbf{A}_c\mathbf{x}(t) + \mathbf{B}\mathbf{E}_c sign_j(\mathbf{S}_e(t)), \tag{5-38}$$

where $\mathbf{A}_c = \mathbf{A} - \mathbf{B}\mathbf{K}_c$.

5.3 Stability Analysis

For a control algorithm, it is very important that the proposed control algorithm be stable for a desired performance. Based on design step 2, the designed state trajectory would optimally track and stay in the sliding surface $\mathbf{S}(t) = 0$ in (5-11). Hence, the

sliding surface variable $S(t)$ for the stability analysis is used. Consider the Lyapunov's function

$$\mathbf{V}(\mathbf{x}_c) = \mathbf{S}(t)^{\mathrm{T}}\mathbf{S}(t), \tag{5-39}$$

or

$$\begin{aligned} &\mathbf{V}(\mathbf{x}) = \mathbf{x}^{\mathrm{T}}\mathbf{C}^{(1)\mathrm{T}}\mathbf{C}^{(1)}\mathbf{x} = \mathbf{x}^{\mathrm{T}}\hat{\mathbf{P}}\mathbf{x} \geq \mathbf{0} \\ &\Rightarrow \hat{\mathbf{P}} = \mathbf{C}^{(1)\mathrm{T}}\mathbf{C}^{(1)} \geq \mathbf{0} \end{aligned}, \tag{5-40}$$

where $\mathbf{C}^{(1)} \in \mathbf{R}^{m\times n}, \mathbf{S}(t) \in \mathbf{R}^{m\times 1}$.

Now,

$$\begin{aligned} \dot{\mathbf{V}}(\mathbf{x}_c) &= \dot{\mathbf{S}}^{\mathrm{T}}\mathbf{S} + \mathbf{S}^{\mathrm{T}}\dot{\mathbf{S}} \\ &= \dot{\mathbf{x}}^{\mathrm{T}}\mathbf{C}^{(1)\mathrm{T}}\mathbf{C}^{(1)}\mathbf{x} + \mathbf{x}^{\mathrm{T}}\mathbf{C}^{(1)\mathrm{T}}\mathbf{C}^{(1)}\dot{\mathbf{x}}. \end{aligned}, \tag{5-41}$$

From (5-38) and (5-40), we have

$$\dot{\mathbf{V}}(\mathbf{x}) = \mathbf{x}^{\mathrm{T}}\left[\mathbf{A}_c^{\mathrm{T}}\hat{\mathbf{P}} + \hat{\mathbf{P}}\mathbf{A}_c\right]\mathbf{x} + \hat{\mathbf{S}}_e^{\mathrm{T}}(\hat{\mathbf{P}}\mathbf{B}\mathbf{E}_c)^{\mathrm{T}}\mathbf{x} + \mathbf{x}^{\mathrm{T}}\hat{\mathbf{P}}\mathbf{B}\mathbf{E}_c\hat{\mathbf{S}}_e, \tag{5-42}$$

where $\hat{\mathbf{S}}_e$ designated as $sign_j(\mathbf{S}_e(t))$ and $\mathbf{A}_c$ is designed to be asymptotically stable, with a positive semi-definite matrix $\hat{\mathbf{P}}$, if (A_c, B) is stabilizable and (A, C) are detectable [99]. According to Lyapunov's equation, for a stable system

$$\mathbf{A}_c^{\mathrm{T}}\hat{\mathbf{P}} + \hat{\mathbf{P}}\mathbf{A}_c = -\hat{\mathbf{Q}}, \tag{5-43}$$

where $\hat{\mathbf{Q}} < \eta$, $\eta \geq 0$ and $\hat{\mathbf{P}} \geq \mathbf{0}$. Equation (5-42) can be written as

$$\dot{\mathbf{V}}(\mathbf{x}) = \begin{bmatrix} \mathbf{x}^{\mathrm{T}} & \hat{\mathbf{S}}_e^{\mathrm{T}} \end{bmatrix}\begin{bmatrix} -\hat{\mathbf{Q}} & \left(\hat{\mathbf{P}}\mathbf{B}\mathbf{E}_c\right) \\ \left(\hat{\mathbf{P}}\mathbf{B}\mathbf{E}_c\right)^{\mathrm{T}} & \mathbf{0} \end{bmatrix}\begin{bmatrix} \mathbf{x} \\ \hat{\mathbf{S}}_e \end{bmatrix} \leq 0. \tag{5-44}$$

When the system states will be on the sliding surface then $\hat{\mathbf{S}}_e = \mathbf{0}$,

$$\Rightarrow \dot{\mathbf{V}}(\mathbf{x}) \leq 0. \tag{5-45}$$

This result implies that the above designed system will be stable in accordance with Lyapunov's second theorem of stability. Thus we can conclude that the optimal sliding mode controller is stable. The proposed controller is applied on two examples on

single input single output (SISO) systems. In the first example, the optimal sliding mode controller performance is compared with the classical sliding mode controller. The system used is a SISO unstable system. For the second example, the proposed controller is implemented as a vibration controller on a smart flexible beam with piezoceramic sensor and actuator. In the following sections, both examples have been explained.

5.4 Example 1: Optimal Sliding Mode Control on SISO System

For comparison, we consider a controllable, observable and unstable system in a controller-type companion form as

$$\begin{aligned} \dot{\mathbf{x}}_{\mathbf{c}}(t) &= \mathbf{A}\mathbf{x}_{\mathbf{c}}(t) + \mathbf{B}\mathbf{u}_{\mathbf{c}}(t) + \mathbf{B}\xi(t) \\ y &= \mathbf{C}\mathbf{x}_{\mathbf{c}}(t) \end{aligned}, \tag{5-46}$$

where $\mathbf{A} = \begin{bmatrix} \mathbf{0} & \mathbf{1} \\ \mathbf{0} & \mathbf{0} \end{bmatrix}, \mathbf{B} = \begin{bmatrix} \mathbf{0} \\ \mathbf{1} \end{bmatrix}, \mathbf{C} = \begin{bmatrix} \mathbf{1} & \mathbf{0} \end{bmatrix}$, and $\xi(t)$ is a band-limited white noise with the magnitude within $\begin{bmatrix} -15 & 15 \end{bmatrix}$ shown in Figure 5-2.

Design step 1: To achieve the robust stability with a sufficient stability margin, we choose $h_1 = 1$. In addition, to create a large non-dominant eigenvalue, we choose $h_2 = 160$. Furthermore, to optimally place the designed eigenvalues of the closed-loop system matrix $\mathbf{A}_c^{(1)} = \mathbf{A} - \mathbf{B}\mathbf{K}_c^{(1)}$ within the vertical strip $\{-160, -1\}$, the first optimal control gain $\mathbf{K}_c^{(1)}$ can be computed as

$$\mathbf{K}_c^{(1)} = \gamma \mathbf{R}^{-1}\mathbf{B}^T\mathbf{P}_1, \tag{5-47}$$

where $\mathbf{P}_1$ is the solution of the Riccati equation,

$$\hat{\mathbf{A}}^T\mathbf{P}_1 + \mathbf{P}_1\hat{\mathbf{A}} - \mathbf{P}_1\mathbf{B}\mathbf{R}^{-1}\mathbf{B}^T\mathbf{P}_1 = 0, \tag{5-48}$$

where $\hat{\mathbf{A}} = \mathbf{A} + h_1\mathbf{I}_2, \gamma = 0.5 + \dfrac{h_2 - h_1}{tr(\mathbf{B}\mathbf{R}^{-1}\mathbf{B}^T\mathbf{P}_1)}$, and $\mathbf{R} = 1$. This provides $\mathbf{K}_c^{(1)} = \begin{bmatrix}161 & 161\end{bmatrix}$, and $\mathbf{A}_c^{(1)} = \mathbf{A} - \mathbf{B}\mathbf{K}_c^{(1)} = \begin{bmatrix}0 & 1\\ -161 & -161\end{bmatrix}$.

The eigenvalues of $\mathbf{A}_c^{(1)}$ are $\left\{\lambda_k^{(1)}, k = 1,2\right\} = \left\{-1.0063,\ -159.9937\right\}$. The small (slow) eigenvalue $\lambda_1^{(1)} = -1.0063$ is chosen as the dominant eigenvalue, its associated dominant eigenvector is determined from (5-12), (5-14) and (5-15) with $\hat{h}_1 = 0$ and $\hat{h}_2 = \dfrac{1}{2}(h_1 + h_2)$ as $\mathbf{M}_1^{(1)} = -\lambda_1^{(1)}\begin{bmatrix}1\\ \lambda_1^{(1)}\end{bmatrix} = \begin{bmatrix}1.0063\\ -1.0126\end{bmatrix}$, and the sliding surface is constructed as

$$\begin{aligned} S(t) &= \mathbf{C}^{(1)}x(t) = \begin{bmatrix}1 & 0.9937\end{bmatrix}x(t)\\ &= \begin{bmatrix}1 & -\dfrac{1}{\lambda_1^{(1)}}\end{bmatrix}x(t) = x_1(t) - \frac{1}{\lambda_1^{(1)}}x_2(t) = 0,,\\ &\Rightarrow x_1(t) = \frac{1}{\lambda_1^{(1)}}x_2(t) \end{aligned} \tag{5-49}$$

and $\mathbf{C}^{(1)}\mathbf{M}^{(1)} = \begin{bmatrix}1 & \dfrac{-1}{\lambda_1^{(1)}}\end{bmatrix}\begin{bmatrix}-\lambda_1^{(1)}\\ -\left(\lambda_1^{(1)}\right)^2\end{bmatrix} = 0$.

Design step 2: The performance index of the tracking problem in (5-20) with $Q = 1, y(t) = x_1(t)$ and $S(t) = 0$ (i.e., $x_1(t) = \left(\dfrac{1}{\lambda_1^{(1)}}\right)x_2(t)$) is reduced to that in (5-23) as

$$\begin{aligned} J &= \int_0^\infty \left[x_1^2(t) + u^T(t)\mathbf{R}u(t)\right]dt\\ &= \int_0^\infty \left[\left(\frac{1}{\lambda_1^{(1)}}\right)^2 x_2^2(t) + u^T(t)\mathbf{R}u(t)\right]dt,\\ &= \int_0^\infty \left[x^T(t)\hat{\mathbf{Q}}x(t) + u^T(t)\mathbf{R}u(t)\right]dt \end{aligned} \tag{5-50}$$

where $\hat{\mathbf{Q}} = diag\{0 \quad \hat{q}_{22}\}, \hat{q}_{22} = \frac{1}{(\lambda_1^{(1)})^2} = 0.9875$ and $\mathbf{R} = 1$. The second optimal control gain was found to be $\mathbf{K}_c^{(2)} = \begin{bmatrix} 0 & 0.0031 \end{bmatrix}$, the total optimal control gain was $\mathbf{K}_c = \mathbf{K}_c^{(1)} + \mathbf{K}_c^{(2)} = \begin{bmatrix} 161 & 161.0031 \end{bmatrix}$, the eigenvalues of closed loop system $\mathbf{A}_c^{(2)}$ are $\left\{\lambda_k^{(2)}, k = 1,2\right\} = \left\{-1.0063, \quad -159.9968\right\}$ and the forward gain $\mathbf{E}_c = 161$. The closed-loop system becomes

$$\begin{aligned} \dot{x}(t) &= \begin{bmatrix} 0 & 1 \\ -161 & -161.0031 \end{bmatrix} x(t) + \begin{bmatrix} 0 \\ 161 \end{bmatrix} sign_j(S_e(t)) + \begin{bmatrix} 0 \\ 1 \end{bmatrix} \xi(t), \\ y(t) &= \begin{bmatrix} 1 & 0 \end{bmatrix} x(t), \end{aligned} \tag{5-51}$$

and initial conditions $x^T(0) = \begin{bmatrix} 3 & 0 \end{bmatrix}$ with the sliding surface $S(t) = \mathbf{C^{(1)}} x(t) = \begin{bmatrix} 1 & 0.9937 \end{bmatrix} x(t)$ and $S_e(t) = \hat{\mathbf{C}} x(t) = 0$. It is noted that based on the specific state-weighting matrix $\hat{\mathbf{Q}}$ in the performance index *j* in design step 2, the optimally designed dominant eigenvalue $\lambda_1^{(2)}$ and its associated dominant eigenvector $M_1^{(2)}$ for the second system matrix $\mathbf{A_c^{(2)}}$ are invariant (i.e. $\lambda_1^{(2)} = \lambda_1^{(1)}$, and $M_1^{(2)} = M_1^{(1)}$). The reason is that the specific state-weighting matrix $\hat{\mathbf{Q}}$ is obtained by pre-substituting the constrained equation $x_1(t) = (1/\lambda_1^{(1)}) x_2(t)$ or the sliding surface $S(t) = 0$ into the performance index *J*. As a consequence, the states (i.e. $x_1(t)$, and $x_2(t)$) of the optimally designed second system must satisfy the constrained equation $x_1(t) = (1/\lambda_1^{(1)}) x_2(t)$ or the sliding surface $S(t) = 0$. Hence, the dominant eigenvalue $\lambda_1^{(1)}$ in the constrained equation must be equal to $\lambda_1^{(2)}$ resulting in $M_1^{(1)} = M_1^{(2)}$ and it is associated with sliding surface $S(t)$ is invariant also.

Design step 3: To determine the $S_e(t)$, we use the modified sliding surface $\hat{\mathbf{C}}x(t)$ in (5-36). For simplicity, the parameters d_1 and d_2 are chosen as $d_1 = d_2 = 0.9$ in the row vector $\hat{C}$ in (5-36). The sign function in (5-51) used in the simulation is

$$sign_j\left(S_e(t)\right) = \frac{(1+\hat{\mathbf{C}}\mathbf{x}_c)^j - (1-\hat{\mathbf{C}}\mathbf{x}_c)^j}{(1+\hat{\mathbf{C}}\mathbf{x}_c)^j + (1-\hat{\mathbf{C}}\mathbf{x}_c)^j}, \tag{5-52}$$

where j=2. A small value of j is used to reduce the magnitude of $sign_j(S_e(t))$. The simulation results are shown in Figure 5-4 and Figure 5-5. From the simulation result in Figure 5-5, we observe that the state trajectory directly tracks to the eigen-surface $(S(t) = 0)$ and converges to the equilibrium point.

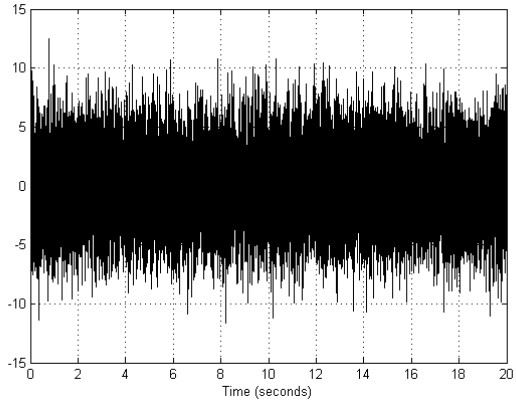

Figure 5-3 Band-limited white noise

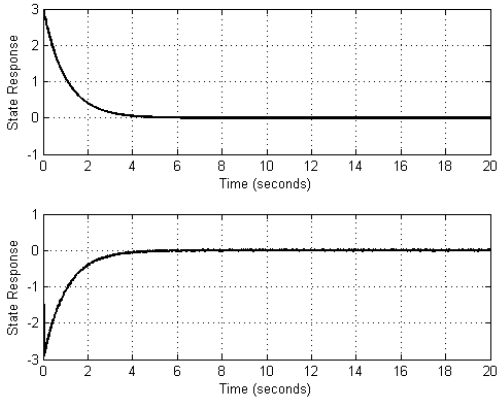

Figure 5-4 State Response with new optimal sliding mode controller

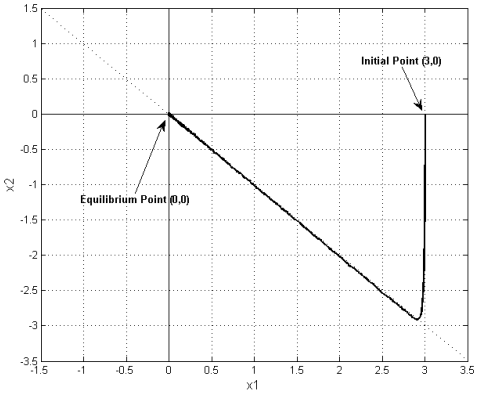

Figure 5-5 Trajectory tracking of sliding surface

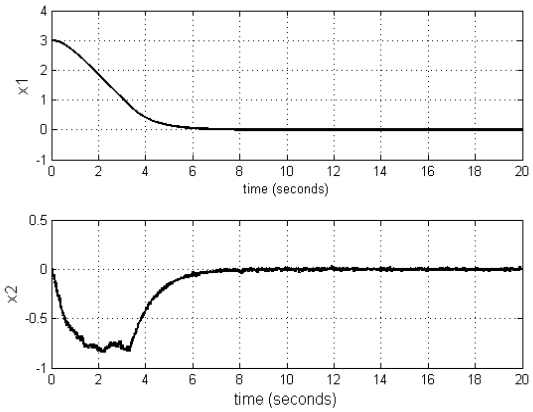

Figure 5-6 State Response of Conventional sliding mode controller

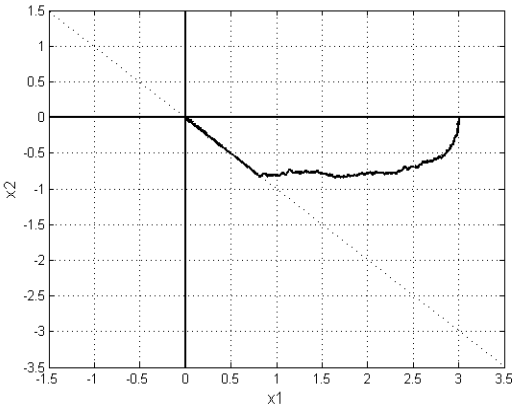

Figure 5-7 Sliding surface tracking with conventional sliding mode controller

The proposed optimal sliding mode controller performance was compared with conventional sliding mode controller described in Zak [8]. The conventional sliding mode control law is defined as

$$u(t) = -K_{eq}x(t) + E_{eq}\,\mathrm{sgn}\left(s(t)\right), \tag{5-53}$$

where $K_{eq} = -(C_s B)^{-1} C_s A; E_{eq} = -C_s B$ and the sliding surface is defined as $s(t) = C_s x(t) = 0$. The conventional sliding mode controller has one condition to satisfy $(C_s B)$ should be non-singular. For comparison purpose, the parameters for conventional sliding mode controller are $C_s = \begin{bmatrix} 1 & -0.9937 \end{bmatrix}, K_{eq} = \begin{bmatrix} 0 & 1.0063 \end{bmatrix}$ and $E_{eq} = -0.9937$. The initial conditions, band limited white noise and sliding surface parameters are kept same for the system with proposed controller. The simulation results for the conventional sliding mode controller are shown in Figure 5-6 and Figure 5-7. From the above comparison, it can be observed that the state response of optimal sliding mode controller is faster than conventional system. Also, the percentage output energy usage before convergence of both controller were calculated by

$$r_s = \frac{\|y_{os}\|_2}{\|y_{sc}\|_2} \times 100, \tag{5-54}$$

where $\|y_{os}(t)\|_2$ is H_2 norm of the output with proposed optimal sliding mode controller and $\|y_{sc}(t)\|_2$ is H_2 norm of output with conventional controller.

It was found that proposed optimal sliding mode controller used about 66% of total energy used by conventional controller, which explains the effectiveness of the proposed approach. Since the chattering occurs when system states converge to the desired sliding manifold, the energy of the states after both states converge to sliding manifold is calculated for proposed sliding mode approach and conventional sliding mode approach. It was found that the state (x_1) has 71.2% less chattering with proposed approach than with conventional sliding mode approach. Similarly, the state (x_2) shows approximately 31% less chattering, which explains the great chattering alleviation performance of the proposed approach.

The proposed optimal sliding mode controller was also compared with conventional sliding mode controller by replacing the discontinuous function with saturation function and tangent hyperbolic function.

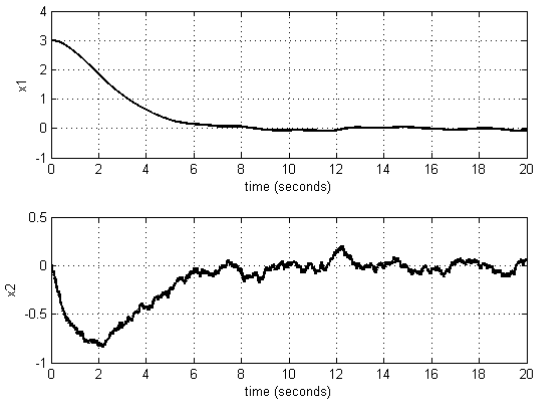

Figure 5-8 State Response with Conventional Sliding Mode Controller with saturation function

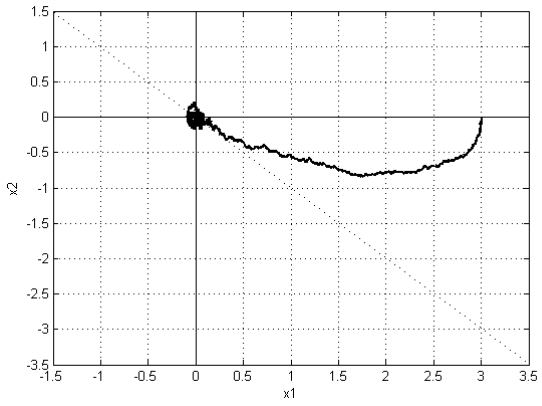

Figure 5-9 Trajectory Response with Conventional Sliding Mode Controller with saturation function

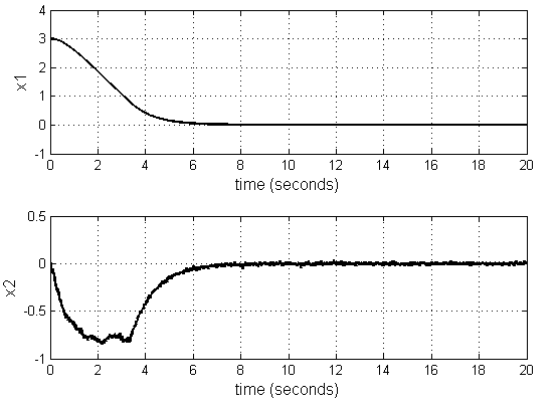

Figure 5-10 State Response with Conventional Sliding Mode Controller with tangent hyperbolic function

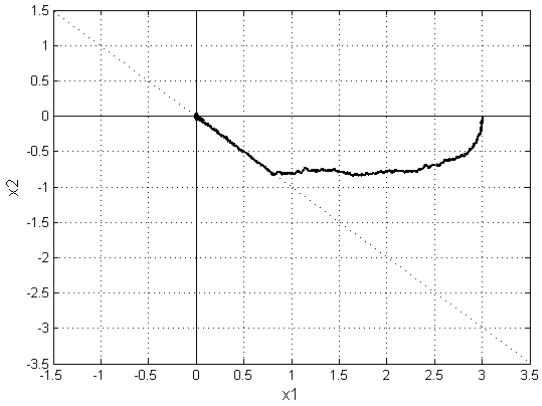

Figure 5-11 Trajectory Response with Conventional Sliding Mode Controller with tangent hyperbolic function

From the above comparison in Figure 5-8-Figure 5-11, it was seen that the tangent hyperbolic function is helping in reducing the chattering of the system with conventional sliding mode controller. However, the optimal sliding mode controller using the sign function method still has less chattering than the conventional sliding mode controller. The x_1 state has about 23% less chattering and x_2 state has about 54% less chattering than conventional sliding mode controller with tangent hyperbolic function. Also, it was seen that the saturation function can be used to replace the discontinuous switching function, however the system will have less disturbance rejection. The robustness of the proposed optimal sliding mode controller is demonstrated by implementing the proposed approach for active vibration suppression of a flexible beam with mass uncertainty and using the piezoceramic actuator and sensor.

5.5 Example 2: Vibration control of Smart Flexible Experiment

The novel optimal sliding mode approach using the sign function was implemented to control the multi-modal vibrations of an aluminum beam. The novel sliding mode approach using the sign function was implemented to control the multi-modal vibrations of an aluminum beam. The experimental setup for this experiment includes a flexible

aluminum beam with a surface bonded piezoceramic sensor and actuator. The aluminum beam properties and piezoceramic sensor and actuator properties are discussed in Table 5-1 and Table 5-2. The integrated system with data acquisition and hardware accessories are shown in Figure 5-12. The beam has very low damping characteristics and the vibration amplitude is considerable upon excitation.

Table 5-1 Beam Properties

Symbol	Quantity	Units	Value
L	Length	(mm)	529.9
W	Width	(mm)	48.7
T	Thickness	(mm)	0.68
P	Beam density	Kg/m^3	2690
E	Y. Modulus	N/m^2	7.03×10^{10}

Table 5-2 PZT actuator and sensor properties

Symbol	Quantity	Units	PZT Actuator	PZT Sensor
L	Length	(mm)	73.3×28×0.12	12.7×6.35×0.25
W	Width	(mm)	28	6.35
T	Thickness	(mm)	0.12	0.25
d_{33}	Strain Coeff.	(C/N)	4×10^{-10}	3.5×10^{-10}
d_{31}	Strain Coeff.	(C/N)	1.79×10^{-10}	1.79×10^{-10}
ρ_p	PZT density	Kg/m^3	7300	7700
E	Young Modulus	N/m^2	3.3×10^{10}	6.9×10^{10}

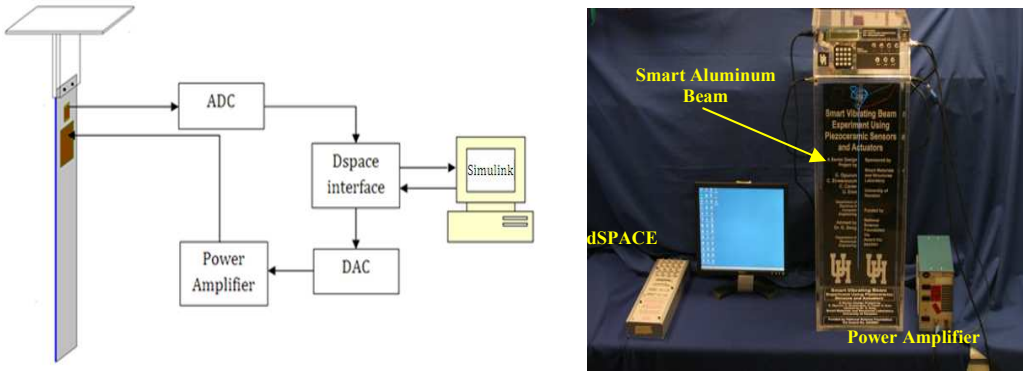

Figure 5-12 Experimental Setup

Two PZT patches, one as actuator (P1-8528) and one as sensor (QP 10s) were used. To activate vibration through the actuator, a piezoceramic amplifier with a negative gain of twenty was used. The system is interfaced with a Matlab Simulink model through the dSPACE Data Acquisition Board RT1103. The sensor signal was fed into the

dSPACE's Analog to Digital Converter (ADC). The actuator signal was broadcast through the Digital to Analog Converter (DAC) from dSPACE. The sampling time for the system was selected to be 0.001 sec.

For implementing the optimal sliding mode control, non-parametric system identification of the smart beam with piezo actuator and sensor was conducted [95, 100, 101]. The modal frequencies were found by plotting the frequency response function with the help of data acquired from the piezoceramic sensor when a frequency rich signal is passed through the actuator to vibrate the beam. The magnitude and phase plots frequency response function of the identified system compared with the model data, as discussed in [95, 100, 101], are shown in Figure 5-13 and Figure 5-14.

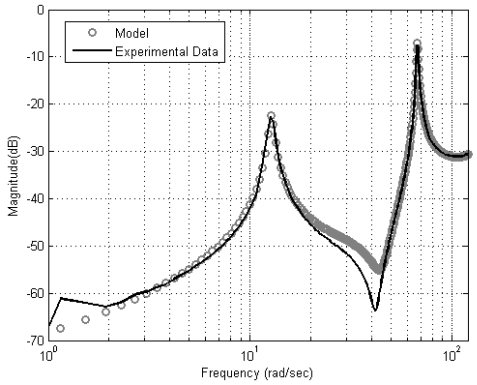

Figure 5-13 Magnitude Plot of FRF for the Beam

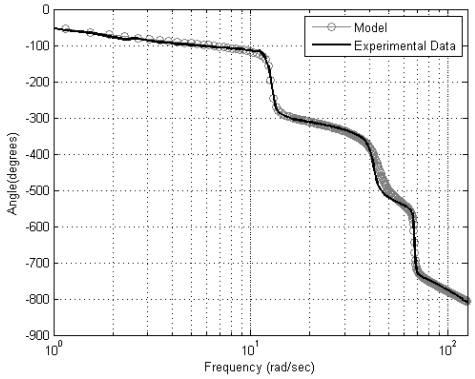

Figure 5-14 Phase Plot of FRF for the Smart Beam

By analyzing the above plots, it can be stated that the system identification is accurate. The first two modal frequencies were considered for vibration control. After cancelling the unobserved poles and zeros, the transfer function of the system was

$$\frac{Y(s)}{U(s)} = \frac{-0.06213s^3 + 35.82s^2 + 271.4s + 7367}{s^4 + 1.999s^3 + 4722s^2 + 3825s + 739400}, \tag{5-55}$$

and its state-space representation in a controller-type companion form is

$$\begin{aligned} \dot{x}(t) &= \mathbf{A}x(t) + \mathbf{B}u(t) \\ y(t) &= \mathbf{C}x(t) \end{aligned}, \; x(0) = \mathbf{0} \tag{5-56}$$

where the system matrices are $\mathbf{A}=\begin{bmatrix} 0 & 1 & 0 & 0 \\ 0 & 0 & 1 & 0 \\ 0 & 0 & 0 & 1 \\ -739400 & -3825 & -4722 & -1.999 \end{bmatrix}, \mathbf{B}=\begin{bmatrix} 0 \\ 0 \\ 0 \\ 1000 \end{bmatrix}$,

and $\mathbf{C}=\begin{bmatrix} 7.367 & 0.2714 & 0.003582 & -0.00006 \end{bmatrix}$. The eigenvalues of the system are $\{-0.3981 \pm 12.7292i, -0.6011 \pm 67.5177i\}$.

For robust stability and to retain the pair of the larger eigenvalues $-0.6011 \pm 67.5177i$ of $\mathbf{A}$ for smaller controller gain design, we choose $h_1 = 0.4$ and $h_2 = 2 = 5h_1$ in Lemma 1. The optimal control gain for the first designed system $\mathbf{A}_c^{(1)}$ in (5-10) was computed from Lemma 1 as $\mathbf{K}_c^{(1)} = \begin{bmatrix} 2.9246 & 7.3121 & 0.0026 & 0.0016 \end{bmatrix}$. The eigenvalues of $\mathbf{A}_c^{(1)}$ are $\{-0.6011 \pm 67.5177i, -1.2 \pm 12.7042i\}$.

It is observed that the pair of eigenvalues $-0.6011 \pm 67.5177i$ is invariant. Then, the other pair of eigenvalues $-1.2 \pm 12.7042i$ was chosen as the dominant eigenvalues since they have a smaller absolute magnitude than the invariant pair, which could provide quickly damped oscillation. To avoid the use of a complex eigenvector to construct the sliding surface, we computed the block eigenvector from (5-12) with $\hat{h}_1 = 0.8$ and $\hat{h}_2 = 4$ as $\mathbf{M}_1^{(1)T} = \begin{bmatrix} M_{11}^{(1)T} \\ M_{12}^{(1)T} \end{bmatrix} = \begin{bmatrix} 0.1804 & -0.1329 & -7.1105 & 37.8719 \\ 0.0008 & 0.1784 & -0.2395 & -6.5426 \end{bmatrix}$. $M_{11}^{(1)}$ is chosen as the dominant eigenvector for constructing the sliding surface. The orthogonal matrix $\mathbf{V}_2 \in \mathbf{R}^{3\times 4}$ for $\mathbf{V}_2 \mathbf{M}_{11}^{(1)} = 0$ can be computed from (5-12). One of the three row vectors in $\mathbf{V}_2$ is chosen as $\mathbf{C}^{(1)} \in \mathbf{R}^{1\times 4}$ to construct the sliding surface as

$$S(t) = \mathbf{C}^{(1)} x_c(t) = 0, \text{ with } \mathbf{C}^{(1)} M_{11}^{(1)} = 0, \tag{5-57}$$

where $\mathbf{C}^{(1)} = \begin{bmatrix} C_1^{(1)} & C_2^{(1)} & C_3^{(1)} & C_4^{(1)} \end{bmatrix} = \begin{bmatrix} 1 & 0 & 0.0218 & -0.0007 \end{bmatrix}$.

Solving a constrained equation from $S(t) = \mathbf{C}^{(1)} x_c(t) = 0$ in (5-57) yields

$$x_{c1}(t) = -\frac{C_2^{(1)}}{C_1^{(1)}} x_{c2}(t) - \frac{C_3^{(1)}}{C_1^{(1)}} x_{c3}(t) - \frac{C_4^{(1)}}{C_1^{(1)}} x_{c4}(t). \tag{5-58}$$

Substituting (5-58) into the output function $y(t)$ in (5-56) gives

$$\begin{aligned} y(t) &= C_1 x_{c1}(t) + C_2 x_{c2}(t) + C_3 x_{c3}(t) + C_4 x_{c4}(t) \\ &= C_1 \left(-\frac{C_2^{(1)}}{C_1^{(1)}} x_{c2}(t) - \frac{C_3^{(1)}}{C_1^{(1)}} x_{c3}(t) - \frac{C_4^{(1)}}{C_1^{(1)}} x_{c4}(t) \right) + C_2 x_{c2}(t) + C_3 x_{c3}(t) + C_4 x_{c4}(t) \\ &= \tilde{C}_1 x_{c1}(t) + \tilde{C}_2 x_{c2}(t) + \tilde{C}_3 x_{c3}(t) + \tilde{C}_4 x_{c4}(t) \\ &= \tilde{\mathbf{C}} x_c(t) \end{aligned}, \tag{5-59}$$

where $\mathbf{C} = \begin{bmatrix} C_1 & C_2 & C_3 & C_4 \end{bmatrix} = \begin{bmatrix} 7.367 & 0.2714 & 0.003582 & -6 \times 10^{-5} \end{bmatrix}$ and $\tilde{\mathbf{C}} = \begin{bmatrix} 0 & -C_1 \frac{C_2^{(1)}}{C_1^{(1)}} + C_2 & -C_1 \frac{C_3^{(1)}}{C_1^{(1)}} + C_3 & -C_1 \frac{C_4^{(1)}}{C_1^{(1)}} + C_4 \end{bmatrix}$. Then, substituting (5-58) and (5-59) into the performance index J in (5-20) with $\mathbf{Q} = \mathbf{I}$ results in $S(t) = 0$ and

$$\begin{aligned} J &= \int_0^\infty \left[y^T(t) y(t) + u_c^T(t) R u_c(t) \right] dt \\ &= \int_0^\infty \left[x_c^T(t) \hat{\mathbf{Q}} x_c(t) + u_c^T(t) R u_c(t) \right] dt \end{aligned}, \tag{5-60}$$

where $\tilde{\mathbf{Q}} = \tilde{\mathbf{C}}^T \tilde{\mathbf{C}} = \begin{bmatrix} 0 & 0 & 0 & 0 \\ 0 & 0.0737 & -0.0338 & 0.0013 \\ 0 & -0.0338 & 0.0156 & -0.0006 \\ 0 & 0.0013 & -0.0006 & 0.00002 \end{bmatrix}$. The second optimal control gain in (5-25) for the second designed system in (5-26) with $R = 1$ and $\hat{\mathbf{Q}}$ in (5-60) yields

$$\mathbf{K}_c^{(2)} = \begin{bmatrix} 0 & 1.0860 & 0.0063 & 0.0043 \end{bmatrix}. \tag{5-61}$$

The total optimal gains $\mathbf{K}_c$ in (5-27) and $\mathbf{E}_c$ in (5-29)become

$$\begin{aligned}\mathbf{K}_c &= \mathbf{K}_c^{(1)} + \mathbf{K}_c^{(2)} = \begin{bmatrix} 2.9246 & 8.3981 & 0.0089 & 0.0059 \end{bmatrix} \\ \mathbf{E}_c &= 100.6771 \end{aligned}. \tag{5-62}$$

The eigenvalues of the optimally designed sliding mode controlled system $\mathbf{A}_c$ are $\{ -1.2437 \pm 12.7063i, -2.7421 \pm 67.4308i \}$. To determine the modified sliding surface $S_e(t)$ in design step 3, we choose $d_i = 0.9$ for $i = 1, \cdots, 4$ and the $j = 2$ in the $sign_j(S_e(t))$. A full order Kalman observer is also designed to approximate the system states. The observer gain was calculated as $\mathbf{L} = \begin{bmatrix} 0.99 & 33.43 & 485.47 & 85130.03 \end{bmatrix}^T$.

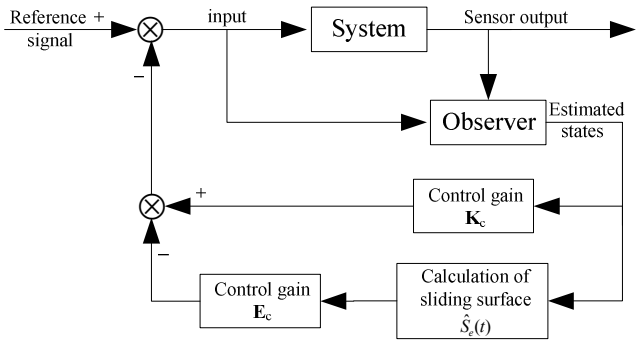

Figure 5-15 Block diagram of control system

The block diagram of the control system is given by Figure 5-15. The block diagram of the noise-free original system in (5-56) and the optimally designed sliding mode control law in (5-62) are shown Figure 5-15.

5.5.1 Simulation Results

For controller implementation, a Simulink model was designed. First, the initial control gains were calculated as discussed in a previous section regarding the optimal sliding mode controller. The system vibrations were analyzed with and without control. They were excited for the first five seconds by applying the first modal frequency signal of 2.07 Hz to the system. After five seconds, the excitation signal was turned off and the control signal turned on.The simulations of various modal vibrations are shown in Figure

5-16, Figure 5-17 and Figure 5-18. The effectiveness of the controller can be seen in the above figures. It can be clearly seen that the vibration of the system was controlled effectively with optimal sliding mode controller, as compared to free vibration damping without control.

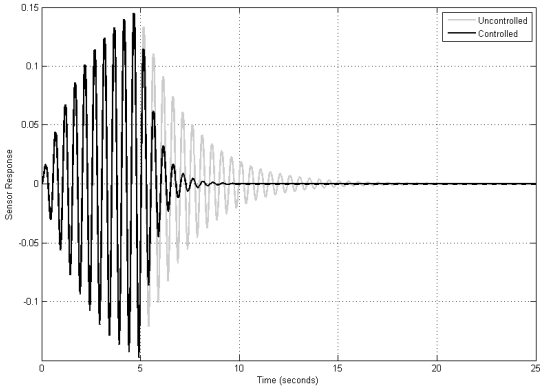

Figure 5-16 First Modal Vibrations

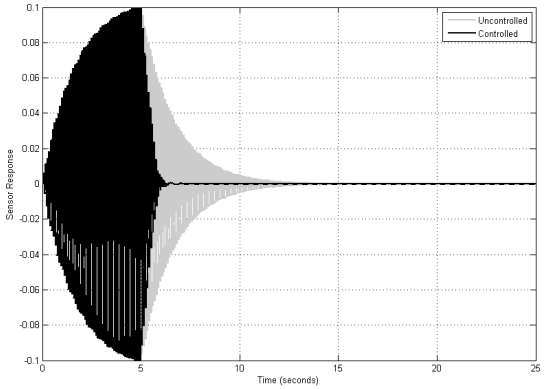

Figure 5-17 Second Modal Vibrations

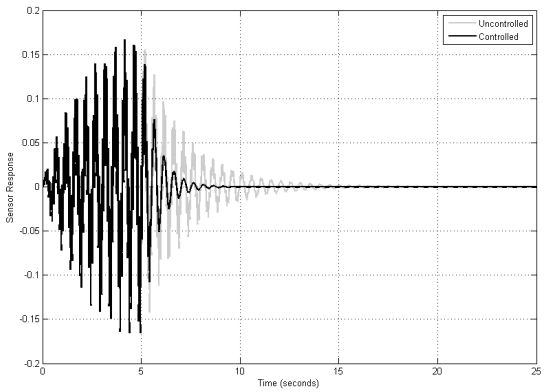

Figure 5-18 Multimodal Vibrations

5.5.2 Experimental Results

For controller implementation, a Simulink model was designed. First, the initial control gains were calculated as discussed in the above section regarding the optimal sliding mode controller. The system vibrations were analyzed with and without control. They were excited for the first five seconds by applying the first modal frequency signal of 2.07 Hz to the system. After five seconds, the excitation signal was turned off and the

control signal turned on. Sensor data was recorded for both with control and without control with a cut-off frequency of 30 Hz. A comparison between the first modal vibration with and without control is shown in Figure 5-19. A Power Spectrum Density (PSD) plot is also shown in Figure 5-20. The effectiveness of the controller can be seen in the above figures. It can be clearly seen that the first modal vibration of the system was controlled in approximately 5 seconds, as compared to more than 15 seconds in free vibration damping without control. The effectiveness of the controller can be seen in the PSD of the system. It can be seen that there is a reduction of around 30 dB for the first modal frequency.

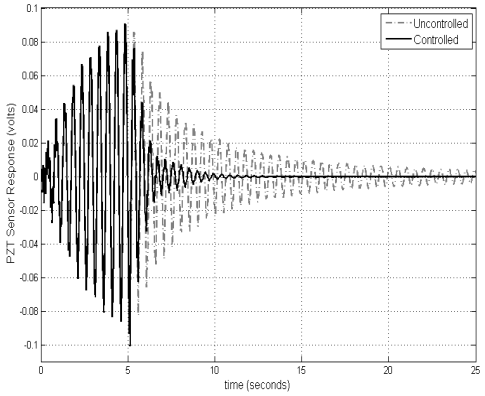

Figure 5-19 Vibration control for first modal frequency

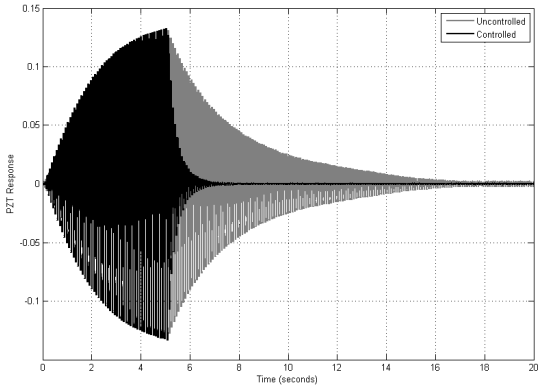

Figure 5-21 Vibration control for second modal frequency

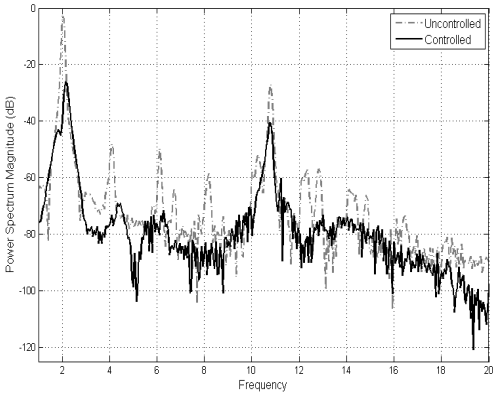

Figure 5-20 PSD comparison for First Modal Vibration Control

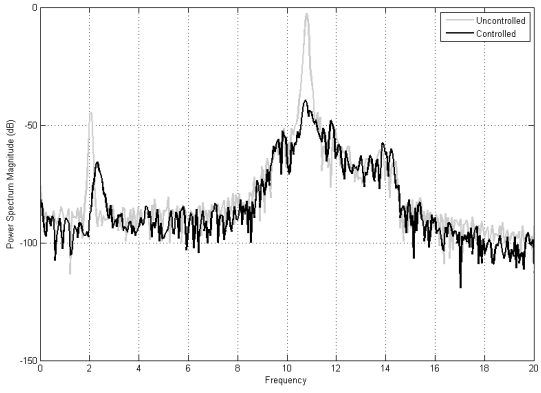

Figure 5-22 PSD comparison for vibration control for second modal frequency

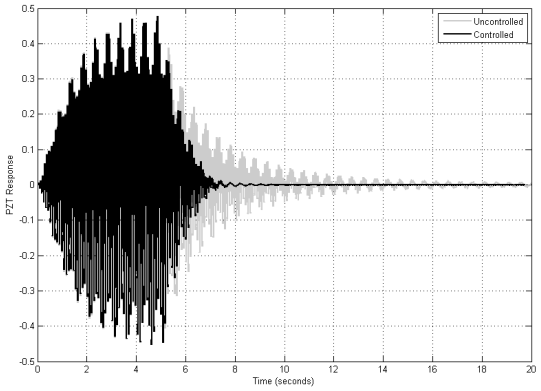

Figure 5-23 Vibration control for multimodal vibrations

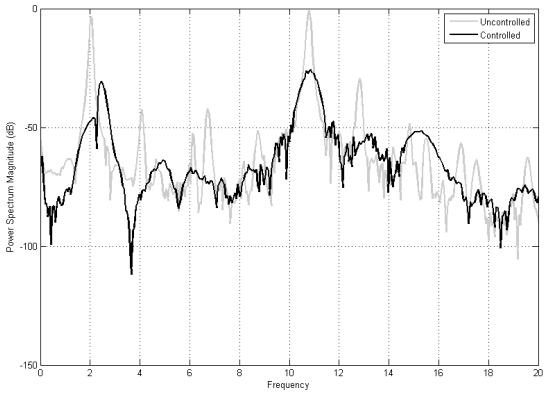

Figure 5-24 PSD comparison for multimodal vibrations with and without control

A multimodal vibration control test was also performed where the system was excited at its first two natural frequencies. The data was compared and shown in Figure 5-23. Again, the controller controlled the multimodal vibration in approximately 4 seconds, as compared to more than 10 seconds of free vibration. The PSD for multimodal vibration control is shown in Figure 5-24. It can be seen that with the optimal sliding mode controller, there is a reduction of 30 dB in the first modal frequency. In addition, the second modal frequency is almost cut off. To test the robustness of the optimal sliding mode controller, a test was performed by adding an uncertain mass to the beam tip. The system's first natural frequency shifted from 2.07 Hz to 1.85 Hz with the uncertain mass.

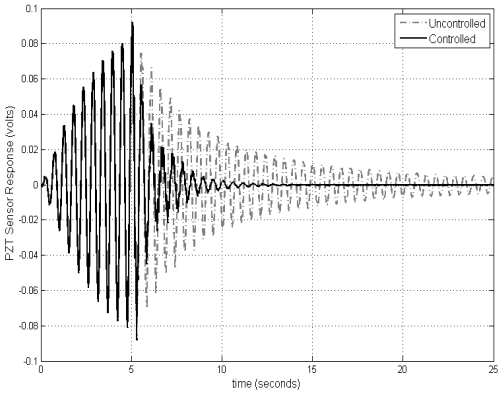

Figure 5-25: Vibration control with Mass Uncertainty

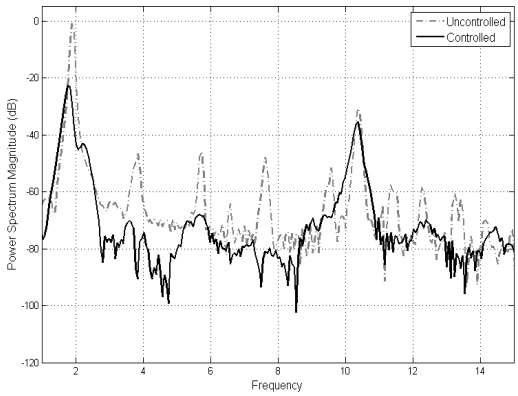

Figure 5-26: PSD plot of System with Mass Uncertainty

The frequency shift due to uncertain mass corresponds to approximately 25% of mass uncertainty. The tests were conducted in the same way as discussed before. First, the system was excited at its new natural frequency for five seconds. Then, control action was turned on. The performances of the controller in both tests are shown in Figure 5-25 and Figure 5-26. It can be seen from the response plot that the optimal sliding mode controller is robust enough to deal with the uncertainties in the system, as vibration can be suppressed in almost 5 seconds even with mass uncertainties.

5.6 Conclusions

In this chapter, a novel optimal sliding mode controller was presented. The scalar sign function approach was used to design the stable sliding surface. The proposed controller was successfully simulated on a single input single output system. The simulation results shows that control performance of the optimal sliding mode controller is better than the conventional sliding mode controller in terms of disturbance rejection and chattering alleviation of up to 71% for one state. The output convergence with optimal sliding mode controller used 34% less energy than the conventional sliding mode controller. Also, the stability of the proposed controller was proved using the energy function. The proposed optimal sliding mode controller was later implemented on the smart flexible beam experiment to suppress the multimodal vibrations of the beam. It was found that the proposed controller is able to suppress the beam's multimodal vibrations effectively. The power spectrum plots show that the optimal sliding mode controller provides approximately 30dB reduction for the first modal vibrations. The controller was successfully tested on the smart beam with constructive mass uncertainty up to 25% of the total mass of the beam and provides approximately about 25dB reduction.

Chapter 6. Robust H_∞ based Optimal Sliding Mode Control

The sliding mode controller is known for its robustness to matched or structured uncertainty. However, for the mismatched or unstructured uncertainty, the sliding mode controller does not guarantee the stability of the controlled system [102]. For unmatched uncertainties, H_∞ norm based approach is always preferred, as the H_∞ norm based approach considers the worst case scenario of an uncertain system for control objectives. Many researchers have used H_∞ approach for effective attenuation of disturbance and in dealing with matched and unmatched uncertainties in the system [103]. In this chapter, a robust state-feedback based optimal sliding mode controller is described as an extension of the previously explained optimal sliding mode controller with LQR approach. The new sliding mode controller guarantees its stability by H_∞ norm.

6.1 Introduction

For matched uncertainties, the sliding mode control approach always stands out among the best approaches. However, for unmatched uncertainties, the control law does not guarantee stability. Many researchers are working on dealing with the issues by employing different approaches with the sliding mode approach [104-107], for example the adaptive approach, reduced order matching and back-stepping design to relax the matching of uncertainties. However, these techniques have some requirements to be fulfilled or have some tradeoffs [102]. The optimal sliding mode controller with the LQR approach discussed in the previous chapter proves only the asymptotic stability of the control system with matched uncertainty. It was proved that the system is robust enough to deal with structural uncertainties. However, for unstructured uncertainties or unmatched

uncertainties which are unknown to the systems, the prescribed degree of stability cannot be proved [108].

In this chapter, the extension of optimal sliding mode controller is discussed for systems with unmatched uncertainties. The first part of the optimal control can be designed with H_∞ approach rather than the LQR approach by taking into account the unmatched properties. The stability of the system is defined with H_∞ norm of the system. The controller is designed based on the hypothesis that if there exists a finite H_∞ norm for the closed loop system i.e., $\left\| T(j\omega) \right\|_\infty < \gamma$ than the system is stable, where T is the transfer function of the closed loop system with respect to the unstructured uncertain input. In the following section, the development of the robust optimal sliding mode controller is discussed. The proposed approach is compared with a conventional sliding mode controller and its performance is evaluated.

6.2 Optimal Sliding Mode Controller for an Uncertain System

Given an uncertain system as

$$\begin{aligned} \dot{x}(t) &= (\mathbf{A} + \Delta\mathbf{A})x(t) + \mathbf{B}u(t) + \mathbf{G_0}w_0(t) \\ y(t) &= \mathbf{C}x(t) + \mathbf{s}v(t) \end{aligned}, \tag{6-1}$$

the selected output to be regulated as

$$z(t) = \begin{bmatrix} \mathbf{H_0}x(t) \\ u(t) \end{bmatrix}, \tag{6-2}$$

where $x(t)$ is the state, $u(t)$ is the control input, $y(t)$ is the measured output, $w_0(t)$ and $v(t)$ are the input and output disturbances, respectively, and $z(t)$ is the controlled output. The initial conditions are $x(0) = \alpha$. The pair $(\mathbf{A}, \mathbf{B})$ and $(\mathbf{A}, \mathbf{H_0})$ are assumed to be

controllable and observable, respectively. Also, the pair $(\mathbf{A},\mathbf{C})$ is observable. The bounded structured uncertainty can be written as

$$\Delta\mathbf{A} = \Delta\mathbf{E} = \mathbf{G}_1 \Delta \mathbf{H}_1 . \tag{6-3}$$

where $\Delta = \pm 1$ and $\mathbf{E}$ is matrix involving the uncertain parameters of the system. To find $\mathbf{G}_1$ and $\mathbf{H}_1$ in (6-3), the $\mathbf{G}_1$ can be chosen as a non-zero column vector of $\mathbf{E}$ and $\mathbf{H}_1$ can be calculated as

$$\mathbf{H}_1 = (\mathbf{G}_1^{\mathrm{T}}\mathbf{G}_1)^{-1}\mathbf{G}_1^{\mathrm{T}}\mathbf{E} . \tag{6-4}$$

The uncertain system in (6-1) can be alternatively represented by an extended system as

$$\begin{aligned} \dot{x}(t) &= \mathbf{A}x(t) + \mathbf{B}u(t) + \hat{\mathbf{G}}\hat{w}(t) \\ y(t) &= \mathbf{C}x(t) + \mathbf{s}v(t) \\ \hat{z}(t) &= \begin{bmatrix} \hat{\mathbf{H}}x(t) \\ u(t) \end{bmatrix} \end{aligned} , \tag{6-5}$$

where $\hat{\mathbf{G}} = \begin{bmatrix} \mathbf{G}_0 & \mathbf{G}_1 \end{bmatrix}, \hat{w} = \begin{bmatrix} w_0(t) & w_1(t) \end{bmatrix}, \hat{\mathbf{H}}^{\mathrm{T}} = \begin{bmatrix} \mathbf{H}_0^{\mathrm{T}} & \mathbf{H}_1^{\mathrm{T}} \end{bmatrix}$. The robust state-feedback control law,

$$u(t) = -\mathbf{K}_{\mathbf{c}}^{(1)} x(t) , \tag{6-6}$$

can be designed from the extended system in (6-5), such that it will stabilize the uncertain system in (6-1) and the closed loop transfer function $T(s)$ from $w_0(t)$ to $z(t)$ satisfies $\left\| T(j\omega) \right\|_\infty \le \gamma$ [109], where $T(s) = \begin{bmatrix} \mathbf{H}_0 \\ \mathbf{H}_1 \end{bmatrix} [s\mathbf{I} - \mathbf{F}]^{-1} \mathbf{G}_0, \mathbf{F} = \mathbf{A} + \Delta\mathbf{A} - \mathbf{B}\mathbf{K}_{\mathbf{c}}^{(1)}$ is a Hurwitz matrix. The feedback gain $\mathbf{K}_{\mathbf{c}}^{(1)}$ in (6-6) can be expressed as

$$\mathbf{K}_{\mathbf{c}}^{(1)} = \mathbf{B}^{\mathrm{T}}\mathbf{P}_1 , \tag{6-7}$$

where $\mathbf{P}_1 > 0$ is solved from the following Riccati equation,

$$\mathbf{P_1 A} + \mathbf{A}^{\mathrm{T}}\mathbf{P_1} + \mathbf{P_1}\left(\frac{1}{\gamma^2}\hat{\mathbf{G}}\hat{\mathbf{G}}^{\mathrm{T}} - \mathbf{B}\mathbf{B}^{\mathrm{T}}\right)\mathbf{P_1} + \hat{\mathbf{H}}^{\mathrm{T}}\hat{\mathbf{H}} = \mathbf{0}\,. \tag{6-8}$$

The stable closed loop system can be described as

$$\begin{aligned} \dot{x}(t) &= \mathbf{A}_{\mathbf{c}}^{(1)} x(t) + \mathbf{G_0} w_0(t) \\ y(t) &= \mathbf{C} x(t) + \mathbf{s} v(t) \end{aligned}, \tag{6-9}$$

where $\mathbf{A}_{\mathbf{c}}^{(1)} = \mathbf{A} + \frac{1}{\gamma^2}\hat{\mathbf{G}}\hat{\mathbf{G}}^{\mathrm{T}} - \mathbf{B}\mathbf{K}_{\mathbf{c}}^{(1)}$.

The dynamic system in (6-9) can be considered as a conventional system, from which the control law can be designed. The states can be estimated using the Kalman filter. The system in (6-9) can be used to design the sliding surface and second control law using the Equations (5-22) to (5-37).

So the final control law can be described as

$$\mathbf{u}(t) = -\mathbf{K}_{\mathbf{c}}\mathbf{x}(t) + \mathbf{E}_{\mathbf{c}} sign_j(\mathbf{S}_{\mathbf{e}}(t))\,, \tag{6-10}$$

where $\mathbf{K}_{\mathbf{c}} = \mathbf{K}_{\mathbf{c}}^{(1)} + \mathbf{K}_{\mathbf{c}}^{(2)}$, and $\mathbf{K}_{\mathbf{c}}^{(1)}$ can be calculated from (6-7**)** and $\mathbf{K}_{\mathbf{c}}^{(2)}$ can be calculated using (5-23), (5-24) and (5-25). $\mathbf{E}_{\mathbf{c}}$ is the optimal tracking gain for the tracking of the sliding surface and can be calculated from (5-29). $\mathbf{S}_{\mathbf{e}}(t)$ is the desired sliding surface calculated using the robust stable system $\mathbf{A}_{\mathbf{c}}^{(1)}$. The desired sliding surface $\mathbf{S}_{\mathbf{e}}(t)$ can be designed using Equations (5-12), (5-14) and (5-15).

The stability of the proposed robust controller can also be explained in a way similar to that described in chapter 4, from Equations (5-39) to (5-45). The proposed robust controller is tested on an uncertain system. The simulation results of the proposed controller are compared with the simulation results of a conventional sliding mode controller.

6.3 Simulation Example

Given the uncertain system as

$$\dot{x}_c(t) = (A + \Delta A)x_c(t) + Bu_c(t) + G_0\omega_0(t), \tag{6-11}$$

the selected output to be regulated is

$$z(t) = \begin{bmatrix} H_0 x_c(t) \\ u_c(t) \end{bmatrix}. \tag{6-12}$$

The measured output is

$$y(t) = Cx_c(t) + \eta_0(t), \tag{6-13}$$

where $\omega_0(t)$ and $\eta_0(t)$ are independent white noise disturbances. In an illustrative example, we select the initial conditions as $x_0 = [0.5 \;\; 0.5 \;\; 0.5]^T$.

The pairs (A, B) and (A, H_0) are assumed to be controllable and observable, respectively. In addition, the pair (A, C) is observable. In this example

$$A = \begin{bmatrix} 0 & 1 & 0 \\ 0 & 0 & 0 \\ 0 & 0 & 0 \end{bmatrix},\; B = \begin{bmatrix} 0 & 0 \\ 1 & 0 \\ 0 & 1 \end{bmatrix},\; G_0 = \begin{bmatrix} 0 \\ 0.1 \\ 0 \end{bmatrix},\; H_0 = q \cdot \mathbf{I}_3,\; C = \begin{bmatrix} 1 & 0 & 1 \\ 0 & 1 & 1 \end{bmatrix}.$$

The matched uncertain matrix ΔA is given by

$$\Delta A = \bar{\Delta} \begin{bmatrix} 0 & 0 & 0 \\ -\Delta k & 0 & \Delta k \\ \Delta k & 0 & -\Delta k \end{bmatrix} = \bar{\Delta} E = G_1 \bar{\Delta} H_1, \tag{6-14}$$

where $q = 10,\; \bar{\Delta} = \pm 1,\; \Delta k = 0.5$, Δk is the variation of the constant, and $rank(E) = 1$. To find G_1 and H_1 in (6-14), we choose G_1, a non-zero column vector of E, as $G_1 = [0 \quad -\Delta k \quad \Delta k]^T$.

Then, the non-zero row vector H_1 can be determined from E as $H_1 = \begin{bmatrix} 1 & 0 & -1 \end{bmatrix}$. The uncertain system in (6-11) can be alternatively represented by an extended system [109] as

$$\begin{aligned} \dot{x}_c(t) &= Ax_c(t) + Bu_c(t) + \hat{G}\hat{\omega}(t) \\ z(t) &= \begin{bmatrix} \hat{H}x_c(t) \\ u_c(t) \end{bmatrix} \\ y(t) &= Cx_c(t) + \eta_0(t) \end{aligned}, \tag{6-15}$$

where $\hat{G} = \begin{bmatrix} G_0 & G_1 \end{bmatrix} = \begin{bmatrix} 0 & 0 \\ 0.1 & -0.5 \\ 0 & 0.5 \end{bmatrix}$, $\hat{H} = \begin{bmatrix} H_0 \\ H_1 \end{bmatrix} = \begin{bmatrix} 10 & 0 & 0 \\ 0 & 10 & 0 \\ 0 & 0 & 10 \\ 1 & 0 & -1 \end{bmatrix}$ and $\hat{\omega}^T = \begin{bmatrix} \omega_0(t) & \omega_1(t) \end{bmatrix}$.

A robust state-feedback control law from (6-6)

$$u_c(t) = -K_c^{(1)} x_c(t), \tag{6-16}$$

and its feedback gain $K_c^{(1)}$ in (6-16) can be expressed as

$$K_c^{(1)} = B^T P_1 = \begin{bmatrix} 20.135 & 24.635 & -12.399 \\ -9.121 & -12.399 & 21.381 \end{bmatrix},$$

where $P_1 > 0$ can be solved from the following Riccati equation,

$$\mathbf{P_1 A + A^T P_1 + P_1 \left(\frac{1}{\gamma^2} \hat{G}\hat{G}^T - BB^T \right) P_1 + \hat{H}^T \hat{H} = 0}, \tag{6-17}$$

where $\gamma = 0.75$. Substituting the robust state-feedback control law in (6-17) into (6-15) results in the stable closed-loop system as

$$\begin{aligned} \dot{x}_c(t) &= A_c^{(1)} x_c(t) + G_0 \omega_0(t) \\ y(t) &= Cx_c(t) + \eta_0(t) \end{aligned}, \tag{6-18}$$

where $A_c^{(1)} = A + \delta^{-2}\hat{G}\hat{G}^T P_1 - BK_c^{(1)} = \begin{bmatrix} 0 & 1 & 0 \\ -6.775 & -7.738 & -2.834 \\ -3.882 & -4.061 & -6.368 \end{bmatrix}$ and the eigen-values of $A_c^{(1)}$ are $\sigma\left(A_c^{(1)}\right) = \left[-9.956 \;\; -1.037 \;\; -3.112\right]$.

To obtain the sliding surface matrix $C^{(1)} \in \mathbf{R}^{2\times 3}$ such that $C^{(1)}M_1^{(1)} = 0_{2\times 1}$, where $M_1^{(1)}$ is the dominant eigenvector vector associated with the dominant eigenvalue $\lambda_1^{(1)} = -1.037$, we compute the following two matrices:

$$M = \frac{1}{2}\left[\operatorname{sign}\left(A_c^{(1)} + \hat{h}_2\mathbf{I}_3\right) - \operatorname{sign}\left(A_c^{(1)} + \hat{h}_1\mathbf{I}_3\right)\right] = \begin{bmatrix} 1.308 & 0.288 & -0.153 \\ -1.357 & -0.299 & 0.159 \\ 0.081 & 0.018 & -0.009 \end{bmatrix},$$

$$N = \frac{1}{2}\left[\operatorname{sign}\left(A_c^{(1)} + \hat{h}_2\mathbf{I}_3\right) + \operatorname{sign}\left(A_c^{(1)} + \hat{h}_1\mathbf{I}_3\right)\right] = \begin{bmatrix} 0.308 & 0.288 & -0.153 \\ -1.357 & -1.299 & 0.159 \\ 0.081 & 0.018 & -1.009 \end{bmatrix},$$

where $\hat{h}_1 = 0,\ \hat{h}_2 = 2$. Next, the associated dominant eigenvector vector $\mathbf{M_1^{(1)}} \in \mathbf{R}^{3\times 1}$ is chosen and the non-dominant eigenvector matrix $\mathbf{M_2^{(1)}} \in \mathbf{R}^{3\times 2}$ from *M* and *N*, respectively. Then, we construct the Hermitian matrix $H = \left[\mathbf{M_1^{(1)}} \quad \mathbf{M_2^{(1)}}\right]$ and its inverse matrix *V* as

$$V \triangleq H^{-1} = \left[M_1^{(1)}M_2^{(1)}\right]^{-1} = \begin{bmatrix} 4.571 & 1 & -0.532 \\ -1 & -0.964 & 0 \\ 0 & -0.060 & -1 \end{bmatrix} = \begin{bmatrix} V_1 \\ V_2 \end{bmatrix}, \qquad \text{(6-19)}$$

where $V_2 \triangleq C^{(1)} = \begin{bmatrix} -1 & -0.964 & 0 \\ 0 & -0.060 & -1 \end{bmatrix}$.

The desirable sliding surface equation can be expressed as

$$S(t) = C^{(1)}x_c(t) = \begin{bmatrix} -1 & -0.964 & 0 \\ 0 & -0.060 & -1 \end{bmatrix} x_c(t).$$

Solving $S(t)=0$ gives the constrained equations as $x_{c1}(t)=-1.098\times x_{c2}(t)$ and $x_{c3}(t)=0.097\times x_{c2}(t)$. Solving the constrained optimal tracking problem gives the weighting matrix $\hat{Q}=diag\{\ 0,\ 1.932,\ 0\ \}$ and $R=\mathbf{I}_2$. Then, the resulting optimal tracking control gain is $K_c^{(2)}=B^TP_2=\begin{bmatrix}-0.017 & 0.136 & -0.029\\ 0.030 & -0.029 & 0.013\end{bmatrix}$, where $P_2>0$ can be solved from the following Riccati equation,

$$\mathbf{A_c^{(1)T}P_2+P_2A_c^{(1)}+\hat{Q}-P_2BR^{-1}B^TP_2=0}. \tag{6-20}$$

The total sliding mode control law becomes

$$u_c(t)=-K_cx_c(t)+E_c\,\mathrm{sign}\left[S(t)\right], \tag{6-21}$$

where $\mathbf{K_c}=\begin{bmatrix}20.117 & 24.772 & -12.428\\ -9.090 & -12.428 & 21.394\end{bmatrix}$ and $\mathbf{E_c=-\left[C\left(A_c\right)^{-1}B\right]^{-1}}=\begin{bmatrix}6.757 & -3.951\\ 3.912 & 2.468\end{bmatrix}$,

and $\mathbf{A_c=A+\frac{1}{\gamma^2}\hat{G}\hat{G}^TP_1-BK_c}=\begin{bmatrix}0 & 1 & 0\\ -6.757 & -7.874 & -2.806\\ -3.912 & -4.032 & -6.380\end{bmatrix}$. The robust sliding mode controlled uncertain system is

$$\dot{x}_c(t)=\left(A+\frac{1}{\gamma^2}\hat{G}\hat{G}^TP_1\right)x_c(t)+Bu_c(t)+G_0\omega_0(t), \tag{6-22}$$

$$u_c(t)=-K_cx_c(t)+E_c\,\mathrm{sign}\left[S(t)\right], \tag{6-23}$$

$$S(t)=C^{(1)}x_c(t), \tag{6-24}$$

$$y_c(t)=Cx_c(t). \tag{6-25}$$

For comparison of the proposed approach with the conventional sliding model control (SMC) approach [8], we are using the nominal system (6-11) without considering noise and uncertainty with the same initial conditions and output functions. The

conventional sliding surface (denoted as $S_s(t)$) for the normal system in (6-11) has been determined in [8] as

$$S_s(t) = C_s^{(1)} x_s(t) = 0_{2\times 1}, \tag{6-26}$$

where $C_s^{(1)} = \begin{bmatrix} 1 & 1 & 0 \\ 0 & 0 & 1 \end{bmatrix}$ is denoted as the conventional sliding surface matrix and $x_s(t)$ is denoted as the corresponding state. The conventional sliding mode control law (denoted as $u_s(t)$) can be expressed [8] as

$$u_s(t) = -K_{eq} x_s(t) + E_{eq}\,\mathrm{sgn}\left[S_s(t)\right], \tag{6-27}$$

where $K_{eq} = \left(C_s^{(1)}B\right)^{-1} C_s^{(1)} A$, $E_{eq} = -\left(C_s^{(1)}B\right)^{-1}$ and $\mathrm{sgn}\left[S_s(t)\right] = \begin{cases} 1, \text{ if } S_s(t) > 0 \\ 0, \text{ if } S_s(t) = 0 \\ -1, \text{ if } S_s(t) < 0 \end{cases}$.

For fair comparison of the proposed SMC method with the conventional SMC method, which utilizes the normal system matrix $\mathbf{A}$ only, we consider the noise-free and uncertain-free normal system in (6-11) as

$$\begin{aligned} \dot{x}_c(t) &= A x_c(t) + B u_c(t), \\ z(t) &= \begin{bmatrix} H_0 x_c(t) \\ u_c(t) \end{bmatrix}, \\ y_c(t) &= C x_c(t), \end{aligned} \tag{6-28}$$

By utilizing the same design methodology for the robust controller design with $\hat{G} = 0$, $\hat{H} = H_0 = q \cdot \mathbf{I}_3$ and $q = 10$, we obtain the optimal sliding mode control law as

$$u_c(t) = -K_c x_c(t) + E_c sign_j\left(S_e(t)\right), \tag{6-29}$$

$$\mathbf{S_e}(t) = \mathbf{S}(t) - \mathbf{S}_i(t) = (\mathbf{C^{(1)}} - \mathbf{C_d})x(t) = \hat{\mathbf{C}}x(t), \tag{6-30}$$

where $\hat{\mathbf{C}} = \mathbf{C^{(1)}} - \mathbf{C_d} = \left[\left(1-d_1\right)C_1^{(1)}, \left(1-d_2\right)C_2^{(1)}, ..., \left(1-d_n\right)C_n^{(1)}\right]$, $d_i \approx sign_j^{\,2}((x_i))$ and $0 \le d_i \le 1$ for even values of j. for simplicity, $d_i = 0.9$ is chosen and $C^{(1)} = \begin{bmatrix} -1.005 & -1 & 0 \\ 0 & 0 & -1 \end{bmatrix}$, $K_c = \begin{bmatrix} 10 & 11.045 & 0 \\ 0 & 0 & 10 \end{bmatrix}$, $E_c = \begin{bmatrix} 10 & -10 \\ 0 & 10 \end{bmatrix}$ and $A_c = A - BK_c = \begin{bmatrix} 0 & 1 & 0 \\ -10 & -11.045 & 0 \\ 0 & 0 & -10 \end{bmatrix}$.

Let us define $u_c(t)$, $x_c(t)$ and $y_c(t)$ in the robustly controlled uncertain system in (6-15) be $u_{rc}(t)$, $x_{rc}(t)$ and $y_{rc}(t)$, respectively. Also, denote the respective $u_c(t)$, $x_c(t)$ and $y_c(t)$ in the optimally controlled normal system using the control law as given in (6-29) as $u_{oc}(t)$, $x_{oc}(t)$ and $y_{oc}(t)$.

6.4 Simulation Results

The performance of the robustly controlled uncertain system in (6-15), the conventional controlled normal system, and the optimally controlled normal system in (6-28) are shown in the following figures.

Figure 6-1 shows the comparison of states trajectories of the proposed optimal sliding mode controlled uncertain system with the proposed controller on an uncertainty free system and the conventional sliding mode controlled system. It can be seen that the proposed robust controller is very effective in dealing with uncertainties.

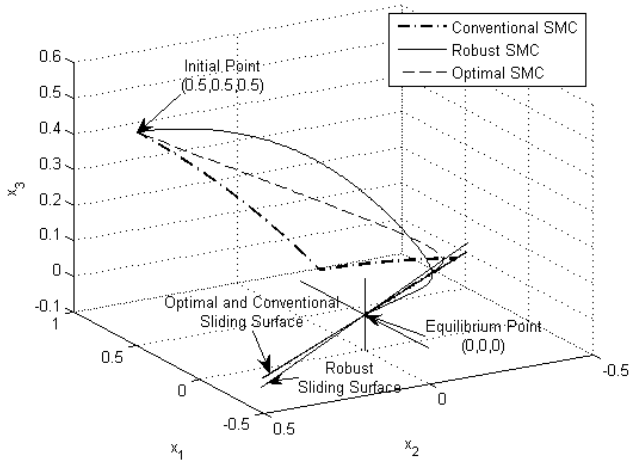

Figure 6-1 Trajectories of the sliding surface

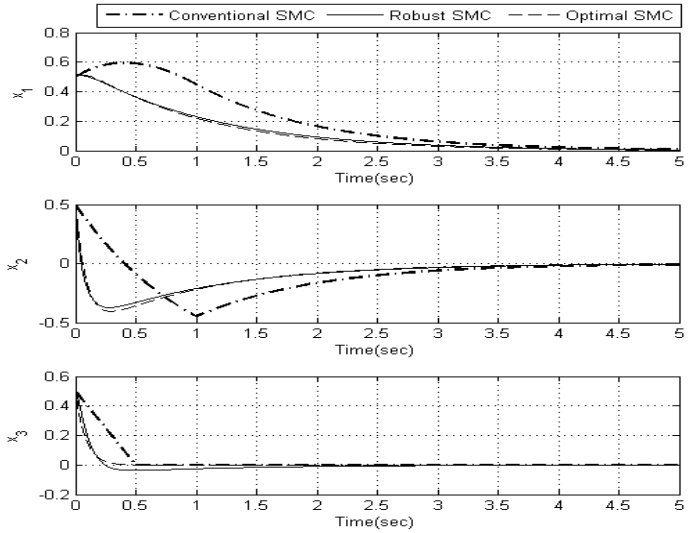

Figure 6-2 Comparison of states response

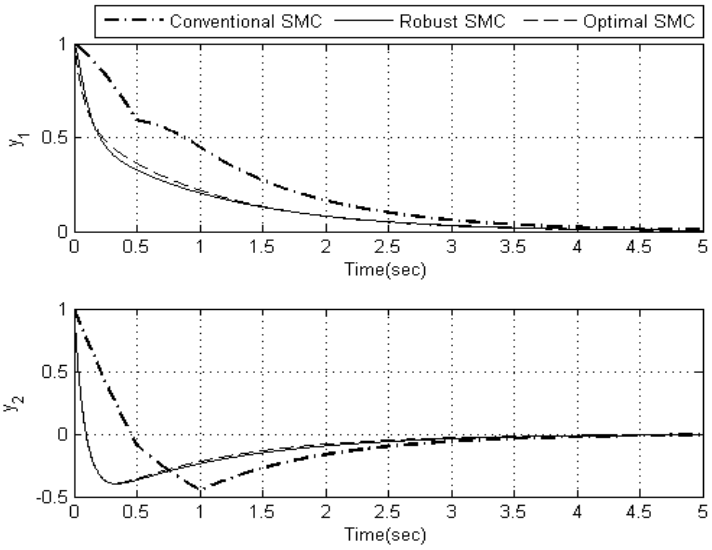

Figure 6-3 Comparison of output response

Figure 6-2-Figure 6-4 show the comparison among the states responses, output responses and the control inputs, respectively. The robust SMC refers to the proposed controller performance while considering the system uncertainties and optimal SMC refers to proposed controller without considering the uncertainties in the system. In Figure 6-2, the states responses are compared. It can be seen clearly that the proposed controller has much better performance than that of conventional sliding mode controller both with and without considering uncertainties.

In Figure 6-3, the output response of the system with these controllers is shown. It is clearly visible that output response of the uncertain system with the proposed robust controller is very much like the output response of the system without considering uncertainty and that both systems converge faster than that of the controlled by the conventional sliding mode controller. The comparison is further analyzed by comparing the energy ratios of the controllers.

The output energy ratios (denoted as r_{yj}) in percentage for $y_{ocj}(t)$ and $y_{sj}(t)$ as

$$r_{yj} = \frac{\left\| y_{ocj}(t) \right\|_2}{\left\| y_{sj}(t) \right\|_2} \times 100\% \quad \text{for} \quad j = 1, 2, , \tag{6-31}$$

where $y_{ocj}^T = \left[y_{ocj}(t_1), y_{ocj}(t_2), \cdots, y_{ocj}(t_N) \right]$, $y_{sj}^T = \left[y_{sj}(t_1), y_{sj}(t_2), \cdots, y_{sj}(t_N) \right]$ are energy usage for the conventional sliding mode controller and the proposed optimal sliding mode controller, respectively, and the sampling time is T = 0.001 seconds . According to (6-31), the percentage energy ratios are given by $r_{y1} = 162.23\%$ and $r_{y2} = 144.95\%$. Based on the computed energy ratios, it can be concluded that the conventional SMC consumes more energy than the proposed optimal SMC.

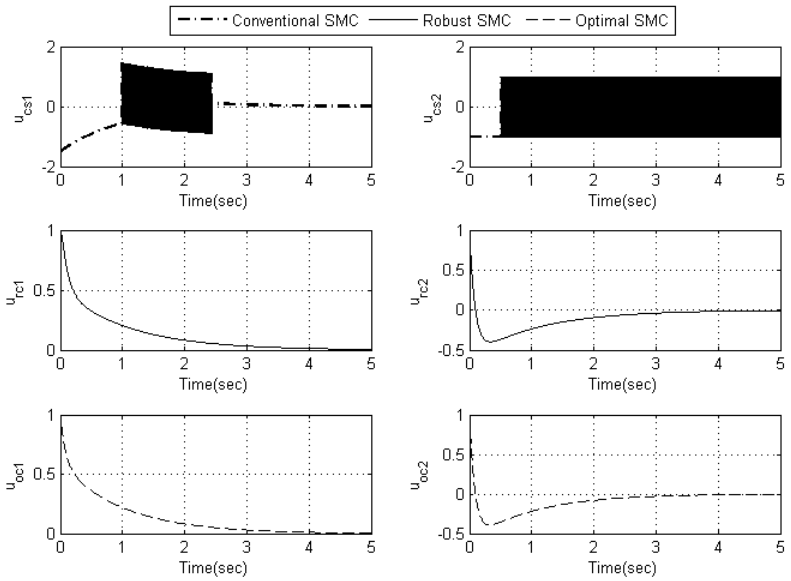

Figure 6-4 Comparison of control input generated by controller

Figure 6-4 shows the comparison of control inputs generated by the discussed sliding mode controllers. The chattering in the conventional controller is very much there however, the control inputs with the proposed sliding mode controller are much smoother. This observation proves that proposed strategy is very effective in chattering alleviation also.

To further test the performance of the proposed controller, the optimal sliding mode controller is implemented on a two story structure with an MR damper installed to control the vibrations of the structure under various earthquake excitations. While implementing the controller on the structure, the controller has to deal with the nonlinear behavior of the MR damper and the model uncertainties of the analytical model of the system. The next chapter describes the implementation and results of the proposed implemented controller to control the vibrations of structures under Kobe, El-Centro and the Northridge earthquake excitation signals.

Chapter 7. Vibration control of Base Isolated Structure with MR Damper using Optimal Sliding Mode Controller

The previous chapter explained the development of the robust optimal sliding mode controller. The simulation results showed that the proposed control approach is very effective in dealing with uncertainties. In this chapter, the robust optimal control approach is implemented on a base isolated two story structure. Nonlinear MR damper is used to control the vibrations of the structure. The nonlinearity of MR damper is used as the matched uncertainty of the system. The system is placed on a shaker table and the earthquake excitation signals are provided to the base of the structure as the external disturbances. This external disturbance is treated as the unmatched uncertainty to the structure. This chapter discusses about the implementation of proposed approach and its ability to reject the effects of uncertainties. The experimental results show that the proposed strategy controls the vibrations of the structure very effectively and, also at the same time, proves its robustness to the uncertainties.

7.1 Introduction and Literature Review

Despite their nonlinear behavior, MR dampers have been used in many vibration control applications such as car suspension systems, medical prosthetic joints and base isolation systems [110-112]. Especially, for base isolation systems, MR dampers have been used to yield better performance through semi-active control techniques [113]. Many different types of controller have been implemented on vibration control of base isolation systems with MR dampers [114]. Yoshioka *et al.* have implemented the H_2/LQG approach with clipped optimal approach on vibration control of base isolated structures [115]. In their approach, the researchers used the Bouc-Wen model to approximate the

nonlinearities of the MR damper. Shirazi *et al.* implemented a linear parameter varying (LPV) approach based semi-active controller [116]. In their research, they compared the LuGre model with the modified Bingham model.

Many different models for nonlinear MR fluids behavior have been discussed such as LuGre [111], Bingham [81], Bouc-Wen and Polynomial models [117]. To employ these models in control algorithms, parameter identification is required. An alternative approach is to use genetic algorithms [118], neural networks [119], adaptive laws [120] and fuzzy logic based approaches [121] to determine the nonlinear dynamic effects of the MR damper on the control system.

In this chapter, the optimal sliding mode controller for uncertain systems approach discussed in the previous chapter is implemented on a base isolated two-story structure under various earthquake signals. The nonlinear behavior of MR dampers is used as the matched uncertainty and earthquake signal excitation is used as an unknown external disturbance or unmatched frequency. The controller performance is later compared with passive control with MR damper and activated MR damper at different power levels. The chapter consists of a system description, development of the optimal controller followed by results and conclusions.

7.2 System Description

The nonlinear experimental setup for the MR damper and two story structure is shown in Figure 7-1. The experimental setup consists of the following major parts: the shaking table and its driving components, a two-story model building, the MR damper, and sensors for displacement and acceleration measurements. Customized earthquake wave signals from real earthquakes are provided for Shaker II (1-D shaker table) from

Quanser. MEMS Accelerometers (ADXL203EB) from Analog Devices are attached at the base floor, middle and top floor for vibration measurement. Also laser sensors (LB-70) from Keyence are used to measure the displacement of each floor.

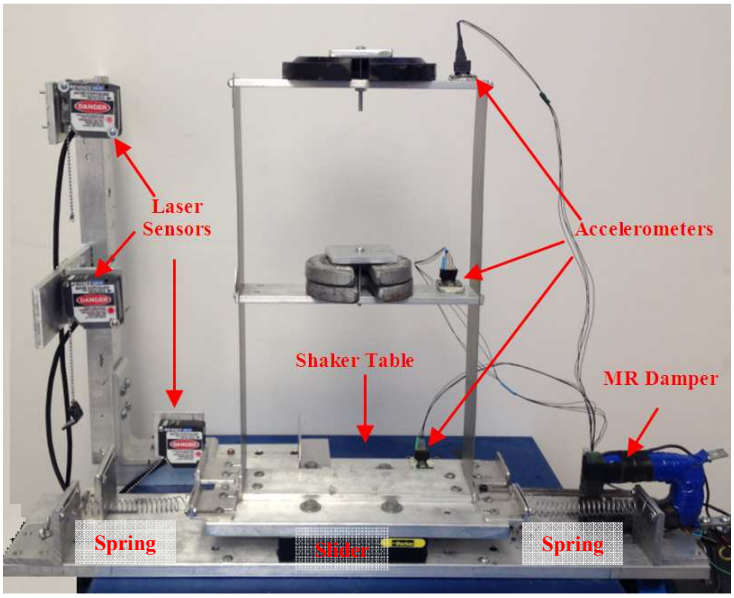

Figure 7-1: Experimental Setup

The MR damper under study is a custom-made device in the Smart Material and Structure Laboratory (SMSL) at the University of Houston. The damper consists of a magnetic coil, MR fluid and a sliding bar. The coil is excited by the voltage applied to the MR damper which increases the viscosity of the MR fluid and consequently the force exerted on the sliding bar. The structure is supported by a slider with low friction for base isolation of the two story structure. Two springs of equivalent stiffness of 338.5 N/m are connected to the base floor of the base isolated structure to restrict the base drift. The mass and spring matrices of the two story structure are $\mathbf{M} = \begin{bmatrix} 1.958 & 0 & 0 \\ 0 & 1.258 & 0 \\ 0 & 0 & 1.212 \end{bmatrix} [kg]$ and $\mathbf{K} = \begin{bmatrix} 1587.1 & -1218.6 & 0 \\ -1218.6 & 2716.3 & -1497.7 \\ 0 & -1497.7 & 1497.7 \end{bmatrix} [N.s/m]$. The damping matrices are calculated using Rayleigh's method [122] to be

$$\mathbf{C} = \alpha_1 \mathbf{M} + \alpha_2 \mathbf{K} = \begin{bmatrix} 1.0426 & -0.6093 & 0 \\ -0.6093 & 1.5182 & -0.7489 \\ 0 & -0.7489 & 0.9030 \end{bmatrix}. \quad (7\text{-}1)$$

The constant $\alpha_1 = 0.1372$ and $\alpha_2 = 0.0005$ are calculated assuming that the damping ratio is 1% for all the modal frequencies.

The state space equation for the system will be

$$\dot{\mathbf{x}} = \begin{bmatrix} \mathbf{0} & \mathbf{I} \\ \mathbf{-M^{-1}K} & \mathbf{-M^{-1}C} \end{bmatrix} \mathbf{x} + \begin{bmatrix} \mathbf{0} & \mathbf{0} \\ \mathbf{-\Lambda} & \mathbf{M^{-1}\Gamma} \end{bmatrix} \begin{bmatrix} \ddot{x}_g \\ F_{mr} \end{bmatrix}, \quad (7\text{-}2)$$

where $\mathbf{x} = \begin{bmatrix} \mathbf{q} \\ \dot{\mathbf{q}} \end{bmatrix}$, $q = \begin{bmatrix} x_b & x_1 & x_2 \end{bmatrix}^T$ and $\mathbf{F_{mr}}$ is the control input (Force from MR damper). The distribution matrices $\mathbf{\Lambda}$ and $\mathbf{\Gamma}$ are defined as $\mathbf{\Lambda} = \begin{bmatrix} \mathbf{1} & \mathbf{1} & \mathbf{1} \end{bmatrix}^\mathbf{T}$ and $\mathbf{\Gamma} = \begin{bmatrix} \mathbf{-1} & \mathbf{0} & \mathbf{0} \end{bmatrix}^\mathbf{T}$. x_b, x_1 and x_2 denote the displacement of the base, middle floor and top floor, respectively, and $\ddot{x}_g$ is the ground acceleration due to earthquake. The matrices $\mathbf{M, C, K}$ are the mass matrix, damping matrix and stiffness matrix of the system, respectively. The natural frequencies of the structure are 0.5045 Hz, 4.69 Hz and 8.94 Hz, respectively, for the 1st, second and 3rd natural frequency.

The nominal base isolation system can be represented as

$$\dot{\mathbf{x}} = \mathbf{A}\mathbf{x} + \mathbf{B}F_{mr} + \mathbf{G_0}\ddot{x}_g, \quad (7\text{-}3)$$

where $\mathbf{A} = \begin{bmatrix} \mathbf{0} & \mathbf{I} \\ \mathbf{-M^{-1}K} & \mathbf{-M^{-1}C} \end{bmatrix}$, $\mathbf{B} = \begin{bmatrix} \mathbf{0} \\ \mathbf{M^{-1}\Gamma} \end{bmatrix}$, $\mathbf{G_0} = \begin{bmatrix} \mathbf{0} \\ \mathbf{-\Lambda} \end{bmatrix}$.

7.3 Control System Development

For the nonlinear MR damper, the modified Bingham model is used for the control system development [116], and is given as

$$F_{mr} = \left(f_a + f_b V\right)\mathrm{sgn}(\dot{x}_b) + \left(c_0 \dot{x}_b + c_{0v} \dot{x}_b V\right) e^{-\left(\frac{\dot{x}_b}{v_0}\right)^2}, \tag{7-4}$$

where the variables and parameters are defined as F_{mr} is the force generated by the MR damper to counter the motion, V is the input voltage, f_a is the Coulomb frictional passive force, f_b Coulomb frictional force influenced by voltage V, c_0 is the viscous damping coefficient and c_{0v} is the viscous damping coefficient influenced by the voltage V, v_o is normalized velocity. The force F_{mr} can be divided in to two parts such that

$$F_{mr} = f_a \,\mathrm{sgn}(\dot{x}_b) + c_0 \dot{x}_b e^{-\left(\frac{\dot{x}_b}{v_0}\right)^2} + \left(f_b \,\mathrm{sgn}(\dot{x}_b) + c_{0v} \dot{x}_b e^{-\left(\frac{\dot{x}_b}{v_0}\right)^2} \right) V, \tag{7-5}$$

or

$$F_{mr} = \square\, d_k \dot{x}_b + \hat{f}_{mrV} V, \tag{7-6}$$

where $\square\, d_k \dot{x}_b = f_a \,\mathrm{sgn}(\dot{x}_b) + c_0 \dot{x}_b e^{-\left(\frac{\dot{x}_b}{v_0}\right)^2}$ and $\hat{f}_{mrV} = f_b \,\mathrm{sgn}(\dot{x}_b) + c_{0v} \dot{x}_b e^{-\left(\frac{\dot{x}_b}{v_0}\right)^2}$.

From the Bingham model in (7-4), it can be seen that, apart from voltage applied, the force generated by the MR damper is influenced by the velocity of the base floor, which is one of the states of the system. The uncertain system under the effect of the MR damper and unmatched uncertainty for external input disturbance matrix, can be written as

$$\dot{\mathbf{x}} = (\mathbf{A} + \Delta\mathbf{A})\mathbf{x} + \mathbf{B}V + (\mathbf{G_0} + \Delta\mathbf{G_0})\ddot{x}_g, \tag{7-7}$$

or

$$\begin{bmatrix} \dot{x}_b \\ \dot{x}_1 \\ \dot{x}_2 \\ \ddot{x}_b \\ \ddot{x}_1 \\ \ddot{x}_2 \end{bmatrix} = \begin{bmatrix} 0 & 0 & 0 & 1 & 0 & 0 \\ 0 & 0 & 0 & 0 & 1 & 0 \\ 0 & 0 & 0 & 0 & 0 & 1 \\ a_{41} & a_{42} & a_{43} & a_{44} + \Delta d_k & a_{45} & a_{46} \\ a_{51} & a_{52} & a_{53} & a_{54} & a_{55} & a_{56} \\ a_{61} & a_{62} & a_{63} & a_{64} & a_{65} & a_{66} \end{bmatrix} \begin{bmatrix} x_b \\ x_1 \\ x_2 \\ \dot{x}_b \\ \dot{x}_1 \\ \dot{x}_2 \end{bmatrix} + \begin{bmatrix} 0 \\ 0 \\ 0 \\ \hat{f}_{mrV} \\ 0 \\ 0 \end{bmatrix} V + \begin{bmatrix} 0 \\ 0 \\ 0 \\ -1 + \Delta\mathbf{G_{01}} \\ -1 + \Delta\mathbf{G_{02}} \\ -1 + \Delta\mathbf{G_{03}} \end{bmatrix} \ddot{x}_g, \tag{7-8}$$

where $\Delta\mathbf{A} = \begin{bmatrix} 0 & 0 & 0 & 0 & 0 & 0 \\ 0 & 0 & 0 & 0 & 0 & 0 \\ 0 & 0 & 0 & 0 & 0 & 0 \\ 0 & 0 & 0 & \Delta d_k & 0 & 0 \\ 0 & 0 & 0 & 0 & 0 & 0 \\ 0 & 0 & 0 & 0 & 0 & 0 \end{bmatrix}$ is the matched uncertainty of the structure due to MR damper force. The uncertainty $\Delta d_k = (-2, 2)$ is assumed to cover the high uncertainty in the nominal system parameter. Also for the above system, the earthquake signal to the system through shaker table is considered as a random unknown external input disturbance. The matrix $\mathbf{G_0}$ is the input disturbance matrix. The matrix $\Delta\mathbf{G_0} = \begin{bmatrix} 0 & 0 & 0 & \Delta\mathbf{G_{01}} & \Delta\mathbf{G_{02}} & \Delta\mathbf{G_{03}} \end{bmatrix}^T$ can be treated as an unmatched uncertainty in the system model.

From Equation (6-3) and (6-4), the parameters $(\mathbf{G_1}, \mathbf{H_1})$ for the matched uncertainty of the system can be calculated. The uncertain matrix $\mathbf{G}_1 = \begin{bmatrix} 0 & 0 & 0 & 1 & 0 & 0 \end{bmatrix}^T$ is can be calculated that.

$$\mathbf{H_1} = \left(\mathbf{G_1^T G_1}\right)^{-1} \mathbf{G_1^T} \Delta\mathbf{A} = \begin{bmatrix} 0 & 0 & 0 & 2 & 0 & 0 \end{bmatrix}. \tag{7-9}$$

The selected output to be regulated is

$$z(t) = \begin{bmatrix} \mathbf{H_0} x(t) \\ V \end{bmatrix}, \tag{7-10}$$

where $H_0 = I \in \mathbf{R}^{6\times 6}$ so that all states of the system can be regulated.

Then, the non-zero row vector H_1 can be determined from E as $H_1 = \begin{bmatrix} 0 & 0 & 0 & 2 & 0 & 0 \end{bmatrix}$. The uncertain system in (7-7) can be alternatively represented by an extended system as

$$\begin{aligned}\dot{\mathbf{x}} &= \mathbf{A}\mathbf{x} + \mathbf{B}V + \hat{\mathbf{G}}\hat{\omega} \\ z(t) &= \begin{bmatrix} \hat{\mathbf{H}}\mathbf{x} \\ V \end{bmatrix}, \\ y(t) &= \mathbf{C}\mathbf{x}\end{aligned} \tag{7-11}$$

where $\hat{G} = \begin{bmatrix} G_0 & G_1 \end{bmatrix} = \begin{bmatrix} 0 & 0 \\ 0 & 0 \\ 0 & 0 \\ -1 & 1 \\ -1 & 0 \\ -1 & 0 \end{bmatrix}$, $\hat{H} = \begin{bmatrix} H_0 \\ H_1 \end{bmatrix} = \begin{bmatrix} 1 & 0 & 0 & 0 & 0 & 0 \\ 0 & 1 & 0 & 0 & 0 & 0 \\ 0 & 0 & 1 & 0 & 0 & 0 \\ 0 & 0 & 0 & 1 & 0 & 0 \\ 0 & 0 & 0 & 0 & 1 & 0 \\ 0 & 0 & 0 & 0 & 0 & 1 \\ 0 & 0 & 0 & 2 & 0 & 0 \end{bmatrix}$,

$\hat{\omega}^T = \begin{bmatrix} f(\dot{x}_b) & \ddot{x}_g \end{bmatrix}$ and $f(\dot{x}_b)$ is the uncertain effect of the MR damper force.

A robust state-feedback control law from (6-6)

$$u_c(t) = -K_c^{(1)} x_c(t), \tag{7-12}$$

and its feedback gain $K_c^{(1)}$ in (7-12) can be expressed as $K_c^{(1)} = B^T P_1 = [0.4635 \quad -1.1175 \quad 0.6819 \quad 0.0063 \quad -0.0145 \quad 0.0087] \times 10^4$, where $P_1 > 0$ can be solved from the following Riccati equation,

$$\mathbf{P_1 A} + \mathbf{A}^{\mathrm{T}}\mathbf{P_1} + \mathbf{P_1}\left(\frac{\mathbf{1}}{\boldsymbol{\gamma}^{\mathbf{2}}}\hat{\mathbf{G}}\hat{\mathbf{G}}^{\mathrm{T}} - \mathbf{B}\mathbf{B}^{\mathrm{T}}\right)\mathbf{P_1} + \hat{\mathbf{H}}^{\mathrm{T}}\hat{\mathbf{H}} = \mathbf{0}, \tag{7-13}$$

where $\gamma = 1$ for the bounded uncertainty. Substituting the robust state-feedback control law in (7-13) into (7-11) results in the stable closed-loop system as

$$\begin{aligned}\dot{\mathbf{x}}(t) &= \mathbf{A}_{\mathbf{c}}^{(\mathbf{1})}\mathbf{x}(t) + \hat{\mathbf{G}}\hat{\omega}(t) \\ y(t) &= \mathbf{C}\mathbf{x}(t)\end{aligned}, \tag{7-14}$$

where $A_c^{(1)} = A + \delta^{-2}\hat{G}\hat{G}^T P_1 - BK_c^{(1)}$ and the eigen-values of $A_c^{(1)}$ are

$$\sigma\left(A_c^{(1)}\right) = \begin{bmatrix} -0.1659 \pm 10.0652i \\ -0.2358 \pm 30.9215i \\ -0.7539 \pm 56.1894i \end{bmatrix}.$$

Now the $\gamma = 1$ is chosen to explain the stability of the controlled system for matched and unmatched uncertainties, so that $\left\|T(j\omega)\right\|_\infty \le \gamma$, where $T(s) = \begin{bmatrix} \mathbf{H_0} \\ \mathbf{H_1} \end{bmatrix}\left[s\mathbf{I} - \mathbf{F}\right]^{-1}(\mathbf{G_0} + \Delta\mathbf{G_0}), \mathbf{F} = \mathbf{A} + \Delta\mathbf{A} - \mathbf{BK_c^{(1)}}$. From the calculation of H_∞ norm of the closed loop system, $\gamma = 1$ is able to stabilize the system with uncertainty in $\mathbf{G_0}$.

Since, the displacement of all three floors $q = \begin{bmatrix} x_b & x_1 & x_2 \end{bmatrix}^T$ are to be controlled, the three states for displacement of each floor will be used to track the sliding surface. The output function is chosen as $y_1(t) = \begin{bmatrix} x_b & x_1 & x_2 \end{bmatrix}^T$.

To obtain the sliding surface matrix, $C^{(1)} \in \mathbf{R}^{3\times 6}$ is calculated such that $C^{(1)}M_1^{(1)} = 0_{3\times 1}$, where $M_1^{(1)}$ is the dominant eigenvector vectors associated with the dominant eigenvalues $\lambda^{(1)} = -0.1659 \pm 10.0652i, -0.2358 \pm 30.9215i$,

$$M = \frac{1}{2}\left[\operatorname{sign}\left(A_c^{(1)} + \hat{h}_2\mathbf{I}_6\right) - \operatorname{sign}\left(A_c^{(1)} + \hat{h}_1\mathbf{I}_6\right)\right] = \begin{bmatrix} 0.0270 & 0.0011 & 0.0045 & 0 & 0 & 0 \\ 0.0064 & 0.0226 & 0.0057 & 0 & 0 & 0 \\ 0.0064 & 0.0016 & 0.0275 & 0 & 0 & 0 \\ -0.0515 & 0.1028 & -0.0581 & 0.0271 & 0.0009 & 0.0046 \\ -0.0607 & 0.1210 & -0.0684 & 0.0065 & 0.0224 & 0.0058 \\ -0.0642 & 0.1277 & -0.0722 & 0.0065 & 0.0014 & 0.0276 \end{bmatrix},$$

$$N = \frac{1}{2}\left[\operatorname{sign}\left(A_c^{(1)} + \hat{h}_2\mathbf{I}_6\right) + \operatorname{sign}\left(A_c^{(1)} + \hat{h}_1\mathbf{I}_6\right)\right] = \begin{bmatrix} 1.0270 & 0.0011 & 0.0045 & 0 & 0 & 0 \\ 0.0064 & 1.0226 & 0.0057 & 0 & 0 & 0 \\ 0.0064 & 0.0016 & 1.0275 & 0 & 0 & 0 \\ -0.0515 & 0.1028 & -0.0581 & 1.0271 & 0.0009 & 0.0046 \\ -0.0607 & 0.1210 & -0.0684 & 0.0065 & 1.0224 & 0.0058 \\ -0.0642 & 0.1277 & -0.0722 & 0.0065 & 0.0014 & 1.0276 \end{bmatrix},$$

where $\hat{h}_1 = 0,\ \hat{h}_2 = 0.5$. Next, the associated dominant eigenvector vector $\mathbf{M_1^{(1)}} \in \mathbf{R}^{6\times 3}$ is chosen and the non-dominant eigenvector matrix $\mathbf{M_2^{(1)}} \in \mathbf{R}^{6\times 3}$ from *M* and *N*, respectively. Then, we construct the Hermitian matrix $H = \left[\mathbf{M_1^{(1)}} \quad \mathbf{M_2^{(1)}}\right]$ and its inverse matrix *V* as

$$V \equiv H^{-1} = \left[\mathbf{M_1^{(1)}} \quad \mathbf{M_2^{(1)}}\right]^{-1} = \begin{bmatrix} V_1 \\ V_2 \end{bmatrix}, \tag{7-15}$$

and $$V_2 \equiv C^{(1)} = \begin{bmatrix} 0.9737 & -0.0010 & -0.0043 & -0.0014 & 0.0015 & -0.0010 \\ 0.730 & 0.9780 & -0.0016 & -0.0016 & 0.0017 & -0.0011 \\ 0.0788 & -0.0014 & -0.0017 & -0.0017 & 0.0018 & -0.0012 \end{bmatrix}. \tag{7-16}$$

For the sliding surface design, any row of $C^{(1)}$ can be chosen from Equation (7-16). The desirable sliding surface equation can be expressed as

$$S(t) = C^{(1)}\mathbf{x}(t). \tag{7-17}$$

Solving $S(t) = 0$ gives the constrained equations as

$$\begin{bmatrix} x_b \\ x_1 \\ x_2 \end{bmatrix} = -\begin{bmatrix} C_{11}^{(1)} & C_{12}^{(1)} & C_{13}^{(1)} \\ C_{21}^{(1)} & C_{22}^{(1)} & C_{23}^{(1)} \\ C_{31}^{(1)} & C_{32}^{(1)} & C_{33}^{(1)} \end{bmatrix}^{-1} \begin{bmatrix} C_{14}^{(1)} & C_{15}^{(1)} & C_{16}^{(1)} \\ C_{24}^{(1)} & C_{25}^{(1)} & C_{26}^{(1)} \\ C_{34}^{(1)} & C_{35}^{(1)} & C_{36}^{(1)} \end{bmatrix} \begin{bmatrix} \dot{x}_b \\ \dot{x}_1 \\ \dot{x}_2 \end{bmatrix} = \mathbf{Z} \begin{bmatrix} \dot{x}_b \\ \dot{x}_1 \\ \dot{x}_2 \end{bmatrix}. \tag{7-18}$$

The constrained optimal tracking problem for displacement of each floor is

$$J = \int \left[\left(y_1(t) - S(t)\right)^T \mathbf{Q} \left(y_1(t) - S(t)\right) + u^T(t) R u(t) \right] dt, \tag{7-19}$$

where $y_1(t) = \begin{bmatrix} x_b(t) \\ x_1(t) \\ x_2(t) \end{bmatrix}$, $S(t) = C^{(1)}\mathbf{x}(t) = 0$, $u(t) = V$ is the control input, and $\mathbf{Q} = \mathbf{I}_6, R = 1$

. This implies that the Equations (7-18) and (7-19) can be rewritten as

$$J = \int \left[x_b^2 + x_1^2 + x_2^2 + V^2 \right] dt, \tag{7-20}$$

or $$J = \int \left(\mathbf{x}^{\mathrm{T}} \hat{\mathbf{Q}} \mathbf{x} + V^2 \right) dt , \tag{7-21}$$

where $\mathbf{x} = \begin{bmatrix} x_b & x_1 & x_2 & \dot{x}_b & \dot{x}_1 & \dot{x}_2 \end{bmatrix}^T$, $\hat{\mathbf{Q}} = \begin{bmatrix} 0_{3\times3} & 0_{3\times3} \\ 0_{3\times3} & \mathbf{Z}^{\mathrm{I}}\mathbf{Z} \end{bmatrix}$ and V is the control input. Then, the resulting optimal tracking control gain is $\mathbf{K}_{\mathbf{c}}^{(2)} = \mathbf{B}^{\mathrm{T}}\mathbf{P}_2 = \begin{bmatrix} 178.92 & -421.24 & 254.48 & 2.77 & -3.49 & 1.11 \end{bmatrix}$, where $\mathbf{P}_2 > 0$ can be solved from the following Riccati equation,

$$\mathbf{A}_{\mathbf{c}}^{(1)\mathrm{T}}\mathbf{P}_2 + \mathbf{P}_2\mathbf{A}_{\mathbf{c}}^{(1)} + \hat{\mathbf{Q}} - \mathbf{P}_2\mathbf{B}\mathbf{R}^{-1}\mathbf{B}^{\mathrm{T}}\mathbf{P}_2 = \mathbf{0} . \tag{7-22}$$

The total sliding mode control law becomes

$$u(t) = -\mathbf{K}_{\mathbf{c}} x_c(t) + \mathbf{E}_{\mathbf{c}} \operatorname{sign}\left[S_e(t) \right], \tag{7-23}$$

where $\mathbf{K}_{\mathbf{c}} = \mathbf{K}_{\mathbf{c}}^{(1)} + \mathbf{K}_{\mathbf{c}}^{(2)}$, $E_c = -\left[C\left(A_c\right)^{-1} B \right]^{-1} = 479.72$, and $S_e(t)$ can be calculated from (7-17) by referring to (5-30) to (5-36).

The closed loop system will be $\mathbf{A}_{\mathbf{c}} = \mathbf{A} + \frac{1}{\gamma^2}\hat{\mathbf{G}}\hat{\mathbf{G}}^{\mathrm{T}}\mathbf{P}_{\mathbf{1}} - \mathbf{B}\mathbf{K}_{\mathbf{c}}$.

The dSPACE DAQ DS1104 RD is used for data acquisition purposes. The optimal controller is implemented in Matlab/Simulink. An Agilent 6542A programmable power supply is used to activate the MR damper. The control voltage signal is provided from the dSPACE board to the power supply and processed through the controlled strategy built on Matlab/Simulink. The states of the system can be obtained from the displacement sensors and accelerometers. The experimental results are discussed in the following section.

7.4 Experimental Results

The optimal controller was implemented on the base isolated system. Earthquake signals, such as Kobe (0.3g), El-Centro (0.6g) and Northridge (0.6g), were used as

excitation signals. For practical consideration, a saturation block was placed to keep the control voltage saturated between 0 and 12 volts. In the following figures, the response of the system with optimal sliding mode controller is compared with the response of the system with the passive effect of the MR damper at 0 volts.

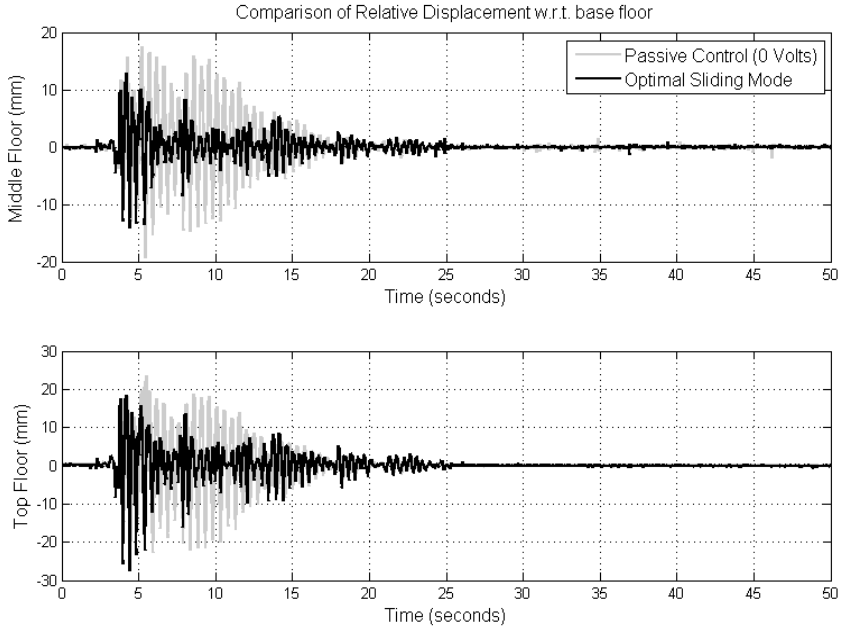

Figure 7-2 Relative Displacement of floors to El-Centro Earthquake (0.6g) Excitation

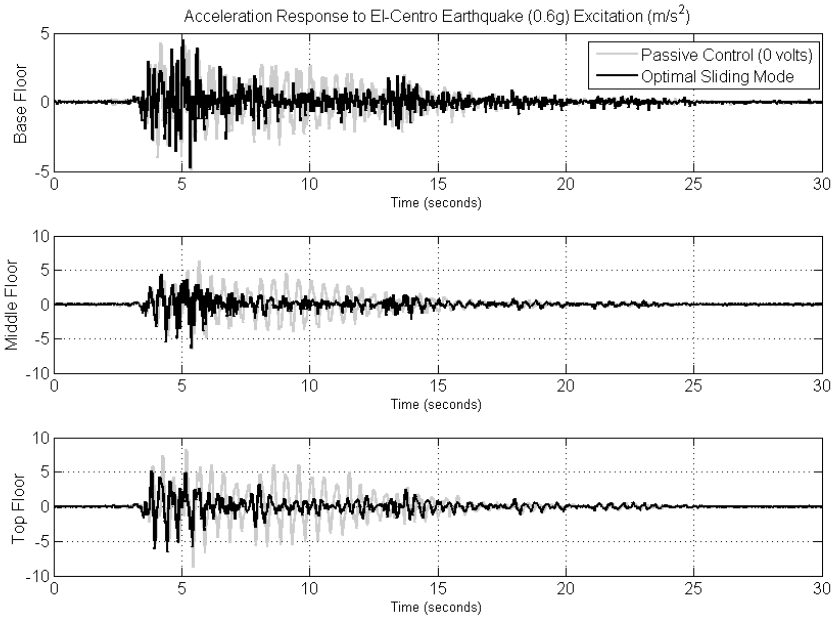

Figure 7-3 Acceleration Response with El-Centro Earthquake (0.6g) Excitation

In Figure 7-2, the comparison of the relative displacement of the middle and top floor with respect to the base floor is shown. It is very clear that the optimal sliding mode controller is very effective in controlling the relative displacement of the top and middle floor throughout the earthquake excitation. The relative displacement of the middle floor with respect to the base floor has about 48% displacement reduction and the top floor has an approximately 54% reduction in Root Mean Square (RMS) average response of the system. Also, the absolute maximum relative displacement for the middle floor has a 26% reduction in maximum absolute displacement and the top floor has a 16% of reduction of the peak value. In Figure 7-3, the acceleration data of each floor is shown. The reduction in peak values for the acceleration of each floor is, respectively, 2.5%, 2.23% and 25% for the base, middle and top floor. However, on analyzing the RMS average of the data, the reduction is approximately 33%, 40% and 46% for the base, middle and top floor respectively, which shows the effectiveness of the approach.

The performance of the proposed sliding mode controller was also evaluated using other earthquake signals such as the Kobe and Northridge earthquakes. The Kobe earthquake signal was scaled down to 0.3g level so that the base movement remains within the slider limits. The Northridge signal was also scaled down to 0.6g for the same reason. The responses for the displacements and acceleration of every floor have been shown in Figure 7-4-Figure 7-7. The effectiveness of the optimal control can be evaluated through these figures. It can be seen that the proposed control algorithm is very robust to system uncertainties and able to deal with external disturbances. A detailed analysis of the control performance is evaluated in Table 7-1 and Table 7.2. In Table 7-1, the percentage reduction in the RMS average of data for the optimal sliding mode controller is provided

in comparison with that of passive control (MR damper at 0 volts). In Table 7-2, the percentage reduction in peak values of displacement and accelerations of every floor is given.

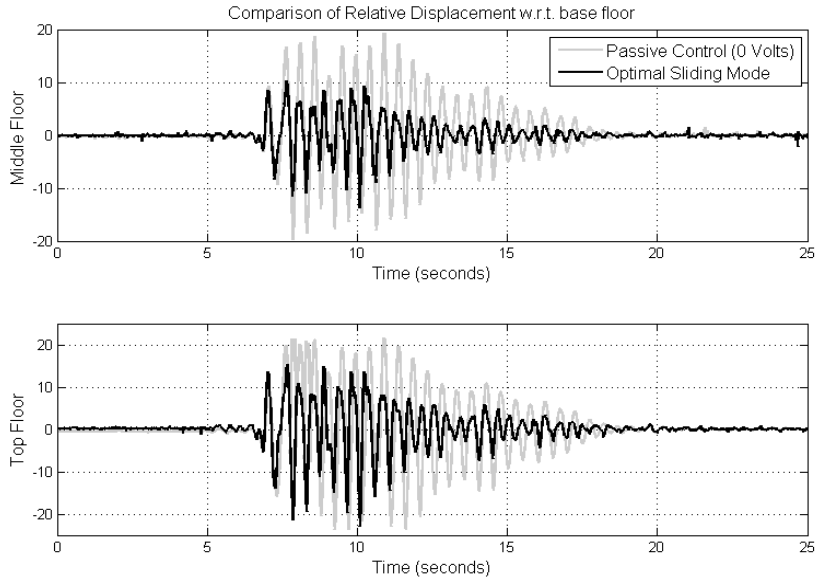

Figure 7-4 Relative Displacement of floors to Kobe Earthquake (0.3g) Excitation

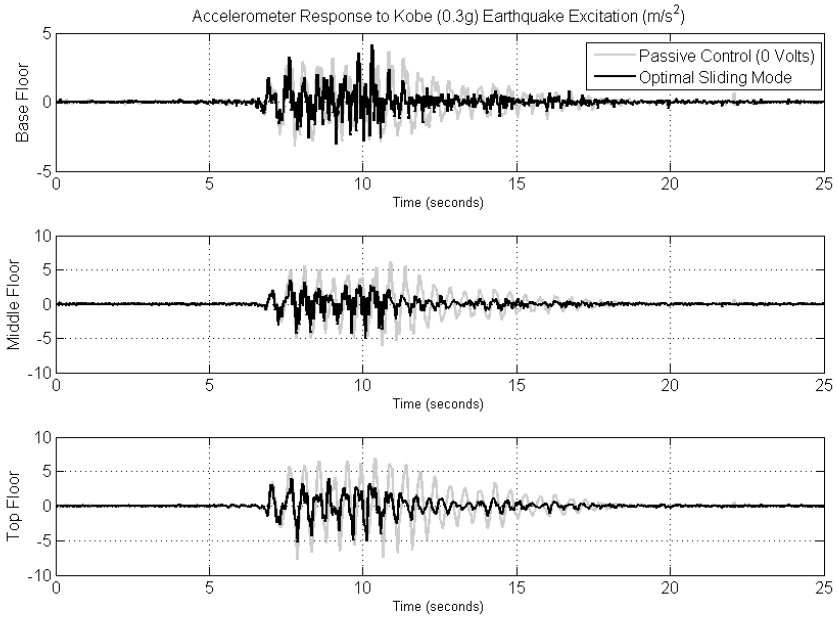

Figure 7-5 Acceleration Response with Kobe Earthquake (0.3g) Excitation

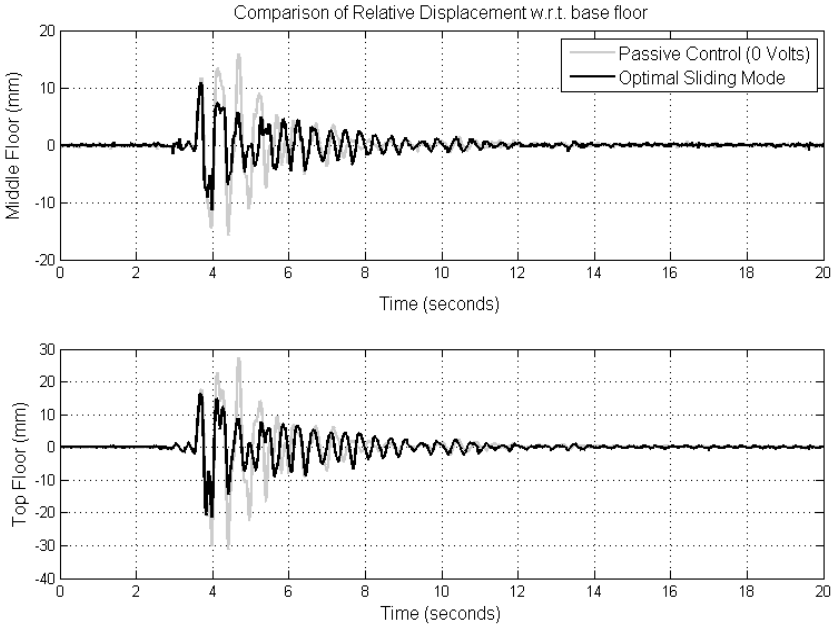

Figure 7-6 Displacement of floors to Northridge Earthquake (0.6g) Excitation

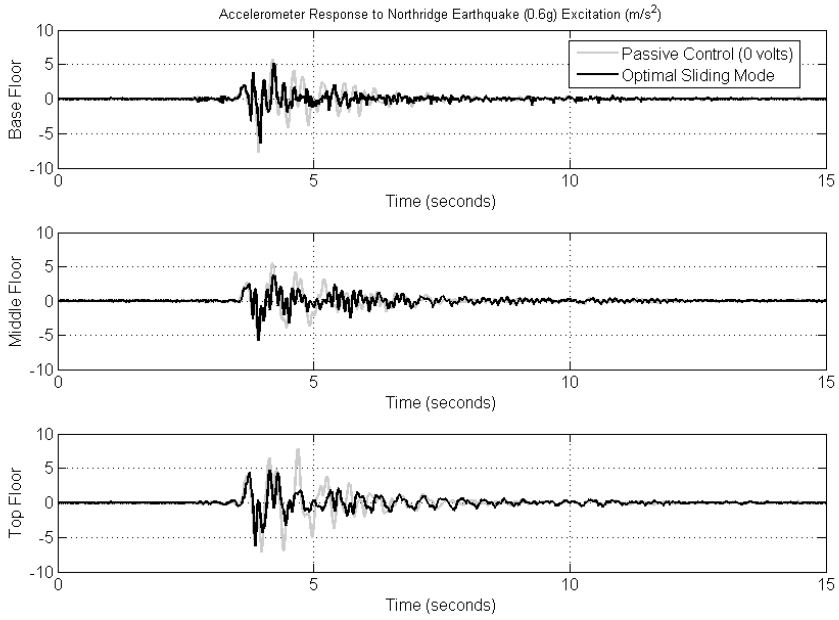

Figure 7-7 Acceleration Response with Northridge Earthquake (0.6g) Excitation

Table 7-1 Performance Analysis for RMS average of system data

	x_{1b}	x_{2b}	x_{ba}	x_{1a}	x_{2a}
El-Centro Earthquake	48%	54%	33%	40%	46%
Kobe Earthquake	53%	58%	37%	50%	51%
Northridge Earthquake	36%	34%	25%	26%	35%

Table 7-2 Performance Analysis for Peak values of system data

	x_{1b}	x_{2b}	x_{ba}	x_{1a}	x_{2a}
El-Centro Earthquake	26%	16%	2.5%	2.23%	25%
Kobe Earthquake	31%	30%	-14%	20%	33%
Northridge Earthquake	28%	36%	18%	-1%	21%

where x_b, x_1 and x_2 correspond to the displacement of the base, middle and top floor, and, x_{ba}, x_{1a} and x_{2a} correspond to the acceleration of these floors, respectively.

From the above analysis in Table 7-1 and Table 7-2, the effectiveness of the proposed controller can be explained. It can be seen that the controller performance is effective throughout the earthquake excitation. For the Kobe and Northridge earthquake excitation, the controller may have a larger peak response for accelerations, but the RMS average data shows that the controller is able to control the overall vibrations of structure.

For the base isolation system, it is expected that the relative displacements and accelerations of each floor are reduced during vibration control. More concentration is given to the reduction of these relative displacements and accelerations than base displacement [114]. The relative displacement depends upon the base displacement. When relative displacements or accelerations of the floors decrease, the base displacement is expected to increase within limits to compensate the displacement of other floors. If the base exceeds or tends to exceed out of limits, or in other words the base bumps into the end of the slider, additional vibrations will be introduced into the system. During the design of the base isolation system, the stiffness of the springs attached to the base of the structure is chosen to keep the motion within limits of the slider. The maximum amplitudes and RMS averages of the selected responses to these earthquakes are considered. The top floor acceleration (x_{2_accel}), relative displacement of the top floor with respect to the base floor (x_{2b}) and base displacement (x_b) are considered. The performance

of the proposed controller is compared with the response of the system with passive control, and semi-active control when the MR damper was activated at different voltages (4 volts, 6 volts, 8 volts and 10 volts). A comparison of the vibration control performance of the proposed robust optimal controller with passive MR damper at different voltage levels is provided in Table 7-3-Table 7-5.

Table 7-3 Experimental Analysis with El-Centro 0.6g Earthquake Excitation

Control method	$x_{2\ accel}$ (m/s^2)		x_{2b} (mm)		x_b (mm)	
	Abs	RMS	Abs	RMS	Abs	RMS
Base fixed	13.00	5.73	47.82	24.90	1.53	0.20
Passive (0 volts)	8.73	3.08	32.81	16.00	25.09	11.86
Passive (4 volts)	6.08	1.70	26.68	8.27	18.09	5.29
Passive (6 volts)	5.48	1.59	22.64	7.80	15.07	4.02
Passive (8 volts)	5.63	1.63	23.33	7.89	14.24	3.47
Passive (10 volts)	5.96	1.70	24.74	8.32	11.89	2.71
Proposed Controller	6.58	1.67	27.54	8.02	14.65	4.36

Table 7-4 Experimental Analysis with Kobe 0.3g Earthquake Excitation

Control method	$x_{2\ accel}$ (m/s^2)		x_{2b} (mm)		x_b (mm)	
	Abs	RMS	Abs	RMS	Abs	RMS
Base fixed	9.43	5.19	35.71	23.73	1.99	0.41
Passive (0 volts)	7.37	4.59	108.37	12.06	25.69	18.56
Passive (4 volts)	5.06	2.36	22.27	12.26	15.85	7.53
Passive (6 volts)	4.64	2.15	20.09	11.14	13.54	4.63
Passive (8 volts)	4.04	2.04	18.01	10.61	11.13	6.11
Passive (10 volts)	4.39	2.13	20.14	10.84	7.68	3.39
Proposed Controller	5.12	2.21	22.85	10.99	12.87	6.07

Table 7-5 Experimental Analysis with Northridge 0.6g Earthquake Excitation

Control method	$x_{2\ accel}$ (m/s^2)		x_{2b} (mm)		x_b (mm)	
	Abs	RMS	Abs	RMS	Abs	RMS
Base fixed	7.36	1.76	27.62	7.18	1.16	0.17
Passive (0 volts)	7.85	1.78	31.10	8.25	27.64	6.68
Passive (4 volts)	5.90	1.30	25.86	6.20	24.39	4.61
Passive (6 volts)	5.13	1.13	23.36	5.46	22.54	3.61
Passive (8 volts)	6.42	1.13	23.06	5.31	22.01	3.29
Passive (10 volts)	6.19	1.00	20.86	4.77	19.07	2.46
Proposed Controller	6.19	1.14	21.33	5.37	21.44	3.29

From the above tables, the best performance, in the case of the strong and long duration based El-Centro earthquake excitation, was from the passive control of the MR damper at 6 volts. For the stronger Kobe earthquake excitation, the passive control of the

MR damper at 8 volts gave the best performance. For the relatively weaker and short duration Northridge earthquake, again the MR damper (activated at a constant of 6 volts) showed the best results. However, the performance of the proposed controller for each excitation is comparable to the performance of the best configuration for each excitation signal. Also, it is not practical and realistic to provide constant actuating voltage to the structure. Therefore, considering the good performance through all excitations, the proposed approach can be treated as a robust and optimal approach.

7.5 Conclusion

In this chapter, the proposed optimal sliding mode controller explained in chapter 5 is implemented on a base isolated system. The controller considers the nonlinearity in the system as matched uncertainty and the unknown external disturbance as unmatched uncertainty. The implemented control strategy was able to control the vibrations of the structure very efficiently. The performance of the controller was evaluated against passive control of the MR damper at a different voltage level. From the comparison results, it was observed that the novel control technique provides optimal performance in controlling the relative displacements of the floors through all earthquake excitations. The experimental results and comparison results showed that the proposed controller is effective in dealing with unknown uncertainties of the system and thus can be treated as a robust control technique.

Chapter 8. Automatic Road De-icing System using Carbon Fiber as the Heating Element

Snow and ice on roads is a big problem in sub-tundra regions which leads to many road hazards. Though many methods are employed to prevent ice or to de-ice the road surface, each one has some disadvantages of their own. Some are not energy efficient, others laborious and costly, and some may cause road damage. In this chapter, a de-icing method is described using carbon fiber as heating elements. A test sidewalk is prepared by embedding continuous carbon fiber into concrete blocks and connecting the carbon fiber to the electric grid. An electric current is used to heat the concrete test slabs to de-ice the surface. A LabVIEW interface is prepared to analyze the de-icing process, which consists of two temperature controllers, an ON-OFF controller and a fuzzy logic based controller, of the test sidewalk. The advanced fuzzy logic controller considers the uncertain environmental parameters such as environmental temperature, chances of rain/snow and dew point to generate the control signal. The LabVIEW interface enables the user to keep track of environmental conditions and to save data on demand.

8.1 Introduction and Literature Review

In freezing climates, snow and ice cause a number of dangerous roadway conditions that are both hazardous and inconvenient. Due to the dramatic increase of driving accidents in slippery conditions caused by snow or sleet, improving road conditions in a timely and safe fashion is imperative. Though there have been a number of strategies developed to de-ice roadways, their disadvantages range from being destructive to the road structure itself to being cost ineffective [123].

8.1.1 Literature Review of De-icing Technologies

The effects of road salting on concrete structures and the environment have been well studied. Williams *et al.* [124] showed a strong relationship between saline pollution in groundwater and springs in urban areas, specifically due to the use of de-icing salts. Elevated concentrations of salt in groundwater and on roadsides damage vegetation and decrease aeration and availability of water in soil [125].

In their review of chloride effects on reinforced concrete, Mussato *et al.* [126] summarized chloride salt's effects on concrete deterioration. The effects of salt on the corrosion of steel reinforcement are well known and extensive studies on the costs and extent of damage due to roadway salting have been conducted [127]. The other alternatives of salt (NaCl) were also studied including magnesium chloride ($MgCl_2$) and calcium chloride ($CaCl_2$) as liquid brines, which reduce the amount of chemical used, speed up the de-icing process, and remain effective longer. Unfortunately, at the same time this process requires additional operation costs for sprayer equipment and special storage tanks for the brine [128]. Furthermore, studies have found mixed effectiveness of these alternatives to reduce structural damage, such as surface scaling and rebar corrosion due to chemical ion gradients, as compared to the use of conventional NaCl [126]. More complex chemical solutions with less damaging side effects to the concrete structure have also been proposed [129, 130], for example, Urea, formadide solutions, calcium magnesium acetate (CMA) and tetrapotassium pyrophosphate (TKPP), etc. However, all of these chemical alternatives are generally less effective and much more expensive than conventional salts; TKPP can cost as much as 15 times the cost of NaCl [129].

Infrared heat lamps as external heating elements were explored in the 1960's on the Mississippi Avenue Bridge in Denver, Colorado [130]. Coupled with the use of an insulation layer, the infrared lamps were mounted on the underside of the bridge structure as part of an ice prevention system. However, heating with infrared heat lamps was not effective in preventing ice on the surface. In addition to the use of external heat lamps to heat roadway surfaces, external application of insulation onto existing concrete structures has been attempted in order to preserve heat in the structure volume and reduce the number of freeze-thaw cycles [131, 132]. Polystyrene, urethane, and Styrofoam were applied to the structure under the surfaces in a number of states with limited success [123]. Polystyrene foam insulation was able to prevent frost action on highway pavements, but urethane was ineffective in both frost prevention and the reduction of freeze-thaw cycles. In fact, in some cases bonding problems between the foam and concrete surface resulted in de-bonding and loss of foam insulation.

Heat pipe and fluid heat exchanger systems, with working fluids such as propylene glycol and Freon, were installed in Wyoming, Oregon, Nebraska, and Virginia with great effectiveness in raising the concrete temperatures thus preventing ice formation on road surfaces [123]. In these systems, installation and maintenance costs are significantly higher, as the heat exchanger and pipe systems must be constructed and maintained through the year. Furthermore, operational costs are high due to the costs of working fluid and power to operate pumps and heat exchangers.

More recent implementations of automated de-icing systems for road surfaces incorporate sensing technology and more conventional chemical de-icing methods in the form of liquid sprays [133]. Fixed Automated Spray Technology (FAST) systems

integrate cast in spray and pump systems with embedded temperature and moisture sensors in the road surface, allowing for remote operation and monitoring. When environmental conditions are favorable for ice formation, chemical de-icers or salt brine solutions are pumped to road surface sprayers and sprayed onto the road surface. Structurally integrated heating elements and FAST systems have been shown to be effective in ice prevention and de-icing operations in the field. However, though the operation of such systems are cost effective in terms of labor costs, additional installation costs for support structures, such as piping, valves, and holding tanks for de-icing chemicals must be considered.

More recently, carbon nanofiber (CNF) materials are also being incorporated into concrete as electrically conductive admixtures. Gau and Sturm studied the relationship between concrete strain and resistivity using different CNF types [134]. They found that the addition of CNF fibers reduced the resistivity of self-consolidating Concrete (SCC) concrete by 80%, though there is a compositional threshold for CNF concentration at which improved electrical conductivity plateaus. Furthermore, they found that SCC aids in fiber dispersion, reduces resistivity, and improves electrical sensitivity to stress and strain when using the SCC concrete as its own strain sensor.

In addition to electrically conductive concrete, self-heating concrete designs have used structurally integrated heating and de-icing methods, most commonly embedded heating wires and hot water pipes. Yehia and Tuan's literature review [123] summarized a mass of efforts between 1970-1996 to incorporate structurally integrated heating elements for highway roadway de-icing and ice prevention. Electrically heated cables have been retrofitted onto highway surfaces with mixed success; a system installed in Newark, New

Jersey in 1961 employed surface installed electrical cables underneath an overlay of asphalt. Though the installation costs of this system were low ($54/ft^2), the system was abandoned when the heat cables were pulled up due to heavy traffic. A similar system installed three years later in Teterboro, New Jersey, operated satisfactorily at similar installation and power costs. Similar electrical systems installed in Ohio, Oregon, Pennsylvania, South Dakota, Texas, and West Virginia were abandoned due to high power consumption or malfunctions of the electrical heating elements.

Later, carbon fiber had shown great potential as a replacement for the heater lamp. A review by Chung of self-heating concrete research showed that uncoated fiber mats were able to achieve a maximum self-heated temperature of 134°C, second only to flexible graphite (which is not suitable as a structural material), at a lower power consumption [135]. The combination of low power and fast response time makes carbon fiber material ideal for use as self-heating elements in concrete. Sun *et al.* used carbon black mortar slabs (CBMS) to form self-heating concrete flooring material [136]. The study found that the CBMS was able to uniformly heat a small room 10°C above the "cold state" temperature in 330 minutes. Yehia *et al.* [123, 137] and Tuan [138] studied the use of steel shavings and fibers in electrically conductive concrete for bridge deck de-icing and snow melting. An optimized mix proportion of 20% steel shavings per volume and 1.5% steel fiber per volume of concrete was found to be effective in resistively heating the bulk concrete model bridge deck for de-icing functions [137]. Both ice melting and ice prevention processes were tested and found to be effective [138].

Preliminary cost analysis showed that the electrically conductive concrete bridge deck was less expensive than conventional concrete de-icing methods, such plowing,

when considering operation and installation costs. Additionally findings include the advantages of AC over DC power sources, physical property testing, and workability evaluation of various mix proportions [139]. Reports from a field test of their steel fiber based conductive concrete on the Roca Spur Bridge in Nebraska indicate high efficiency and effectiveness in de-icing and ice prevention applications [140]. However, steel fibers are not very effective in preventing crack propagation due to their high modulus of elasticity [141].

From the above literature review, it can be seen that there are many ways which have been tried to deal with icing issues on the roads. Each idea has one or more problems. Salting on roads is laborious and also at the same time, it can cause damage to roads. Heating lamps and heat exchangers are effective but they are very costly and power inefficient. Electrically conductive concrete with steel fiber is being used recently where concrete can be heated electrically. However, steel fibers ineffectiveness against crack propagation comes as a big problem for concrete lifespan. The steel fiber can be replaced with carbon fiber based concrete which is lighter material and helps in enhancing structural strength also. The resistive property of carbon fiber can be used to melt/prevent the ice by heating the concrete surface above freezing temperature. The efficiency of system can be further reduced by employing an intelligent temperature controlled system which can save the additional cost when heating is still on while no ice or snow is on the surface or while weather conditions are unlikely for ice formation. Temperature control is one of the most used control application in many industries. Many different temperature controllers have been proposed and successfully implemented. A brief literature review of different temperature controllers in different industries is presented.

8.1.2 Literature Review for Temperature Control

In most cases, temperature is the most important and easiest parameter to control in de-icing applications. Frequently changing environmental conditions, time delays inherent in heating systems, and temperature dependence upon the heat absorption by the concrete structure make it very difficult to model the system. Experimental results show that the variations in surface temperature of the concrete structure due to heating are significantly different from ambient [142] and that the system response for heating the concrete is very slow [143]. For slow responsive system, generally, ON-OFF control and PID schemes are employed in commercial products for automatic feedback control system [144]. Design of a temperature controller with faster response time and with smaller steady state error is a challenge in the control research field.

Many control algorithms have been studied and implemented for temperature control. Widely used in industry, the PID controller was first proposed in 1936. There are techniques to tune the PID controller, such as Zeigler and Nicholas method and Internal Model Control (IMC) method, for accurate dynamic models of a given system. Apart from these methods, a trial and error process can also be used to get better performance with the PID controller. However, PID performance may deteriorate with external disturbance or uncertainty in the system. This problem leads researchers' attention to model free and robust control algorithms. Various self-tuning techniques have been discussed to make the temperature controller robust to external disturbances and uncertainties [145-147]. Recently, the fuzzy control theory has been employed in many applications. Great robustness and easy implementation has attracted many control researchers. Many

different type of controller were implemented using fuzzy approach for temperature controller [148-151].

In this report, a fuzzy logic based temperature controller which deals with uncertain environmental parameters, such as environmental temperature, probability of rain/snow and dew point relative to the surface temperature of the concrete block, is proposed and implemented. Before the development of the temperature control system, a simple modeling of the surface temperature with respect to electrical power for the de-icing process is discussed.

8.2 Modeling of Surface Temperature with respect to Electrical Power

A simple analytical model is determined for the concrete block heating. The surface temperature is considered as the output and electrical power is considered as the input. Initial temperature of the concrete surface is assumed to be -10 ºC and environmental temperature is considered to be -10 ºC. The properties of materials (carbon fiber and concrete) are taken from American Society for Materials (ASM) standards [152]. An analytical model is prepared using Gambit version 2.4 for geometry and meshing, and, FLUENT solver version v.6.3 from ANSYS.

The dimension of concrete block is $72\times48\times4$ inch^3. For simplicity, the carbon fiber heating element is considered as a constant layer and placed after 3 inch thickness of concrete. The thickness of carbon fiber element is considered as 0.001 inch. The surface temperatures of each concrete layers along its length and width are assumed to be uniform. The equation of heat transfer in solid regions is used to model the de-icing process [153], which is

$$S_h = \frac{\partial}{\partial t}(\rho h) - \nabla \cdot (k \nabla T), \tag{8-1}$$

where S_h is volumetric heat source, $\rho = 2400 \frac{kg}{m^3}$ is density of concrete materials, $h = \int_{T_{ref}}^{T} c_p dT$ is sensible enthalpy and $c_p = 837 J/kg.K$ is specific heat of concrete, $k = 2.07 watt/m.K$ is thermal conductivity and T is the surface temperature of concrete layer. It is assumed that 300 watt of electrical power is continuously provided to the carbon fiber heating element and all of heat energy is transferred towards the outer surface of the concrete which is exposed to environment. After considering the heating of concrete block for 11.11 hours, the temperature profile of the concrete block along the thickness of the block is shown in Figure 8-1.

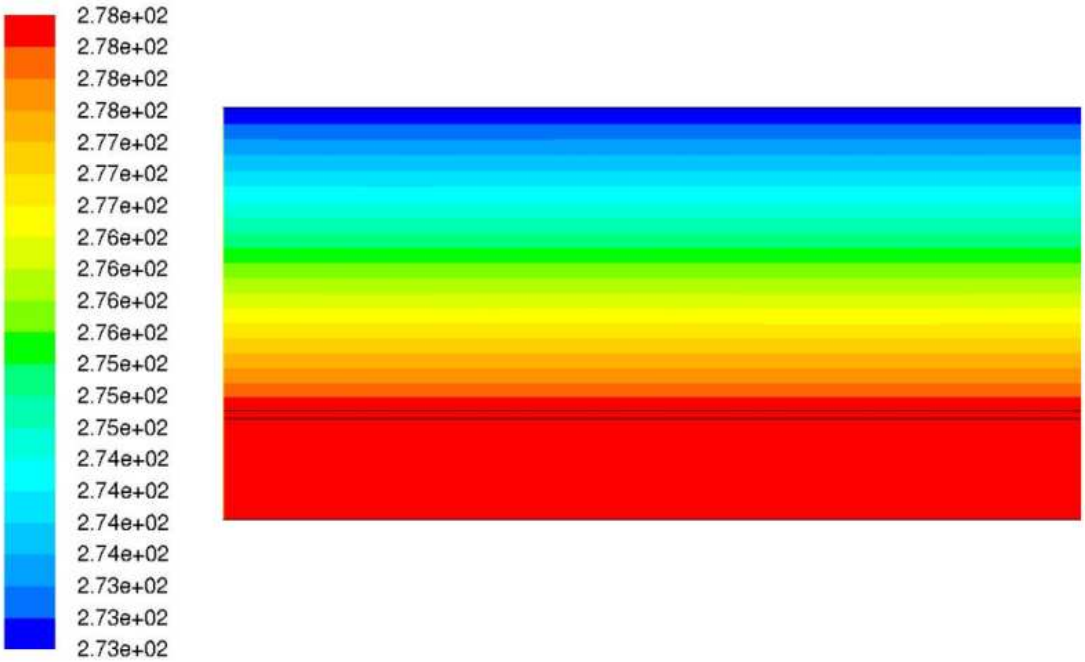

Figure 8-1 Temperature profile along the thickness of concrete block

The surface temperature with respect to electrical power is modeled as a single order system. It is found that the heating process has a delay of 0.1 hour. After comparing the data with step response of a single order system, the first order model is estimated as

$$T.F. = \frac{2.26}{s + 0.1852} e^{-0.1s}, \tag{8-2}$$

where t is time in hours. The time constant for the heating process is 5.4 hrs. Figure 8-2 shows the comparison of the step response of the modeled system with analytical model. It can be seen that first order model of heating process matches the analytical data very well.

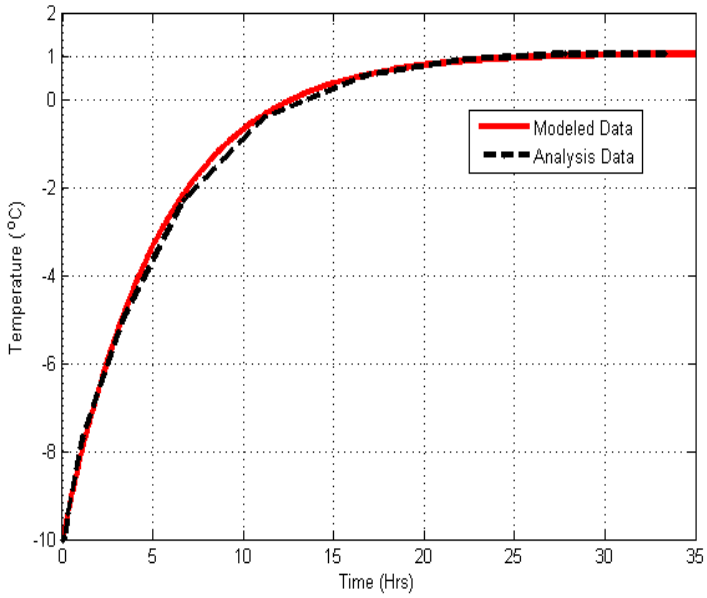

Figure 8-2 Modeling of heating process of concrete with carbon fiber

From the above estimated model, it can be seen that the heating of concrete for de-icing purposes is a slow process. To make it faster and cost effective in terms of power usage, an adequate control system is needed. In the following section, the control system development of de-icing process is discussed.

8.3 Control System Development

A LabVIEW based interface was developed for data acquisition and temperature control in Figure 8-3. The LabVIEW interface has the following capacities.

- Web Based Weather Monitoring of test site
- Manual Turn On/OFF electrical heating of carbon fiber

- ON-OFF Control for Surface Temperature of Sidewalk
- Fuzzy Logic based temperature Control
- Data Saving

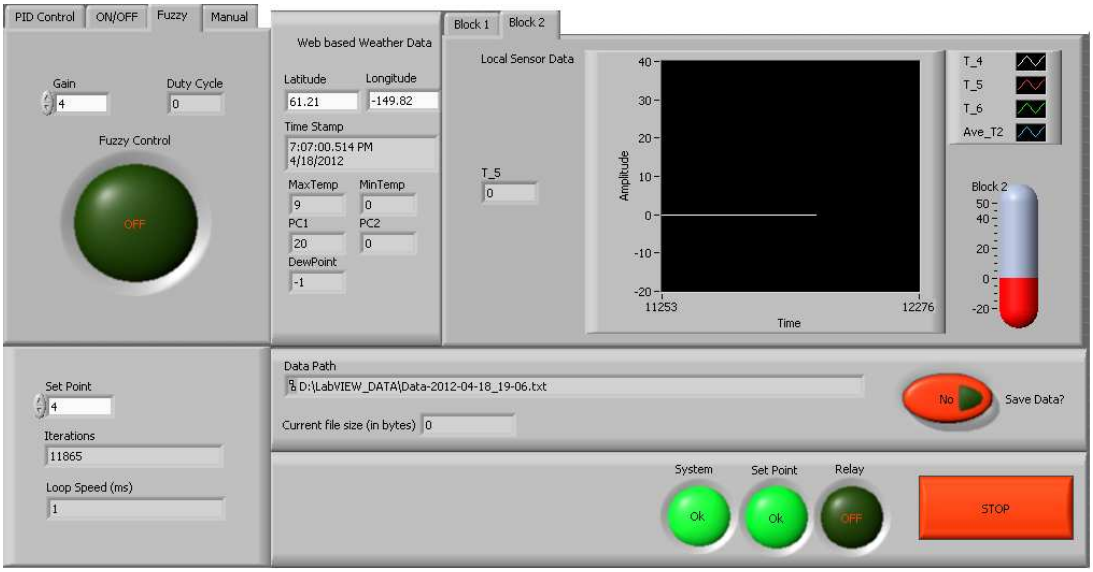

Figure 8-3 LabVIEW based user interface

8.3.1 Web Based Weather Monitoring

A web based weather monitoring was included in the LabVIEW interface. The LabVIEW interface used Simple Object Access Protocol (SOAP) server. The SOAP server provides different sub VIs which can be used to get the information about the location of interest and environmental data at that location. For this project, The SOAP is used to get the weather information by putting the longitude and latitude information of the test site location.

The information about weather forecast data is collected from the National Digital Forecast Database (NDFD) XML service, which is a service providing the public, government agencies, and commercial enterprises with data from the National Weather Service's (NWS) digital forecast database. The SOAP connects the LabVIEW interface to NDFD database when requested. The NDFD database gets updated after 45 minutes – 1

hour. The following Figure 8-4 describes the process of collecting weather data from national weather services.

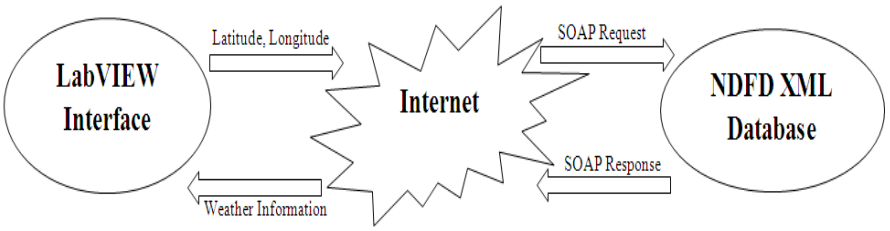

Figure 8-4 Collection of Weather Data from LabVIEW interface

The following information is collected by LabVIEW interface through SOAP request.

- Maximum Temperature
- Minimum Temperature
- Percentage chances of Rain/Snow
- Dew Point

8.3.2 Manual Turn On/off

The user interface is programmed to manually turn on/off the electrical heating of the concrete structure. A software manual switch is programmed to send high signal to the solid state relay (SSR) through NI DAQ to turn on the electric current from the transformer to the carbon fiber. Apart from a software manual switch, every block is connected to a 3-way switch to activate the heating. One side of the switch keeps the heating off, the second side manually turns on/off the heating. The 3rd side keeps system controlled via user interface. The user interface has an on/off controller and a fuzzy logic based temperature controller to control the surface temperature of test sidewalk. The description of both controllers is given in the following section.

8.3.3 On/OFF Controller

The heating of a concrete block to raise the surface temperature is a slow process. It takes a few hours to raise the temperature from sub-zero to above melting point at a limited control power. For this type of systems, ON-OFF controller generally shows optimized performance [144].

The ON-OFF controller is the simplest form of control and is often used in temperature controlled heating processes. When the temperature of the system is less than the set-point temperature the heater is turned on at maximum power and once the system temperature is above the set-point, the heater is switched off completely. To keep the system temperature near the set-point temperature, the turn-on and the turn-off temperature are kept at very small difference. This can be done by in many ways by introducing a hysteresis or a dead zone in actuation. In this study, a dead-zone is introduced to eliminate the temperature fluctuations. The block diagram of ON-OFF controller is given in Figure 8-5.

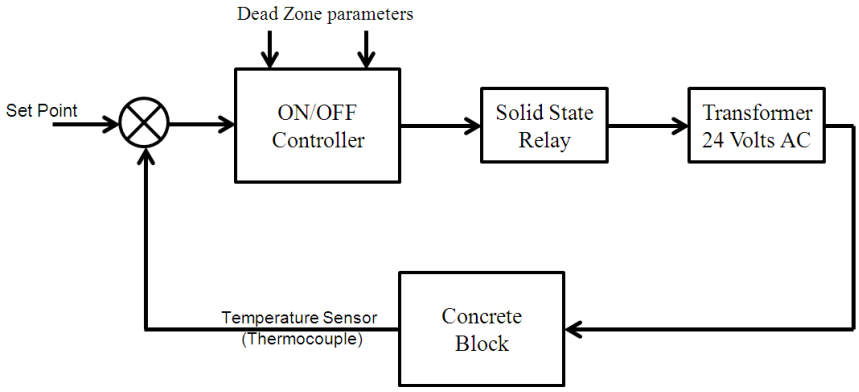

Figure 8-5 Block Diagram of ON-OFF Controller

The ON-OFF controller explained above can give optimal performance only under similar ambient conditions. However, environmental conditions are always changing and are sometimes very unpredictable. These fluctuating conditions affect the performance of

the controller. To overcome this, a fuzzy logic based controller is employed to take into account environmental parameters and also help the system to behave in a more economical way.

8.3.4 Fuzzy Logic Based Temperature Controller

The fuzzy logic control approach is based on the ability of humans to learn, represent, manipulate and implement any idea to control the system accordingly. This ability makes the fuzzy control approach very interesting and popular among engineers. Fuzzy controllers are very robust and handle nonlinearities and model uncertainties of the system very well. However, design of a fuzzy logic controller requires an in-depth knowledge of the system and its behavior. A general fuzzy logic controller block diagram can be represented with four elements as shown in Figure 8-6.

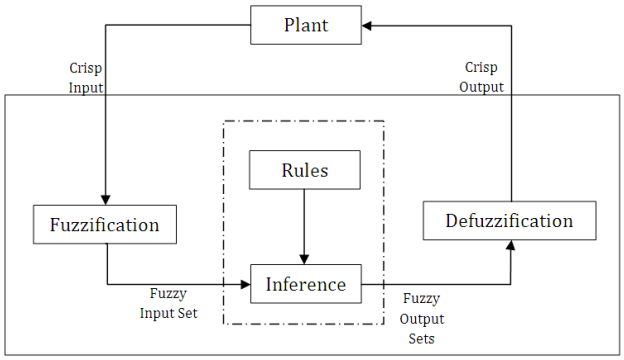

Figure 8-6 Block Diagram of Fuzzy Logic Controller

The set of rules, which contains the fuzzy logic quantification of expert knowledge of the system for good control, is as follows:

Inference Mechanism: An inference mechanism describes the fuzzy outputs based on the expert's knowledge of the system. The inference mechanism basically has two tasks:

1. Determining the extent to which each rule is relevant to the current situation.
2. Formulate a decision based on the current input and information from the rule-base.

In general, the inference mechanism works on the if/then principle and decides the output of the controller based on information from the sensor.

Fuzzification: Fuzzy sets are used to quantify the information in the rule-base. It can be defined as an interface which converts controller inputs into a fuzzy input set that can be understood by the inference mechanism, or "fuzzify" the raw input of the sensor. Generally, a Singleton function is used, which produces a fuzzy set that defines a membership function to quantify the information in the rule-base for the control output.

Defuzzification: Defuzzification is the interface used to convert decisions made by the inference mechanism to physical output for the controller to control the plant. There are different types of defuzzification strategies that exist in fuzzy logic control systems. Some of these are as follows:

1. Center of gravity (COG): The crisp output is chosen by the center of the area and the area of each implied fuzzy set.
2. Center Average: The crisp output is chosen using the centers of each of the output and membership functions and the maximum certainty of each of the conclusions that represent the implied fuzzy set.
3. Max criterion: The crisp output is chosen as the maximum value that can be achieved for the overall fuzzy set.
4. Mean of maximum: The crisp output in this strategy is the mean value of all elements having maximum membership in their defined fuzzy set.

Generally, center average defuzzification technique is used as it is easy to compute. A model of a fuzzy system can be expressed by using the product inference engine, Singleton fuzzifier, and center average defuzzifier, as

$$u_D\left(\mathbf{x}\middle|\theta\right)=\frac{\sum_{l_1=1}^{m_1}\sum_{l_2=1}^{m_2}\bar{y}_u^{l_1l_2}\left(\prod_{i=1}^{2}\mu_{A_i^{l_i}}\left(x_i\right)\right)}{\sum_{l_1=1}^{m_1}\sum_{l_2=1}^{m_2}\left(\prod_{i=1}^{2}\mu_{A_i^{l_i}}\left(x_i\right)\right)}, \tag{8-3}$$

where the parameter matrix $\theta\in R^{\prod_{i=1}^{2}m_i}$ and consists of the adjustable parameter $\bar{y}_u^{l_1l_2}$. Then the fuzzy controller can be rewritten as

$$u_D\left(\mathbf{x}\middle|\theta\right)=\theta^T\xi\left(\mathbf{x}\right), \tag{8-4}$$

where $\xi\left(\mathbf{x}\right)$ is defined as

$$\xi^{l_1l_2}\left(\mathbf{x}\right)=\frac{\prod_{i=1}^{2}\mu_{A_i^{l_i}}\left(x_i\right)}{\sum_{l_1=1}^{m_1}\sum_{l_2=1}^{m_2}\left(\prod_{i=1}^{2}\mu_{A_i^{l_i}}\left(x_i\right)\right)}. \tag{8-5}$$

The fuzzy controller described above can be used to estimate the nonlinearities and uncertainties of the system by analyzing the crisp input by the fuzzy approach. For temperature control of the concrete test-sidewalk, the input parameters for the fuzzy logic controller are

1. Local surface temperature of concrete test block (T_L ^oC)
2. Environmental minimum temperature from NDFD website (T_W ^oC)
3. Dew point < relative local environmental temperature
4. Percentage chance of precipitation

The output parameter of the fuzzy logic based controller is the duty cycle for the pulse width modulation (PWM) signal to activate the SSR. The range of duty cycle ranges from (0%-100%). The block diagram of the fuzzy logic based controlled heating of surface temperature is given in Figure 8-7.

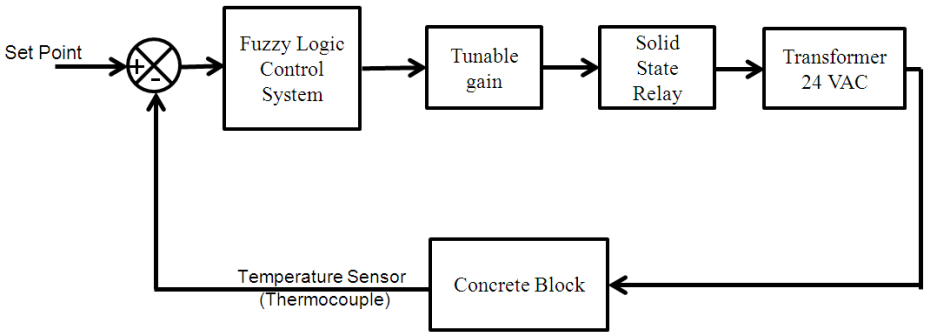

Figure 8-7 Block diagram of fuzzy logic based temperature controller

Generally, if the dew point is lower than the environmental temperature, chances are high that snow/rain will happen in the area. For the fuzzy logic controller it is considered that if the chances of precipitation is greater than 40%, there are moderate chances that rain/snow will happen and for chances of precipitation to be greater than 60%, the chances are considered to be very high. Chances of precipitation under 40% are considered to be low for rain/snow. The fuzzy rules for the temperature controller are given in the following Table 8-1 and Table 8-2.

The temperature range for these rules is defined as "Very Low" = less than -15ºC, "Low" = (-10ºC, -5ºC), "Less Zero" = (-5ºC, -2ºC), "Zero" = (-2ºC, 2ºC), "High" = (2ºC, 5ºC), and "Very High" = greater than 5ºC.

Table 8-1 If Precipitation>40%, Dew Point > Minimum Temperature

T_L / T_W	Very Low	Low	Less Zero	Zero	High	Very High
Very Low	Low/Moderate	Low/Moderate	High/Moderate	High/Moderate	Zero	Zero
Low	High/Moderate	High	High	High	Zero	Zero
Less Zero	High	High	High	High	Zero	Zero
Zero	High	High	High	High	Zero	Zero
High	Moderate	Moderate	Moderate	Low	Zero	Zero
Very High	Moderate	Moderate	Low	Low	Zero	Zero

Table 8-2 If Probability of Rain/Snow>60, Dew Point > Minimum Temperature

T_L / T_W	Very Low	Low	Less Zero	Zero	High	Very High
Very Low	High	High	High/Moderate	High/Moderate	Zero	Zero
Low	High	High	High	High	Zero	Zero
Less Zero	High	High	High	High	Zero	Zero
Zero	High	High	Moderate	Moderate	Zero	Zero
High	Moderate	Moderate	Low	Low	Zero	Zero
Very High	Moderate	Moderate	Low	Low	Zero	Zero

8.4 Experimental Setup in Lab

For the de-icing project, a concrete block with embedded carbon fiber tape was casted at the University of Houston. The dimension of the concrete block was 12″×18″×6″. The carbon tape of 3″ width was embedded in to the block as shown in Figure 8-8. The tape was clamped between two copper rods on each side as electrodes.

Figure 8-8 Configuration of Concrete Block with embedded Carbon Fiber Tape

To simulate the real time cold weather effect on the block, the concrete block was kept in a freezer. The temperature inside the freezer was set to be -15 ºC. Three thermocouples were placed on the surface of the block to measure the temperature and the weighted average of these thermocouples was used as the surface temperature reading. Water was poured on to the surface of the concrete block to produce surface ice

formations, as shown in Figure 8-9. The aluminum roads were connected to the electrical system via electrical cables as shown in Figure 8-10.

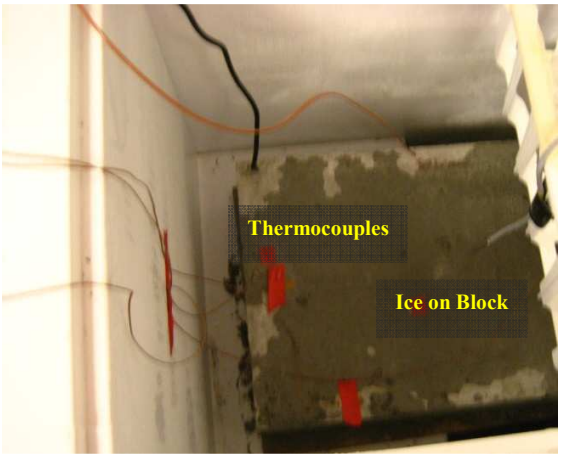

Figure 8-9 Concrete Block inside Freezer

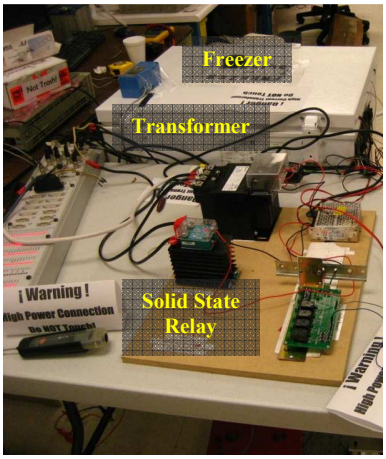

Figure 8-10 Electrical System

The layout of the above mentioned electrical system is shown in Figure 8-11. The USB based NI Data Acquisition Board is connected to a computer with a LabVIEW interface.

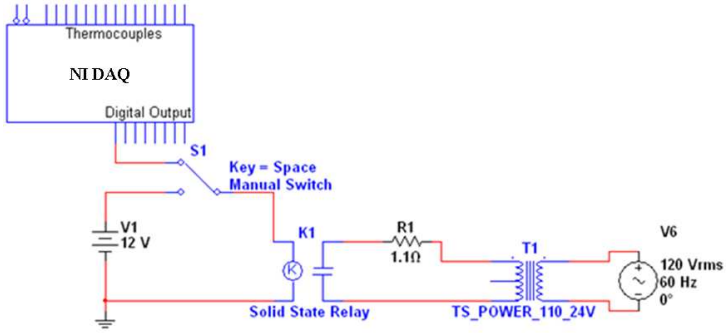

Figure 8-11 Electrical Circuit Diagram

8.5 Lab Experimental Results

Many experiments were conducted for the de-icing process with both the ON/OFF controller and the fuzzy logic based controller. The thermocouples were placed on the surface of concrete block and the average of these thermocouple readings are used as feedback. Different environmental conditions were assumed to test the performance of the

fuzzy logic based controller. The following figures demonstrate the performance of both controllers.

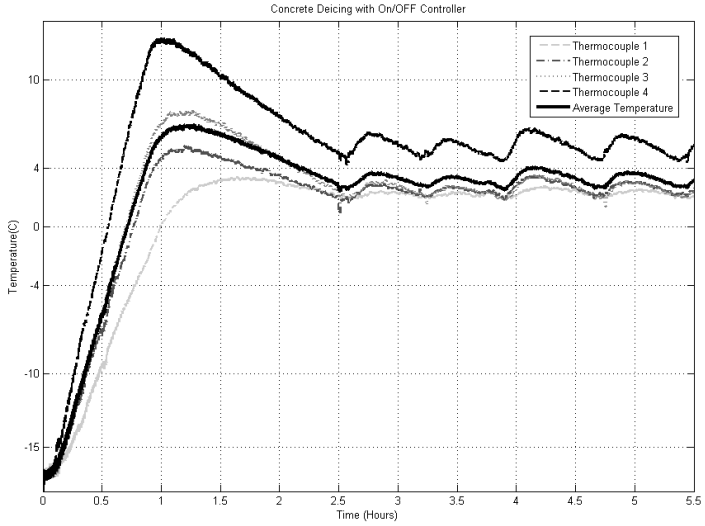

Figure 8-12 De-icing with ON/OFF controller

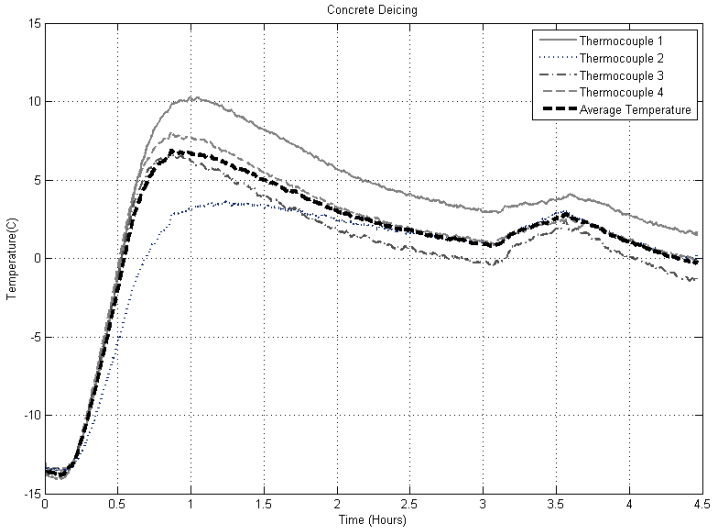

Figure 8-13 De-icing with fuzzy logic based controller

It can be seen in Figure 8-12 and Figure 8-13 that both controllers were able to raise the surface temperature of the concrete test specimen above the freezing point effectively. It was found that the temperature at the edges of the concrete test specimen where the electrodes are placed show higher readings due to high contact resistance between the metal electrodes and the carbon fiber tape. Due to this high resistance, the

heat generated is greater in this area, resulting in higher surface temperature at the edges. This issue can be resolved by adopting a distributive temperature controller.

8.6 Field Experiment Setup

A test sidewalk with a conventional surface pavement was constructed at the University of Alaska Anchorage (UAA) campus following the concrete standards in the Municipality of Anchorage Standard Specifications (MASS). The completed sidewalk is shown in Figure 8-14. Besides the sidewalk with embedded heating panels, there were installed a power supply box and a data acquisition/control box which house the power supply and data acquisition/control equipment of the field experiment facility, respectively. The three heating panels were powered and controlled individually. Figure 8-15 describes the carbon fiber frame in each block of the test sidewalk. Block 2-Block 4 have an embedded carbon fiber frame. Figure 8-16 describes the cross sectional area of test sidewalk.

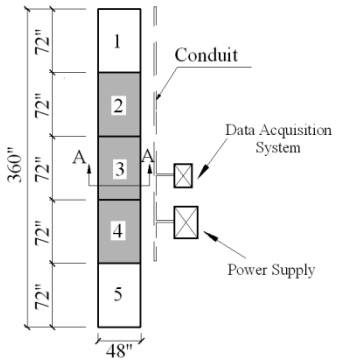

Figure 8-14 Test Sidewalk Dimensions

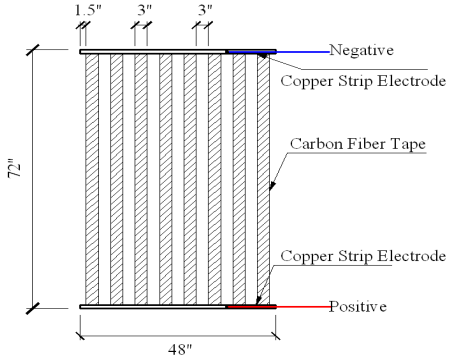

Figure 8-15 Carbon Fiber Frame

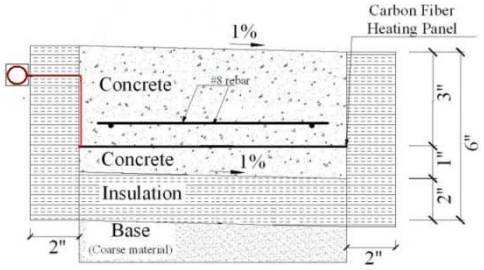

Figure 8-16 Cross Sectional View of Test Sidewalk

Figure 8-17 describes the block diagram of the automatic de-icing system. The electrical power supply box consists of a power meter, three step-down transformers and solid state relays. Power and energy usage can be tracked from the power meter. The transformers used in this de-icing system are PH1000PG HPS Machine Tool Industrial Control Transformers with a primary voltage of 120/240V, a secondary voltage of 12/24 V, and a VA rating of 1000VA. In the experiments, the transformers were connected to 110V/60Hz AC power outlet and the heating panels were charged with by 24V AC for heat generation.

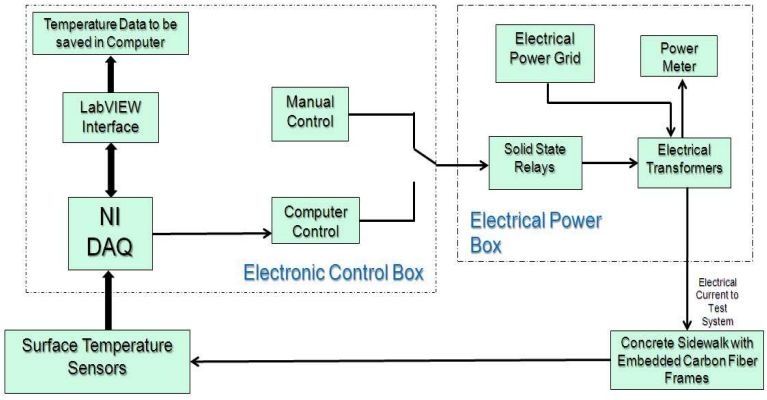

Figure 8-17 Block Diagram of Automatic De-icing System

The electronic control box houses three main units: an industrial computer, a data acquisition unit (NI 9188) and a power-switching unit. The NI-9188 is an Ethernet chassis manufactured by National Instruments. It consists of a 16-channel thermocouple reader (NI 9213) and an 8-channel solid state relay driver (NI 9485). The data were retrieved through a remote computer via internet.

8.7 Field Experimental Results

The automatic de-icing system was tested under natural conditions at the UAA campus. It was found that during the day, direct sunlight falling on the concrete blocks also helps temperature to rise. Now, since the thermocouple used to sense the surface

temperature is also exposed to sunlight, it also gives higher temperature reading. The fluctuations in the surface temperature reading can be attributed towards the environmental effects beyond human control.

The temperature profile of a concrete block with fuzzy logic based controller is shown in Figure 8-19. The target surface temperature was chosen to be around 4^{o}C. It can be seen that fuzzy logic based controller took about 4 hours to raise the temperature from less than -5^{o}C to above 0^{o}C. Also it is able to keep the temperature around 4^{o}C as environmental conditions were almost the same for the whole duration.

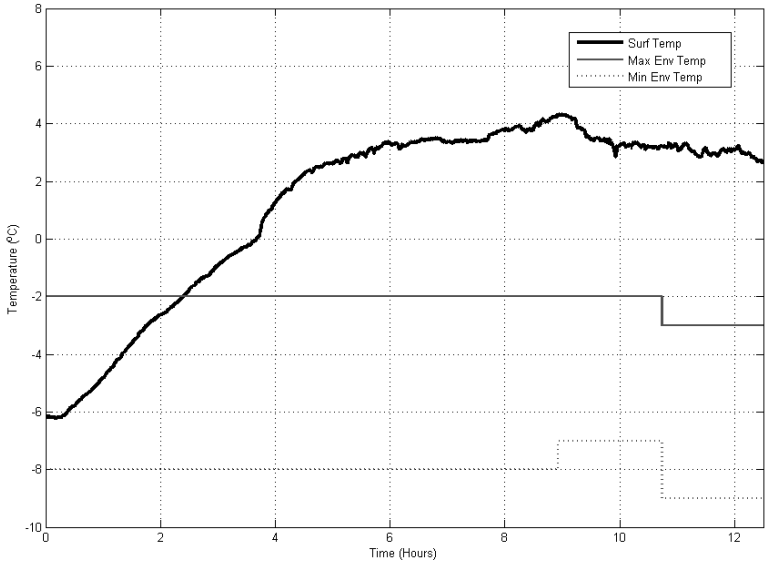

Figure 8-18 Temperature Control with Fuzzy Logic based Controller

The temperature profile of a concrete block with fuzzy logic based controller is shown in Figure 8-19 over a longer time (approx. 260 hours). The high temperature peaks in the range of (5^{o}C – 10^{o}C) are due to direct sunlight on these concrete blocks. The target surface temperature was chosen to be around 4^{o}C. It can be seen that fuzzy logic based controller is able to keep the temperature above freezing point under different environmental conditions.

The temperature profile of the concrete block with the ON/OFF controller is shown in Figure 8-20 and Figure 8-21. Again fluctuation due to sunlight and other environmental effects can be seen. The concrete test sidewalk was not cooled down to below freezing point under natural condition before putting it under ON/OFF controller. This is the reason why the temperature data in Figure 8-21 with the ON/OFF controller starts from above 0^{o}C.

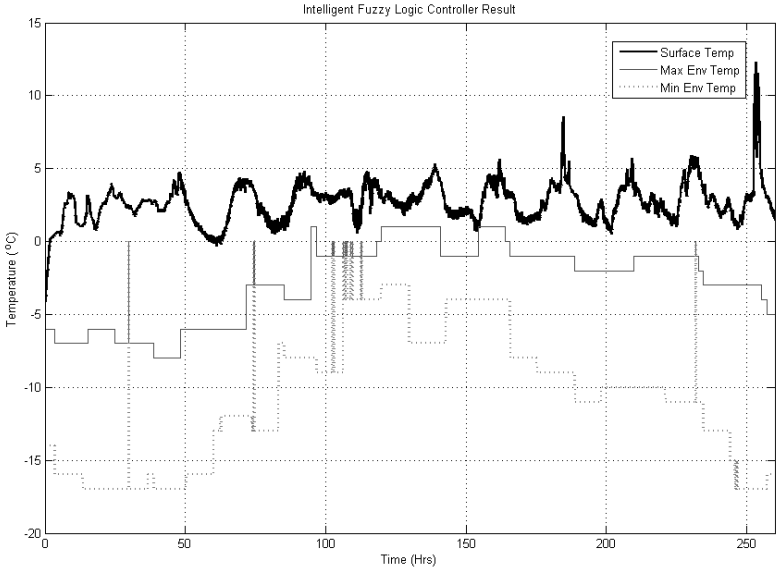

Figure 8-19 Surface Temperature with fuzzy logic based controller

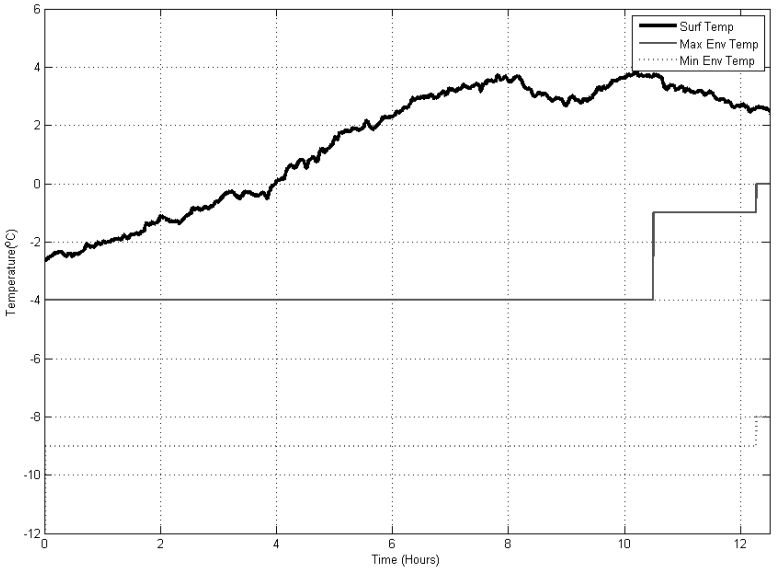

Figure 8-20 Temperature control with ON/OFF Controller

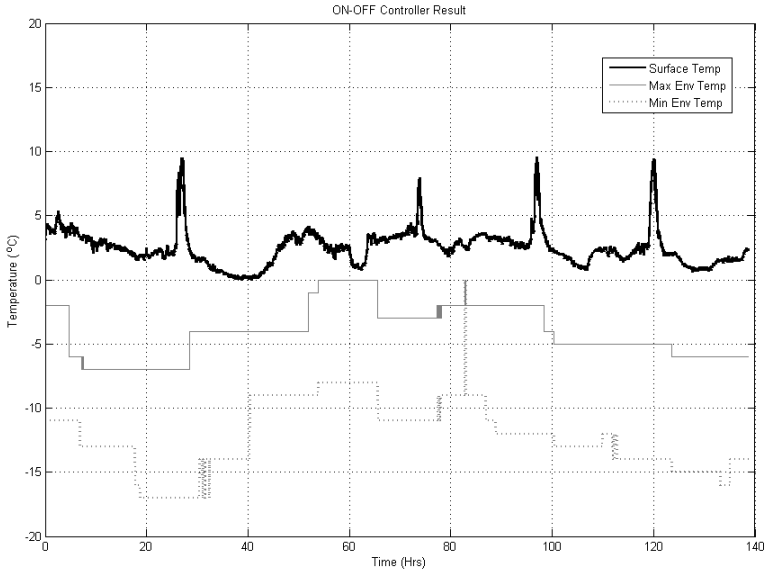

Figure 8-21 Surface Temperature with ON/OFF controller

To test the surface temperature profile, IR images were taken using the Thermal Imaging Camera from FLIR. The images from the thermal IR camera show that the temperature along the surface is almost constant. The following figures show the images taken from the thermal imaging camera.

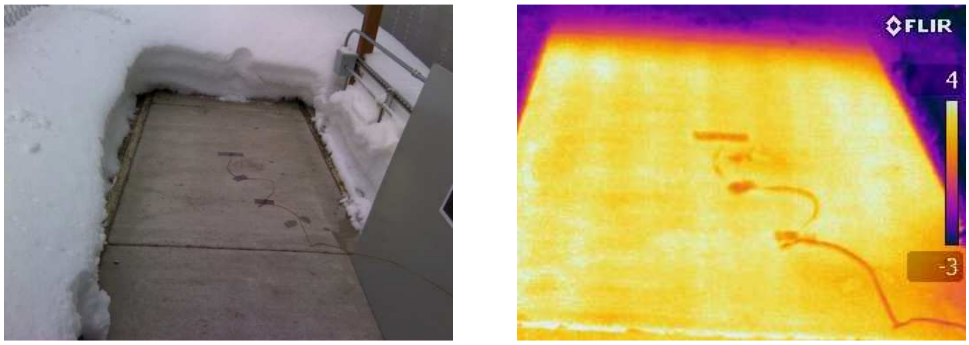

Figure 8-22 Thermal camera images (Block with ON/OFF Controller)

Figure 8-23 Thermal camera images (Block with Fuzzy Logic based Controller)

From the above images, it can be seen that the surface temperature is uniform along the whole surface of the concrete block. Also, the surface temperature of the concrete block is around 4^{o}C as desired. Since the surface temperature is uniform, the thermocouple used for temperature feedback can be placed anywhere on the concrete surface.

8.8 Power Consumption Analysis

Cost effectiveness has always been a very important factor for employing a new system. It is very important to compare the recurring cost for the electrical power that the system will consume. The power consumption data was recorded and compared with power consumption by manual control in the earlier study of the same system [154]. In an earlier study, after analyzing the data it was found that power consumption for de-icing and anti-icing tests was almost same. Also on comparing with other existing technologies, the proposed de-icing system was proved to be much cheaper. It was envisioned that the system can be made more efficient if used in a controlled way by preventing waste of power consumption when there is no ice or no chances of rain and snow. Also, it was stated that the installation cost for the physical system that included cost of heating panels, electrical and control equipment was relatively lower than that of other existing technologies. In addition to it, remote access of the system made it cheaper in terms of labor cost. During testing of these temperature controllers for the test sidewalk, the electrical power consumed by the system is recorded and compared with other technologies. During this time, the system was running under one control algorithm either ON/OFF Control or Fuzzy Logic based Control. A detailed power consumption analysis

for the ON/OFF controller and fuzzy logic based controller are given in Table 8-3 and Table 8-4.

Table 8-3 Power Consumption of test sidewalk (ON/OFF controller)

Date	Time b/w	Energy Usage	Energy Cost	Energy	Cost/Unit
03/02~05/2012	80	22.157	4.4314	1.3294	0.298
03/05~06/2012	22	4.03	0.8060	0.8784	0.197
03/06~07/2012	20	3.81	0.7620	0.9144	0.205
03/07~09/2012	48.33	8.786	1.7572	0.8736	0.196
Total	170.33	38.7830	7.7566	**1.0929***	**0.245***

Table 8-4 Power Consumption of test sidewalk (fuzzy logic temperature controller)

Date	Time b/w	Energy Usage	Energy Cost	Energy	Cost/Unit
03/09~12/2012	76.5	15.197	3.0394	0.9535	0.208
03/12~13/2012	23.5	4.545	0.9090	0.9283	0.151
03/13~14/2012	22.33	3.142	0.6284	0.6753	0.156
03/14~19/2012	123	17.79	3.5580	0.6942	0.166
Total	245.33	40.6740	8.1348	**0.7968***	**0.178***

The comparison of power consumption cost among the manual control, ON/OFF control and fuzzy logic based controller for de-icing of the test sidewalk is given in Table 8-5.

Table 8-5 Comparison of power consumption cost

Controller Type	Energy Cost	Cost/Unit Area
Manual	4.1088*[a]	0.9214*[a]
On-Off Controller	1.0929*	0.249*
Fuzzy Logic	0.7968*	0.178*

Note: Cost for sidewalk preparation and system components is not considered.
*average energy cost/day and average energy cost/[day.m^2], energy cost assumed =$0.2/kWh
[a] values calculated from earlier study [154].

From above tables of comparison, it can be stated that the de-icing system with the ON/OFF controller and fuzzy logic based controller are very efficient in terms of power consumption cost. The de-icing system with the ON/OFF controller is 72.97% more

efficient than the always ON manual controller, with the fuzzy logic controller, the system is 80.68%. Also, the de-icing system with the fuzzy logic controller is 27.35% more efficient than with the ON/OFF controller.

8.9 Conclusion

In this study, the design, development, and testing of a carbon fiber based de-icing system for concrete structures was presented. A carbon fiber fabric based heating element was embedded in a concrete pavement and field tested at the University of Alaska Anchorage using an internet based remote control system. A LabVIEW interface was built to enable the remote access and monitoring of the de-icing system. Two control algorithms, the ON/OFF controller with dead-zone and an advanced fuzzy logic based controller, were implemented and tested over the winter of 2011-2012. The controller performances were satisfactory and helped lower the cost of power consumption as compared to always ON, manual control. The designed fuzzy logic based advanced controller was over 25% more energy efficient than the ON/OFF controller. It is envisioned that after employing the models for effects of environmental changes, such as daily temperature cycles and wind conditions, on the de-icing system, the de-icing process can be made even more economical.

Chapter 9. General Conclusions and Future Work

Smart materials have been used for many commercial engineering applications. These applications require some controllers to achieve high performance. This dissertation includes the development of an advanced optimal sliding mode controller and its applications using smart materials. The optimal sliding mode controller consisted of two parts. The first guarantees the robust stability of the controller and the second keeps the states of the system in a desired sliding surface trajectory. The desired sliding surface trajectory was designed using the stable eigenvectors. The stability of the proposed controller was explained.

A simulation example was used to evaluate the performance of the proposed approach. According to the simulation results comparison, the optimal sliding mode controller demonstrates better performance than the conventional sliding mode control and uses 34% less energy to converge the states with less chattering (71% and 31% for both the states). To further test the proposed approach, the optimal approach was successfully implemented to control the multimodal vibrations of a smart flexible beam with piezoceramic sensor and actuator. To test the robustness of the controller, the proposed controller was effectively tested on the smart beam with uncertain mass. The random mass uncertainty added to the system was about 25%. It was found that the proposed optimal controller was able to provide 30dB reduction in power for the first modal frequency and approximately 25dB reduction in power for the uncertain modal vibrations.

It was found that the LQR approach guarantees controller stability for matched system uncertainties; however, for unmatched uncertainties the stability of the controller cannot be explained properly. In order to deal with both, matched and unmatched

uncertainties, the optimal control gains are calculated using H_∞ approach. The improved sliding mode controller was again compared with a conventional sliding mode controller on a multiple input multiple output simulation system with uncertainties. The improved proposed approach was found to be highly effective in dealing with these uncertainties and proved to be better than the conventional sliding mode approach. The performance of the robust optimal controller was evaluated by implementing the controller to suppress the vibrations of a two story structure with base isolation and a nonlinear MR damper. The MR damper nonlinearity was considered a matched uncertainty and the earthquake disturbance to base isolated structure was considered an unmatched uncertainty. The experimental results of the optimal sliding mode controller were compared with the passive damping of the MR damper at different voltages level for different earthquake excitations. The experimental results showed that the proposed vibration control was optimally designed for all earthquake excitations and dealt with uncertainties effectively.

The passive control systems are the oldest and still, the most preferred way to control the vibrations of the structures. Many types of passive systems have been introduced and implemented from time to time. Generally, active/semi-active control systems are designed using specific control algorithms to have better results. For passive control systems, even for a simple design, the mathematical model could be very complex. In this study, a passive vibration control device was modeled as a passive sliding mode controller. An analogy was made between the analytical model of the force generated by the passive device (PTMD) and the sliding mode control law to suppress the vibrations of a jumper used in the oil and gas industry. A simulation was done on the jumper model with the PTMD as a passive sliding mode controller. The simulation results were

compared with experimental results. The comparison between experimental data and simulation data of the passive sliding mode controller model of the PTMD verified the proposed hypothesis. Thus, it can be stated that the proposed passive sliding model can be helpful in designing and understanding vibration suppression of the system with PTMD.

A cost effective de-icing system was developed using carbon fiber as the heating element. A mathematical model was developed for the de-icing process considering the carbon fiber heating as input and surface temperature as output. Two control algorithms, the ON/OFF controller and fuzzy logic based controller, were designed to control the surface temperature of the road. The fuzzy logic controller was developed by taking the surface temperature and weather parameters, such as environmental temperature, dew point and chances of rain/snow into consideration. The experimental lab and field results showed that the electrical heating of carbon fiber is very efficient for the de-icing of roads in cold regions. The power cost analysis for the fuzzy logic based temperature controller of the de-icing system was compared with an ON-OFF controller and manual controller. The comparison results showed that the fuzzy logic based automatic system is about 27% more economical than ON-OFF control based system and about 80% cheaper than manual operation.

Although, the power analysis shows that the fuzzy logic based temperature controlled de-icing method is very economical in comparison with other existing technologies, it can be improved further by employing more environmental parameters such as wind speed and historical weather data comparison to present data, etc.

This dissertation will be able to generate four journal papers. The papers have been submitted for journal publications and, currently, the authors are waiting for the approval. The list of papers is as follows

1. Mithun Singla, Leang-San Shieh, Gangbing Song, Linbo Xie, Yongpeng Zhang, "Development of a Novel Optimal Sliding Mode Controller with LQR Approach and Matrix Sign Function," 2012.
2. Mithun Singla, Chen-Yin Woo, Leang-San Shieh, Gangbing Song, Linbo Xie, Jason Tsai, "Optimal Vibration Control of Base-Isolated Structure with Robust H_∞ Based Sliding Mode Controller with Matrix Sign Function for Matched and Unmatched Uncertainties," 2012.
3. Mithun Singla, Gangbing Song, Peng Zhang, Leang-San Shieh, "Pounding Tuned Mass Damper: An Innovative Realization of Sliding Mode Control using a Passive Approach," 2012.
4. Mithun Singla, Christiana Chang, Gangbing Song, Zhaohui Yang, "Development of a Novel De-icing System with Advanced Temperature Control for Roads using Carbon Fiber as Heating Element," 2012.

Reference

[1] V. K. Wadhawan, *Smart Structures :Blurring the Distinction between the Living and the Nonliving* vol. 65: Oxford Science Publications, 2007.

[2] R. S. Lakes and J. Quackenbush, "Viscoelastic behaviour in indium tin alloys over a wide range of frequency and time," *Philosophical Magazine Latters,* vol. 74, pp. 227-232, 1996.

[3] "www. fiberglast.com," Fiberglast Inc.

[4] R. L. Powell and G. E. Childs, "American Institute of Physicas Handbook," vol. 4, pp. 142-160, 1972.

[5] V. I. Utkin, "Variable structure systems with sliding modes: a survey," *IEEE transactions of Automation and Control,* vol. 22, pp. 212-222, 1977.

[6] K. D. Young, V. I. Utkin, and U. Ozguner, "A Control Engineer's Guide to sliding Mode Control," *IEEE Transactions on Control Systems Technology,* vol. 7, pp. 328-342, May, 1999.

[7] J.-J. E. Slotine and W. Li, *Applied Nonlinear Control*. New Jersey: Prentice Hall International Inc., 1991.

[8] S. H. Zak, *Systems and Controls*. New York: Oxford University Press, 2003.

[9] R. Xu, "Optimal Sliding Mode Controller and Stablization of Underactuated Systems," in *Department of Electrical and Computer Engineering*. vol. Ph. D.: Ohio State University, 2007, p. 167.

[10] C. Vecchio, "Sliding Mode Control: theoretical developments and applications to uncertain mechanical systems," in *Department of Computer and System*. vol. Ph. D. Pavia, Italy: University of Pavia, 2008, p. 250.

[11] I. Boiko, A. Pisano, and E. Usai, "Analysis of Chattering in Systems with Second-Order Sliding Modes," *IEEE Transactions on Automatic Control,* vol. 52, pp. 2085-2102, 2007.

[12] M. Basin and D. Calderon-Alvarez, "Sliding mode regulator as solution to optimal control problem for non-linear polynomial systems," *Journal of the franklin Institute,* vol. 347, pp. 910-922, 2010.

[13] M. Basin, "Integral sliding mode design for robust filtering and control of linear stochastic time-delay system," *Internation Journal of Robust and Nonlinear Control,* vol. 15, pp. 407-421, 2005.

[14] M. Basin, L. Fridman, and M. Skliar, "Optimal and Robust sliding mode filter for systems with continuous and delayed measurements," in *Proceeding of the 41st Conference on Decision and Control* Las Vegas, NV, 2002.

[15] K. D. Young, V. I. Utkin, and U. Ozguner, "A Control Engineer's Guide to Sliding Mode Control," *IEEE Transaction on Control System Technology,* vol. 7, pp. 328-342, 1999.

[16] S. Wang, S. Habibi, and R. Burton, "The Smooth Sliding Mode Controller and Filter," *Control and Intelligent Systems,* vol. 38, pp. 130-139, 2010.

[17] L. Hsu, R. R. Costa, and J. P. V. S. d. Cunha, "Model-Reference Output-feedback Sliding Mode Controller for a Class of Multivariable Nonlinear Systems," *Asian Journal of Control,* vol. 5, pp. 543-556, 2003.

[18] J.-L. Chang, "Output Feedback Sliding Mode Controller Design via H∞ Theory," *Asian Journal of Control,* vol. 5, pp. 24-31, 2003.

[19] H. J. Shieh, J. H. Siao, and Y.-C. Liu, "A Robust Optimal Sliding Mode Control Approach for Magnetic Levitation Systems," *Asian Journal of Control,* vol. 12, pp. 480-487, 2010.

[20] Y.-F. Li and J. Wikander, "Model reference discrete-time sliding mode control of linear motor precision servo systems," *Mechatronics,* vol. 14, pp. 835-851, 2004.

[21] K. S. You, M. C. Lee, and W. S. Yoo, "Sliding Mode Controller with Sliding Perturbation Observer Based on Gain Optimization using Genetic Algorithm," *KSME International Journal,* vol. 18, pp. 630-639, 2004.

[22] Z. Mohammadi, M. Teshnehlab, and M. A. Shoorehdeli, "Designing Flexible Neuro-Fuzzy System Based on Sliding Mode Controller for Magnetic Levitation Systems," *International Journal of Computer Science Issues,* vol. 8, pp. 160-171, 2011.

[23] A. Hazzab, I. K. Bousserhane, M. Kamli, and M. Rahil, "A New Fuzzy Sliding Mode Controller for Induction Motor Speed Control," in *Proceedings of Second International Symposium on Communications, Control and Signal Processing*, Marrakech, Morocco, 2006.

[24] G. L. Hou, J. H. Zhang, J. Wang, and Q. H. Wu, "Adaptive Sliding Mode and Fuzzy Gain Scheduling Control for Steam Temperature in Power Plants," in *International Control Conference* Glasgow, Scotland, 2006.

[25] S.-J. Huang, H.-Y. Chen, and C.-C. Wang, "Fuzzy Sliding Mode Controller with Gain Auto-tuning for Un-symmetric Input Temperature Control System," in *IEEE International Conference on Systems, Man, and Cybernetics* Taipei, Taiwan, 2006.

[26] J. Jing and Q.-H. Wu, "An Intelligent Sliding Mode Control Algorithm for Position Tracking Servo System," *International Journal of Information Technology,* vol. 12, pp. 57-62, 2006.

[27] M. Singla and G. Song, "Positive Position Feedback and Fuzzy Logic Based Active Vibration Control of a Smart Beam with Mass Uncertainty," in *Structures, Structural Dynamics, and Materials Conference* Schaumberg, IL, USA, 2008.

[28] M. C. Pai, "Design of adaptive sliding mode controller for robust tracking and model following," *Journal of the Franklin Institute,* vol. 347, pp. 1837-1849, 2010.

[29] M.-L. Chan, C. W. Tao, and T.-T. Lee, "Sliding mode controller for linear systems with mismatched time-varying uncertainties," *Journal of Franklin Institute,* vol. 337, pp. 105-115, 2000.

[30] H. H. Choi, "An Explicit Formula of Linear Sliding Surfaces for a Class of Uncertain Dynamic Systems with Mismatched Uncertainties," *Automatica,* vol. 34, pp. 1015-1020, 1998.

[31] A. Levant and A. Michael, "Adjustment of high-order sliding mode controllers," *International Journal of Robust and Nonlinear Control,* vol. 19, pp. 1657-1672, 2009.

[32] A. Levant, "Higher-order sliding modes, differentiation and output-feedback control," *International Journal of Control,* vol. 76, pp. 924-941, 2003.

[33] A. Levant, "Universal Single-Input-Single-Output (SISO) Sliding Mode Controller with Finite Time Convergence," *IEEE Transactions on Automatic Control,* vol. 46, pp. 1447-1451, 2001.

[34] G. Bartolini, A. Pisano, and E. Usai, "Digital second-order sliding mode control for uncertain nonlinear systems," *Automatica,* vol. 37, pp. 1371-1377, 2001.

[35] N. K. Yadav and R. K. Singh, "Discrete time nonlinear sliding mode controller," *International Journal of Engineering, Science and Technology,* vol. 3, pp. 94-100, 2011.

[36] W.-C. Yu, G.-J. Wang, and C.-C. Chang, " Discrete sliding mode control with forgetting dynamic sliding surface," *Mechatronics,* vol. 14, pp. 737-755, 2004.

[37] M. Basin, "Optimal sliding mode algorithms for dynamic systems," *Editorial in Journal of The franklin Institude,* vol. 349, 2012.

[38] K. D. Young and U. Ozguner, "Sliding Mode Design for Robust Linear Optimal Control," *Automatica,* vol. 33, pp. 1313-1323, 1997.

[39] Z. Lu, L. S. Shieh, G. Chen, and N. P. Coleman, "Simplex sliding mode control for nonlinear uncertain systems via chaos optimization," *Chaos, Solitons and Fractals,* vol. 23, pp. 747-755, 2005.

[40] F. Dinuzzo and A. Ferrara, "Higher order Sliding mode Controllers with Optimal Reachning," *IEEE Transactions on Automatic Control,* vol. 54, pp. 2126-2136, 2009.

[41] N. Sakamoto, "Optimal Control Problem via Self-Adaptation Sliding Mode Controller with Neural Network," *Electronics and Communications in Japan,* vol. 94, pp. 1043-1049, 2011.

[42] C. Pukdeboon and A. S. I. Zinober, "Control Lyapunov function optimal sliding mode controllers for attitude tracking of spacecraft," *Journal of Franklin Institute,* vol. 349, pp. 456-475, 2012.

[43] S. Laghrouche, F. Plestan, and A. Glumineau, "Higher Order Sliding Mode Control based on Optimal Linear Quadratic Control," *Automatica,* vol. 43, pp. 531-537, 2007.

[44] C. Edwards, "A practical method for the design of sliding mode controllers using linear matrix inequalities," *Automatica,* vol. 40, pp. 1761-1769, 2004.

[45] M. Nikkhah, H. Ashrafiuon, and K. R. Muske, "Optimal Sliding Mode Control for Underactuated Systems," in *Proceedings of the 2006 American Control Conference*, Minneapolis, Minnesota, USA, 2006.

[46] Y. Niu, D. W. C. Ho, and Z. Wang, "Improved sliding mode control for discrete time systems via reaching law," *IET Control Theory and Applications,* vol. 4, pp. 2245-2251, November, 2010.

[47] V. Azhmyakov, "On the set-valued approach to optimal control of sliding mode processes," *Journal of The Franklin Institute,* vol. 349, pp. 1323-1336, 2012.

[48] V. I. Utkin and H. Lee, "Chattering Problem in Sliding Mode Control Systems," in *Proceedings of the 2006 International Workshop on Variable Structure Systems*, Alghero, Italy, 2006, pp. 346-350.

[49] W.-C. Su, S. V. Drakunov, U. Ozgiiner, and K. D. Young, "Sliding Mode with Chattering Reduction in Sampled Data Systems," in *Proceedings of the 32nd Conference on Decision and Control*, San Antonio, TX, 1993, pp. 2452-2457.

[50] K. D. Young and S. V. Drakunov, "Sliding Mode Control with Chattering Reduction," in *American Control Conference, 1992*, 1992, pp. 1291-1292.

[51] G. Song and R. Mukherjee, "A Comparative Study of Conventional Nonsmooth Time-Invariant and Smooth Time-Varying Robust Compensators," *IEEE Transaction of Control Systems Technology,* vol. 6, pp. 571-576, 1998.

[52] G. Song and H. Gu, "Active Vibration Suppression of a Smart Flexible Beam using a Sliding Mode Based Controller," *Journal of Vibration and Control,* vol. 13, pp. 1095-1107, 2007.

[53] J. D. Roberts, "Linear Model Reduction and Solution of the Algebraic Riccati Equations by Use of Sign Function," *International Journal of Control,* vol. 130, pp. 677-687, 1980.

[54] L. S. Shieh, Y. T. Tsay, and R. Yates, "Some Properties of Matrix Sign Function Derived from Continued Fractions," *IEEE Proceedings of Control Theory and Applications,* vol. 130, pp. 111-118, 1983.

[55] F. Attarzadeh, "Relative Stability Test for Continuous and Sampled-Data Control Systems " *Proceedings of IEE,* vol. 129, pp. 189-192, 1982.

[56] R. L. Mattheys, "Stability Analysis via the Extended Matrix Sign Function," *Proceedings of IEE,* vol. 125, pp. 241-243, 1978.

[57] J. S. H. Tsai, L. S. Shieh, and R. E. Yates, "Fast and Stable Algorithms for Computing the Principal nth Root of a Complex Matrix and The Matrix Sector Function," *Computers & Mathematics with Applications,* vol. 15, pp. 903-913, 1988.

[58] J. S. H. Tsai, C.-C. Huang, S.-M. Guo, and L.-S. Shieh, "Continuous to Discrete Model Conversion for the System with a Singular System Matrix based on mAtrix Sign Function," *Applied Mathematical Modeling,* vol. 35, pp. 3893-3804, 2011.

[59] V. Utkin, J. Guldner, and J. Shi, *Sliding Mode Control in Electromechanical Systems*. Bristol PA: Taylor and Francis, 1999.

[60] J. Fei and M. Xin, "Robust Adaptive Sliding Mode Controller for Semi-active Vehicle Suspension System," *Interbational Journal of Innovative Computing, Information and Control,* vol. 8, pp. 691-700, 2012.

[61] S.-H. Lee, Y. Joo, J. Back, J.-H. Seo, and I. Choy, "Sliding Mode Controller for Torque and Pitch Control of PMSG Wind Power Systems," *Journal of Power Electronics,* vol. 11, pp. 342-349, 2011.

[62] B. Afkham and S. Ehteram, "Nonlinear Control of Buildings Subjected to Earthquakes by Using Sliding Mode Controller (SMC)," *Modern Applied Science,* vol. 4, pp. 170-176, 2010.

[63] C. Pukdeboon, "Optimal Sliding Mode Controllers for Attitude Stabilization of Flexible Spacecraft," in *Mathematical Problems in Engineering*. vol. 2011, 2011, pp. 1-20.

[64] O. Camacho and R. Rojas, "A General Sliding Mode Controller for Nonlinear Chemical Processes," *Transaction of the ASME,* vol. 122, pp. 650-655, 2000.

[65] O. Camacho, C. Smith, and W. Moreno, "Development of an Internal Model Sliding Mode Controller," *Industrial and Engineering Chemistry Research,* vol. 42, pp. 568-573, 2003.

[66] C.-T. Chen and S.-T. Peng, "Design of a sliding mode control system for chemical processes," *Journal of Process Control,* vol. 15, pp. 515-530, 2005.

[67] U. Demirci and F. Keresteciogl u, "A re-configuring sliding-mode controller with adjustable robustness," *Ocean Engineering,* vol. 31, pp. 1669-1682, 2004.

[68] K. Takahashi, K. Tateishi, Y. Tomita, and S. Ohsawa, "Application of the Sliding-Mode Controller to Optical Disk Drives," *Japanese Journal of Applied Physics,* vol. 43, pp. 4801-4805, 2004.

[69] H. Gu, G. Song, and H. Malki, "Chattering-free fuzzy adaptive robust sliding-mode vibration control of a smart flexible beam," *Smart Material and Structures,* vol. 17, pp. 1-7, 2008.

[70] L. Li, G. Song, and J. Ou, "Nonlinear Structural Vibration Suppression Using Dynamic Neural Network Observer and Adaptive Fuzzy Sliding Mode Control," 2009.

[71] G. W. Housner, L. A. Bergam, T. K. Cauchy, A. G. Chassiakos, R. O. Claus, S. M. Skelton, T. T. Soong, B. F. Spencer, and J. P. T. Yao, "Structural Control: Past, Present and Future Control," *Journal of Engineering Mechanics,* vol. 123, pp. 897-971, 1997.

[72] S.-G. Luca, F. Chira, and V.-O. Rosca, "Passive, Active and Semi-Active Control systems in Civil engineering," *Bulletin of the Polytechnic Institute of Iaşi,* pp. 23-31, 2005.

[73] C. Pastia, S.-G. Luca, F. Chira, and C.-O. Rosca, "Structural control systems implemented in civil engineering," *Bulletin of the Polytechnic Institute of Iaşi,* pp. 41-49, 2005.

[74] M. A. Lackner and M. A. Rotea, "Passive structural control of offshore wind turbines," *Wind Energy,* vol. 14, pp. 373-388, 2011.

[75] J. Ou and H. Li, "Design approaches for active, semi-active and passive control systems based on analysis of characteristics of active control force," *Earthquake Engineering and Engineering vibrations,* vol. 8, pp. 493-506, 2009.

[76] J. Ou and H. Li, "Analysis of capability for semi-active or passive damping systems to achieve the performance of active control systems," *Structural Control and Health Monitoring,* vol. 17, pp. 778-794, 2010.

[77] T. R. M. Rao, G. V. Rao, k. S. Rao, and A. Purushottam, "Analysis of Passive and Semi-Active controlled suspension systems for ride comfort in an omnibus passing over speed bump," *International Journal of Research and Reviews in Applied Sciences,* vol. 5, pp. 7-17, 2010.

[78] M. D. Symans and M. C. Constantinou, "Semi-active control systems for seismic protection of structures: a state-of-the-art review," *Engineering Structures,* vol. 21, pp. 469-487, 1999.

[79] M. H. Chey, "Passive and Semi-active tuned mass damper building systems," in *Civil and Natural Resources Engineering* Christchurch, New Zealand: University of Canterbury, 2007.

[80] S. J. Dyke, B. F. S. Jr., M. K. Sain, and J. D. Carlson, "Modeling and Control of Magnetorheological Dampers for Seismic Response Reduction," *Smart Material and Structures,* vol. 5, pp. 565-575.

[81] B. F. J. Spencer, S. J. Dyke, M. K. Sain, and J. D. Carlson4, "Phenomenological Model of a Magnetorheological Damper," *Journal of Engineering Mechanics,* vol. 123, 1997.

[82] B. F. J. Spencer and T. T. Soong, "New applications and development of active, semi-active and hybrid control techniques for seismic and non-seismic vibration in the USA," in *Proceedings of International Post-SMiRT Conference Seminar on Seismic Isolation*, Cheju, Korea, 1999.

[83] M. Singla, J. B. Dabney, and G. Song, "Development of an interactive smart vibration beam experiment," in *Proceedings of the 11th International Conference on Engineering, Science, Construction, and Operations in Challenging Environments* Long Beach, CA, 2008.

[84] A. D. Nashif, "Control of Noise and Vibration with damping materials," *Sound and Vibration,* vol. 17, pp. 28-36, 1983.

[85] C. K. Crosby, "Utilizing Viescoelastic Dampers in Seismic Retrofit of a Thirteen Story Steel Frame Building," in *Structures Congress XII* Atlanta, GA, 1994.

[86] P. R. Mahmoodi, L. E. Robertson, M. Yontar, C. Moy, and L. Feld, "Performance of Viescoelastic Dampers in World Trade Center Towers," in *Dynamics if structures, Proceedings of the sessions of Structural Congress*, Orlando, FL, 1987.

[87] D. R. Morgenthaler, "Design and Analysis of of Passive Damped Large Space Structures," *ASME,* vol. 5, pp. 1-8, 1987.

[88] T. T. Soong and G. F. Dargush, "Passive Energy Dissipation and Active Control," in *Structural Engineering Handbook*, Chen-Wai-Fah, Ed.: CRC Press LLC, 1999.

[89] M. A. Franchek, M. W. Ryan, and R. J. Bernhard, "Adaptive Passive Vibration Control," *Journal of Sound and Vibration,* vol. 189, pp. 565-585, 1995.

[90] H. S. Jing and M. Young, "Impact interactions between two vibration systems under random excitation," *Earthquake Engineering and Structural Dynamics,* vol. 20, pp. 667-681, 1991.

[91] X. Ma and C. P. Pantelides, "Linear and Nonlinear pounding of structural systems," *Computers and Structures,* vol. 66, pp. 79-92, 1998.

[92] B. F. Maison and K. Kaisai, "Analysis for type of structural pounding," *Journal of Structural Engineering (ASCE),* vol. 116, pp. 957-977, 1990.

[93] B. F. Maison and K. Kaisai, "Dynamics of pounding when two buildings collide," *Earthquake Engineering and Structural Dynamics,* vol. 21, pp. 771-786, 1992.

[94] R. Jankowski, "Non-linear viscoelastic modeling of earthquake-induced structural pounding," *Earthquake Engineering and Structural Dynamics,* vol. 34, pp. 595-611, 2005.

[95] M. Singla, "Advanced Control of Piezoceramic Devices," in *Electrical Engineering*. vol. Master of Science Houston, TX: University of Houston, 2008.

[96] L. S. Shieh, Y. T. Tsay, and R. Yates, "Some Properties of Matrix Sign Function derived from continued time fractions," *IEEE Proceeding of Control Theory and Applications,* vol. 130, pp. 111-118, 1983.

[97] L. S. Shieh, H. M. Dib, and B. C. Mcinnis, "Linear Quadratic Regulators with Eigen-value Placement in a Vertical Strip," *IEEE Transaction on Automatic Control,* vol. 31, pp. 241-243, 1986.

[98] J. Wu, M. Singla, C. Olmi, L. S. Shieh, and G. Song, "Digital Controller Design for Absolute Value Function Constrained Nonlinear Systems via Scalar Sign Function Approach," *ISA Transactions,* vol. 49, pp. 302-310, 2010.

[99] S. Kilicaslan and S. P. Banks, "Existence of Solutions of Riccati Differential Equations," *Journal of Dynamics Systems, Measurement, and Control,* vol. 134, p. 11, 2012.

[100] V. Sethi and G. Song, "Multimodal Vibration Control of a Flexible Structure using Piezoceramic Sensor and Actuator," *Journal of Intelligent Material Systems and Structures,* vol. 19, pp. 573-582, 2007.

[101] V. Sethi, M. Franchek, and G. Song, "Active multimodal vibration suppression of a flexible structure with piezoceramic sensor and actuator by using loop shaping," *Journal of Vibration and Control,* vol. 17, pp. 1994-2006, 2011.

[102] S. H. Jang and S. W. Kim, "A new sliding surface design method of linear Systems with Mismatched Uncertainties," *IEICE Transaction Fundamentals,* vol. 88, pp. 387-391, 2005.

[103] S.-G. Wang, H. Y. Yeh, and P. N. Roschke, "Robust Control for Structural Systems with Parametric and Unstructured Uncertainties," *Journal of Vibration and Control,* vol. 7, pp. 753-772, 2001.

[104] A. S. I. Zinober and P. Liu, "Robust control of nonlinear uncertain systems via sliding mode with backstepping design," Exeter, UK, 1996, pp. 281-286.

[105] P. Swaroop, J. K. Hedrick, and P. P. Yip, "Dynamic surface control for a class of nonlinear systems," *IEEE Transaction on Automatic Control,* vol. 45, pp. 1893-1899, 2000.

[106] J. Hu, J. Chu, and H. Su, "SMVSC for a class of time delay uncertain systems with mismatched uncertainties," *IEEE Proceedings of Control Theory and Applications,* vol. 147, pp. 687-693, 2000.

[107] H. P. M. and S. M. C., "Structurally Constrained Robust Optimal Control," *Chilean Journal of Engineering,* vol. 14, pp. 276-283, 2006.

[108] B. D. O. Anderson and J. B. Moore, *Linear Optimal Control*. Englewood Cliffs, NJ: Prentice Hall, 1971.

[109] R. J. Veillette, J. V. Medanic, and W. R. Perkins, "Robust Stabilization and Disturbance Rejection for System with Structured Uncertainty," in *28th Conference on Decision and Control*, Tampa, Florida, 1989.

[110] M. Kciuk and R. Turczyn, "Properties and application of magnetorheological fluids," *Journal of Achievements in Materials and Manufacturing Engineering,* vol. 18, pp. 127-130, 2006.

[111] S. J. Dyke, B. F. S. Jr., M. K. Sain, and J. D. Carlson, "Modeling and Control of Magnetorheological Dampers for Seismic Response Reduction," *Smart Material and Structures,* vol. 5, pp. 565-575, 1996.

[112] A. Do, O. Sename, and L. Dugard, "An LPV Control Approach for Semi active Suspension Control with Actuator Constraints," in *Proceedings of American Control Conference*, Baltimore, USA, 2010, pp. 4653-4658.

[113] F. A. Shirazi, K. M. Grigoriadis, and G. Song, "Parameter varying control of an MR damper for smart base isolation," in *American Control Conference* San Francisco, CA, 2011.

[114] H. Wang, "Advanced Controls on Base Isolation System," in *Electrical and Computer Engineering*. vol. Master's of Science Houston: University of Houston, 2009.

[115] H. Yoshioka, J. C. Ramallo, and B. F. S. Jr., "Smart Base Isolation Strategies Employing Magnetorheological Dampers," *Journal of Engineering Mechanics,* vol. 128, pp. 540-551, 2002.

[116] F. A. Shirazi, J. Mohammadpour, K. M. Grigoriadis, and G. Song, "Identification and Control of an MR Damper with Stiction Effect and its Application in Structural Vibration Mitigation," *IEEE Transaction of Control System Technology,* vol. 1, pp. 1-17, 2011.

[117] H. Du, K. Y. Sze, and J. Lam, "Semi-active H_∞ Control of Vehicle Suspension with Magnetorheological Dampers," *Journal of Sound and Vibration,* vol. 283, pp. 981-996, 2005.

[118] M. Giuclea, T. Sireteanu, D. Stancioiu, and C. W. Stammers, "Modeling of Magnetorheological Damper Dynamic Behaviour By Genetic Algorithms based Inverse Method," *Proceedings of the Roman Academy,* vol. 5, pp. 1-10, 2004.

[119] M. Zapateiro and N. Luo, "Neural Network Modeling of a Magnetorheological Damper," in *Proceedings of the 2007 conference on Artificial Intelligence Research and Development*, Sant Julia De Loria, Andorra, 2007, pp. 351-358.

[120] C. Sakai, T. Terasawa, and A. Sano, "Integration of Bilinear H∞ Control and Adaptive Inverse Control for Semi-Active Vibration Isolation of Structures," in *Proceedings of 44th IEEE Conference on Decision and Control*, Seville, Spain, 2005, pp. 5310-5316.

[121] W. Han, H. A. Malki, and S. Gangbing, "Fuzzy semi-active control of MR damper for structural base isolation," in *Fuzzy Systems, 2009. FUZZ-IEEE 2009. IEEE International Conference on*, 2009, pp. 2035-2040.

[122] I. Chowdhury and S. P. Dasgupta, "Computation of Rayleigh damping coefficients for large systems," *The Electronic Journal of Geotechnical Engineering,* vol. 8, 2003.

[123] S. Yehia and C. Tuan, "Conductive concrete overlay for bridge deck deicing," *American Concrete Institute Materials Journal,* vol. 96, pp. 382-390, 1999.

[124] D. Williams, N. Williams, and Y. Cao, "Road salt contamination of ground water in major metropolitan area and development of a biological index to monitor its impact," *Water Research,* vol. 34, pp. 127-138, 2000.

[125] P. H. Jones, B. A. Jaffrey, P. K. Watler, and H. Hutchon, *Environmental impact of road salting: Chemical deicers and the enviroment*. Chelsea, MI: Lewis Publishers, 1992.

[126] B. Mussato, O. Gepraegs, and G. Farnden, "Relative Effects of Sodium Chloride and Magnesium Chloride on Reinforced Concrete: State of the Art," *Transportation Research Record,* vol. 1866`, pp. 59-66, 2004.

[127] T. R. Menzies, "National cost of damage to infrastructure from highway deicing," in *Corrosion forms and control for infrastructure* San Diego, CA, 1991.

[128] S. Birst and M. Smadi, "Evaluation of North Dakota's Fixed Automated Spray Technology Systems," North Dakota State University, Fargo, ND 2009.

[129] D. E. Kuemmel, "Managing Roadway Snow and Ice Control Operations," 1994.

[130] J. A. Zenewitz, "Survey of Alternatives to the Use of Chlorides for Highway Deicing," Department of Transportation 1977.

[131] H. B. Britton, "The Value of Insulated Forms for Winter Bridge Construction," *Highway Research Record,* vol. 111, pp. 79-93, 1963.

[132] M. D. Oosterbahn and G. A. Leonards, "Use of Insulating Layer to Attenuate Frost Action in Highway Pavements," *Highway Research Record,* vol. 1318, pp. 23-27, 1965.

[133] B. L. Ward, "Evaluation of a Fixed Anti-Icing Spray Technology (FAST) System," 2002.

[134] D. Gao, M. Sturm, and Y. L. Mo, "Electrical resistance of carbon-nanofiber concrete," *Smart Material and Structures,* vol. 18, pp. 1-7, 2009.

[135] D. D. L. Chung, "Self Heating structural materials," *Smart Material and Structures,* vol. 13, pp. 562-565, 2004.

[136] M. Sun, X. My, Z. Wang, Z. Hou, and Z. Li, "Experimental studies on the indoor electrical floor heating system with carbon black mortar slabs," *Energy and Buildings,* vol. 40, pp. 1094-1100, 2008.

[137] S. Yehia, C. Tuan, D. Ferndon, and B. Chen, "Conductive concrete overlay for bridge deicing: Mixture proportioning, optimization, and properties," *American Concrete Institute Materials Journal,* vol. 97, pp. 172-181, 2000.

[138] C. Tuan, "Electrical resistance heating of conductive concrete containing steel fibers and shavings," *American Concrete Institute Materials Journal,* vol. 101, pp. 65-70, 2004.

[139] S. Yehia and C. Tuan, "Current Events," *Roads and Bridges,* vol. 46, pp. 32-35, 2008.

[140] S. Yehia, "No-stick surface," *Roads and Bridges,* vol. 42, pp. 26-28, 2004.

[141] P. Rossi, "Steel or Synthetic Fiber Reinforcement?," in *Structure Magazine*. vol. 11, 2011.

[142] J. P. D. Charpin, T. G. Myers, A. D. Fitt, Y. Ballim, and A. Patini, "Modeling Surface Heat Exchanges from a Concrete Block into the Environment," *Mathematics in Industry,* 2004.

[143] C. Chang, M. Ho, G. Song, Y.-L. Mo, and H. Li, "A Feasibility Study of Self-Heating Concrete Utilizing Carbon Nanofiber Heating Elements," *Smart Material and Structures,* vol. 18, December, 2009 2009.

[144] M. Sen, "A review of the principles and applications of thermal control," *Journal of the Mexican Society of Mechanical Engineering,* vol. 1, pp. 115-131, 2004.

[145] E. Grassi and K. Tsakalis, "PID controller tuning by frequency loop-shaping," in *35th IEEE Conference on Decision and Control*, Kobe, Japan, 1996, pp. 4776-4781.

[146] S.-J. Huang and Y.-h. Lo, "Metal Chamber Temperature control by Using Fuzzy PID Gain Auto-tuning strategy," *WSEAS Transactions on Systems and Control,* vol. 4, pp. 1-10, January, 2009 2009.

[147] R. Yusof, S. Omatu, and M. Khalid, "Application of self-tuning PI(PID) controller to a temperature control system," in *3rd IEEE Conference on Control Applications*, Glasgow, UK, 1994, pp. 1181-1186.

[148] S.-Z. He, S. Tan, F.-L. Xu, and P.-Z. Wang, "Fuzzy self-tuning of PID controllers," *Fuzzy Sets and Systems,* vol. 56, pp. 37-46, May, 1993 1993.

[149] C. Jia-Xin and L. Wei, "Application of fuzzy control PID algorithm in temperature controlling systems," in *2nd International Conference on Machine Learning and Cybernetics*, Henan, China, 2003, pp. 2601-2604.

[150] U.-C. Moon and K. Y. Lee, "Temperature control of glass melting furnace with fuzzy logic and conventional PI control," in *Proceedings of American Control Conference*, Chicago, IL, USA, 2000, pp. 2720-2724.

[151] A. Visioli, "Tuning of PID controllers with fuzzy logic," *Control Theory and Applications,* vol. 148, pp. 1-8, Jan 2001 2001.

[152] ASM, "Material about Materials."

[153] FLUENT, *FLUENT 6.3 Tutorial Guide: Tutorial: Heat Transfer Theory*.

[154] T. Yang, Z. J. Yang, M. Singla, G. Song, and Q. Li, "Experimental study on Carbon Fiber based Deicing Technology," *Journal of Cold Regions Engineering,* pp. 1-30, 2011.

[155] P. Zhang, "Pounding Tuned Mass Damper (PTMD): An Innovative Device to Control the Vibration of Subsea Jumpers," Houston: University of Houston, , 2012.

Appendix I

Modeling of Jumper used in chapter 4 for realizing the active sliding mode control law by analyzing the PTMD is found by SAP2000 by Zhang *et al.* [155]. The jumper was divided into 11 nodes and the mass and the stiffness matrix were calculated. The damping of the system is assumed to be 2% and the damping matrix was calculated using Rayleigh's Method.

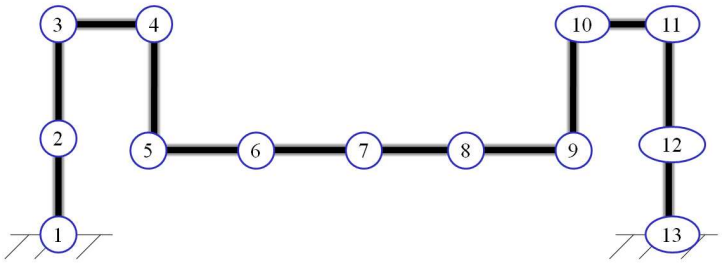

Figure. Modeling of Jumper with 11 nodes

The mass and stiffness matrix for in-plane vibrations are

Mass Matrix of Jumper (Kgs)

74.19	0	0	0	0	0	0	0	0	0	0
0	5.54	0	0	0	0	0	0	0	0	0
0	0	44.34	0	0	0	0	0	0	0	0
0	0	0	54.96	0	0	0	0	0	0	0
0	0	0	0	72.78	0	0	0	0	0	0
0	0	0	0	0	68.56	0	0	0	0	0
0	0	0	0	0	0	72.78	0	0	0	0
0	0	0	0	0	0	0	54.96	0	0	0
0	0	0	0	0	0	0	0	44.34	0	0
0	0	0	0	0	0	0	0	0	5.54	0
0	0	0	0	0	0	0	0	0	0	74.20

In-plane Stiffness Matrix (N/m)

From Column 1 to 7

4776697	-1700979	231983.5	-232362	506.0766	-576.146	428.6348
-1700979	1072744	-437771	88423.04	112137.2	-29345.7	7372.364
231983.5	-437771	399720.7	-50253.7	-112299	29533.98	-7513.59
-232362	88423.04	-50253.7	258266.3	-216344	122659.5	-31263.9
506.0766	112137.2	-112299	-216344	488010.3	-407980	167534.7
-576.146	-29345.7	29533.98	122659.5	-407980	570694	-407980
428.6348	7372.364	-7513.59	-31263.9	167534.7	-407980	488010.3
4375.315	-4751.78	26114.21	-18861.9	-31263.9	122659.5	-216344
-4783.46	3154.996	-24388.3	26114.21	-7513.59	29533.98	-112299
2084.908	-757.284	3154.996	-4751.78	7372.364	-29345.7	112137.2
-4044.42	2084.908	-4783.46	4375.315	428.6348	-576.146	506.0766

From Column 8 to 11

4375.315	-4783.46	2084.908	-4044.42
-4751.78	3154.996	-757.284	2084.908
26114.21	-24388.3	3154.996	-4783.46
-18861.9	26114.21	-4751.78	4375.315
-31263.9	-7513.59	7372.364	428.6348
122659.5	29533.98	-29345.7	-576.146
-216344	-112299	112137.2	506.0766
258266.3	-50253.7	88423.04	-232362
-50253.7	399720.7	-437771	231983.5
88423.04	-437771	1072744	-1700979
-232362	231983.5	-1700979	4776697

For out-plane vibrations, the same mass matrix is used as in-plane vibrations and the stiffness matrix for out-plane vibrations are

From Column 1 to 7

4458250	-1587580	216518	-216872	472.3382	-537.736	400.0592
-1587580	1001227	-408586	82528.17	104661.4	-27389.3	6880.873
216518	-408586	373072.7	-46903.5	-104813	27565.05	-7012.69
-216872	82528.17	-46903.5	241048.6	-201922	114482.2	-29179.6
472.3382	104661.4	-104813	-201922	455476.3	-380781	156365.8
-537.736	-27389.3	27565.05	114482.2	-380781	532647.7	-380781
400.0592	6880.873	-7012.69	-29179.6	156365.8	-380781	455476.3
4083.628	-4435	24373.26	-17604.4	-29179.6	114482.2	-201922
-4464.57	2944.663	-22762.4	24373.26	-7012.69	27565.05	-104813
1945.914	-706.799	2944.663	-4435	6880.873	-27389.3	104661.4
-3774.79	1945.914	-4464.57	4083.628	400.0592	-537.736	472.3382

From Column 8 to 11

4083.628	-4464.57	1945.914	-3774.79
-4435	2944.663	-706.799	1945.914
24373.26	-22762.4	2944.663	-4464.57
-17604.4	24373.26	-4435	4083.628
-29179.6	-7012.69	6880.873	400.0592
114482.2	27565.05	-27389.3	-537.736
-201922	-104813	104661.4	472.3382
241048.6	-46903.5	82528.17	-216872
-46903.5	373072.7	-408586	216518
82528.17	-408586	1001227	-1587580
-216872	216518	-1587580	4458250